# The synthesis and characterization of films and nanofibres from novel poly(N,N'-dimethyl acrylamide)-*graft*-poly(dimethyl siloxane) amphiphilic hydrogels

**by**

**Stefan Wagenaar**

**Thesis presented in fulfilment of the requirements for the degree of Master of Science in the Faculty of Science (Polymer Science) at Stellenbosch University**

Supervisor: Professor P.E Mallon

March 2017

_____

# Declaration

By submitting this thesis/dissertation electronically, I declare that the entirety of the work contained therein is my own, original work, that I am the sole author thereof (save to the extent explicitly otherwise stated), that reproduction and publication thereof by Stellenbosch University will not infringe any third party rights and that I have not previously in its entirety or in part submitted it for obtaining any qualification.

March 2017

_____

# **Abstract**

A series of graft copolymers comprised of poly(N,N'-dimethyl acrylamide) (PDMAA) and poly(dimethyl siloxane) (PDMS) were synthesized for the first time by way of free radical polymerization. The copolymer compositions were found to closely match the feed ratios of each reaction. HPLC separation showed that the samples were composed of a hompolymer and copolymer fraction, with the homopolymer fraction rapidly diminishing as the amount of PDMS monomer in the feed was increased. Nanofibres were successfully produced from the material by single needle electrospinning to produce fibres with an average diameter of around 700 nm. Films and nanofibres of the material were then analysed by way of DSC, FTIR, HPLC, SEM, Solid state NMR, TGA and WAXD, as well as conventional swelling studies. The presence of the hydrophobic PDMS grafts was effective in producing a physically crosslinked hydrogel network, as the materials were able to absorb up to 1.6 times their own weight in water and were held together by the hydrophobic clusters. The nanofibres were able to absorb as much as 10 times their weight in water, with water retention undergoing a sharp reduction with increasing PDMS content. Swelling occurred rapidly, with the films reaching around 90% of their equilibrium swelling in less than 5 minutes when immersed in water. SEM images of the nanofibres before and after water exposure revealed that they lacked dimensional stability and lose their fibrous structure when wet. The stability improved with increased PDMS content. The effective crosslinking density of the samples was calculated in order to investigate the effect of the PDMS content on crosslinking density, and it was shown that a non-linear relationship existed between the PDMS content and the resultant swelling of the material. DSC analysis was used to elucidate the water structure inside of the films and fibres, and the relative fractions of freezing and non-freezing water was determined. DSC analysis of dry films showed that the material's glass transition occurred around 90°C, which is near the expected value for poly(N,N'-dimethyl acrylamide). However, the physical properties more closely resembled that of a rubber-like compound due to the large weight percentage of included PDMS. Determination of the material's morphology showed that it underwent a morphological transition above a threshold PDMS content, changing from a highly phase segregated system to one with a higher degree of homogeneity. $T_{1\rho}$ relaxation data from solid state NMR showed that the respective values for the PDMAA and PDMS segments differed significantly in the low PDMS content samples, but converged with increasing PDMS content. Additionally, in the nanofibre state it was also found that the samples showed a lower degree of phase separation and that the PDMS grafts were more isolated, which would result in a lower effective crosslinking density. This correlated well with other observed data. SEM images of fracture surfaces from swollen samples revealed island-like structures which are believed to be primarily associated with the PDMS domains. This correlated well with other evidence from solid state NMR and swelling studies. Finally, tensile tests illustrated that the new material had improved physical properties over the homopolymer material.

_____

# Opsomming

'n Reeks van entkopolimere, poli(N,N'-dimetiel akrilamied)-*ent*-poli(dimetiel siloksaan), is vir die eerste keer gesintetiseer deur middel van vrye radikaal polimersasie. HPLK skeiding het aangedui dat die monsters homo- en kopolimeer fraksies bevat, en dat die fraksie homopolimeer vining afneem met toenames in in PDMS inhoud. Nano-vesels is gevorm met electrospinning en vesels met 'n gemiddelde deursnit van 700 nm is verkry. Films en vesels van die materiaal is geanaliseer met DSK, FTIR, HPLK, SEM, vaste fase KMR, TGA en X-straal analise, sowel as water absorbsie studies. Dit is bevind dat die teenwoordigheid van die hidrofobiese poli(dimetiel siloksaan) (PDMS) doeltreffend was in die skepping van 'n hidrogel, aangesien die materiaal tot 1.6 keer sy eie gewig in water kon absorbeer, as gevolg van die samespanning van die hidrofobiese PDMS. Die nano-vesels kon tot 10 keer hul gewig in water absorbeer, maar dit was hoogs afhanklik van die PDMS inhoud. Die films het baie vinnig water geabsorbeer en omtrent 90% versadiging bereik na slegs 5 minute. Die vesels was egter onstabiel in water en het geneig om hul strukteer te verloor na 'n kort tydperk. Hierdie stabiliteit het verbeter met verhogings in die PDMS inhoud. Die kruis bindings digtheid is uitgewerk om die effek van die PDMS inhoud daarop te bepaal, and dit is bevind dat daar 'n nie-lineêre verhouding was tussen die twee veranderlikes bestaan as gevolg van die teenwoordigheid van komplekse morfologiese rangskikkings. DSK analise is gebruik om die water struktuur met betrekking tot die vriesbare en onvriesbare water fraksies te bepaal. DSK analise van droë monsters het aangedui dat die polimeer se glas oorgangs temperatuur om en by 90°C was, naby aan die verwagte temperatuur vir poli(N,N'-dimetiel akrilamied). Die fisiese eienskappe was egter meer kenmerkend van 'n rubberagtige materiaal as gevolg van groot gewig persentasie PDMS. 'n Ondersoek om die materiaal se morfologie te bepaal het aangedui dat dit 'n morfologiese oorgang ondergaan bo 'n kritieke PDMS inhoud, en dat dit dan verander vanaf 'n hoogs geskeide stelsel na 'n meer homogene een. T1ρ data vanaf vaste fase KMR het verskil in die monsters met 'n lae PDMS inhoud vir die PDMAA en PDMS gedeeltes, maar was eenders in die monsters met n hoër hoeveelheid PDMS. In die nano-vesels was die skeiding tussen die gedeeltes amper onopmerkbaar aangesien die PDMS gedeeltes hoogs geisoleerd was, wat sou veroorsaak dat die vesels 'n lae kruis bindings digtheid sou hê. Mikro beelde vanaf electron mikroskopie op die oppervlaktes van monsters wat volledig geswel is en toe oopgekraak is onder lae temperatuur het 'n rangskikking van "eiland" strukture aangetoon wat waarskynlik afkomstig is vanaf PDMS reike areas. Die bevindings het sterk ooreengstem met alle vorige gevolgtrekkings.Laastens, meganiese toetse het aangetoon dat die nuwe materiaal se fisiese eienskappe 'n verbeter het teenoor die homopolimeer.

_____

# Acknowledgements

I would like to thank the following people and organizations for their assistance during the course of this project:

The National Research Fund (NRF), for their financial support.

Colleagues in the Polymer Science department for their assistance and insight with various instruments and techniques.

Dr. Jaco Brand for his assistance and training in the use and interpretation of solid state NMR.

Professor P.E Mallon for his mentorship, guidance and patience.

My father and stepmother, for their endless moral and financial support over the course of my university career.

## Table of contents

Table of contents
_____

Table of contents
_____

_____

## List of figures

List of figures

_____

List of figures
_____

_____

## **List of tables**

# Glossary

## List of abbreviations

| | |
|---|---|
| AIBN | 2,2'-azobisisobutyronitrile |
| APCN | Amphiphilic Cone Network |
| BIS | N,N'-methylenebisacrylamide |
| °C | Degrees celsius |
| cm | Centimetres |
| CP | Cross Polarization |
| $dm^{-3}$ | Decimeters (liters) |
| DDI | Distilled and deionized (Water) |
| DMAA | N,N'-dimethyl acrylamide |
| DMF | N,N'-dimethyl formamide |
| DSC | Differential Scanning Calorimetry |
| EGDMA | Ethylene glycol dimethacrylate |
| EWC | Equilibrium Water Content |
| FE-SEM | Field Emission Scanning Electron Miscroscopy |
| FTIR | Fourier Transform Infrared Spectroscopy |
| $f_H$ | Water fraction by mass |
| $g.ml^{-1}$ | Grams per millilitre |
| GPC | Gel Permeation Chromtography |
| HPLC | High Performance Liquid Chromatography |
| J/g | Joules per gram |
| kN | Kilo Newtons |
| $kJ.mol^{-1}$ | Kilojoules per mole |
| kV | Kilovolts |
| LCST | Lower Critical Solution Temperature |
| MAS | Magic Angle Spinning |
| mins | Minutes |
| $ml.min^{-1}$ | Millilitres per minute |
| mm | Milimetres |
| N | Newtons |
| NIPAAM | N-isopropyl acrylamide |
| nm | Nanometres |
| NMR | Nuclear Magnetic Resonance Spectroscopy |

Glossary

_____

| | |
|---|---|
| PDMAA | Poly(N,N'-dimethyl acrylamide) |
| PDMS | Poly(dimethyl siloxane) |
| PEG | Poly(ethylene glycol) |
| PHEMA | Poly(2-hydroxy ethyl methacrylate) |
| PIB | Poly(isobutylene) |
| PNIPAAM | Poly(N-isopropyl acrylamide) |
| ppm | Part per million |
| Q | Swelling in water |
| $Q_s$ | Swelling of the water swellable fraction in water (exclusively) |
| RAFT | Reversible addition-fragmentation chain-transfer polymerization |
| R.H | Relative Humidity |
| SAXS | Small Angle X-ray Scattering |
| SEC | Size Exclusion Chromatography |
| SET-LRP | Single Electron Transfer Living Radical Polymerization |
| SP | Single Pulse |
| T1 | Spin-lattice relaxation time (laboratory frame) |
| $T1\rho$ | Spin-lattice relaxation time in the rotating frame |
| T2 | Spin-spin relaxation time |
| Tg | Glass transition temperature |
| TGA | Thermogravimetric Analysis |
| THF | Tetrahydrofuran |
| TRIS | Tris(hydroxyl methyl)amino methane |
| UCST | Upper Critical Solution Temperature |
| UV/Vis | Ultraviolet/Visible Light Spectroscopy |
| WAXD | Wide Angle X-ray Diffraction |
| $W_{fb}$ | Freezing bound water fraction |
| $W_{ff}$ | Free water fraction |
| $W_{nf}$ | Non-freezing water fraction |
| wt.% | Weight percentage |
| w/v% | Weight to volume percentage |
| Z | Swelling in hexane |
| $Z_S$ | Swelling of the hexane swellable fraction in hexane (exclusively) |

_____

# Chapter 1: Introduction and objectives

## 1.1 Introduction

Hydrogels are an interesting class of materials that have been extensively researched due to their high biocompatibility.[1-3] This has made them attractive for a range of biomedical applications in the form of contact lenses, pharmaceuticals and sanitary products.[4] With continued research and development, they will likely find widespread use in drug delivery systems, wound dressings, scaffolds for tissue engineering, biosensors and catalysis.[5-7] Hydrogels are primarily characterized based on their ability to absorb large quantities of water relative to their own weight. In order for a hydrophilic material to be a hydrogel, it needs to be crosslinked in some way so that it will not undergo complete dissolution in water.[6] This has mostly been accomplished by chemical crosslinking processes, however a number of physical crosslinking processes, in which the material is held together by non-covalent interactions, have also been reported.[8,9] In this study, we have focused on developing novel hydrogel materials by crosslinking via hydrophobic interactions that arise from the introduction of a hydrophobic comonomer. These water insoluble segments bundle together and are then able to act as linkages between the polymer chains.[10] This not only provides a simpler method of crosslinking, since no further chemical treatment is required, but can also potentially be used to improve the properties of the material by selecting the appropriate type and amount of comonomer.

A basic prerequisite for this type of approach is that the copolymers need to be reasonably miscible so that a cohesive material can be formed in the film state. Without this, phase segregation can lead to a weak material that would break easily under tension or from abrasion. Secondly, it is vital that the addition of the hydrophobic component does not lead to the formation of an entirely hydrophobic material. It is also desirable that the physical crosslinks should allow dissolution in some organic solvents for the purpose of processing and analysis. This provides a decisive advantage over traditional chemically crosslinked hydrogels, and is particularly important for the purpose of producing nanofibre hydrogels, since the material needs to be soluble in order to form nanofibres via the electrospinning process.

A large number of possible monomer combinations exist that could produce such materials, and therefore we will focus on one type of hydrophobic comonomer, which will be copolymerized with a selection of hydrophilic monomers, namely 2-hydroxy ethyl methacrylate (HEMA), acrylic acid and N,N'-dimethyl acrylamide (DMAA). A methacrylate terminated poly(dimethyl siloxane) macromonomer was selected which can form graft copolymers via a routine free radical copolymerization process. Relatively few reports exist on the utilization of graft copolymer hydrogels,[11] specifically in relation to silicones, and to our knowledge, none that do not make use of conventional chemical crosslinking methods. This, in turn, implies that virtually no reports exist on the production of hydrogel nanofibres from these materials, since chemically crosslinked materials are insoluble. Nanofibres are of great interest due to their improvements in catalytic activity, drug loading capacity and release efficiency, lowered toxicity, and solvent responsiveness in comparison to hydrogel films.[12-15]

_____

In this study, the swelling behaviour of films and nanofibres made from physically crosslinked poly(N,N'-dimethyl acrylamide)-graft-poly(dimethyl siloxane) will be explored extensively, and the relationship between the silicone content and the swelling properties examined and utilized in conjunction with an array of analytical techniques to determine the morphology of the system. The crosslinking of these materials is dependent on the morphology, and it is therefore necessary to understand what effect the hydrophobic copolymer content will have on the material's final properties. Chapter 2 will focus on providing the reader with the necessary literature background to introduce all of the concepts related to the work conducted in this study. Chapter 3 contains the technical details of all the experimental procedures utilized, and in Chapter 4 the experimental results will be analysed and discussed extensively. Finally, Chapter 5 will provide a brief summary of the all the findings and provide future recommendations, including some potential applications for the novel material.
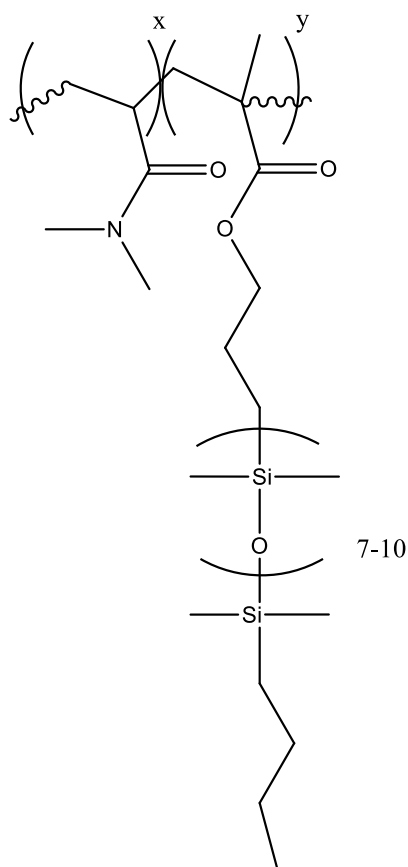


**Figure 1-1:** Structure of poly(N,N'-dimethyl acrylamide)-*graft*-poly(dimethylsiloxane)

_____

## 1.2 Objectives

The key objectives may be summarized as the following:

- To synthesize a new class of amphiphilic hydrogels, with the following basic requirements:
    - Able to undergo swelling in water and non-polar solvents (amphiphilic)
    - Biocompatible
    - Crosslinking induced by non-covalent interactions, specifically hydrophobic interactions arising from the presence of PDMS groups
    - Improved mechanical properties over that of the homopolymer
    - Soluble in organic solvents for ease of processing
    - Stimuli responsive

- Electrospinning of this material to produce nanofibre hydrogels

- Full characterization and analysis of the films and nanofibres of this material
    - Contact angles of nanofibre surfaces
    - Determination of morphology by WAXD, SEM and solid state NMR
    - Mechanical testing
    - SEC and HPLC for determination of molecular weight and composition
    - Swelling studies
    - Thermal analysis by DSC and TGA

_____

## 1.3 References

**1**   Nguyen, K. T.; West, J. L. *Biomaterials* **2002**, *23*, 4307–4314.

**2**   Bennour, S.; Louzri, F. *Adv. In Chem.* **2014**, *2014,* 10.

**3**   Micic, M.; Rogic Miladinovic, Z.; Suljovrujic, E. *Int. J. Polym. Mater. Polym. Biomater.* **2016**, *65*, 18–27.

**4**   Hoffman, A. S. *Adv. Drug Deliv. Rev.* **2012**, *64*,18–23.

**5**   Xu, J.; Qiu, M.; Ma, B.; He, C. *ACS Appl. Mater. Interfaces* **2014**, *6*, 15283–15290.

**6**   Mahdavinia, G. R.; Pourjavadi, A.; Hosseinzadeh, H.; Zohuriaan, M. J. *Eur. Polym. J.* **2004**, *40*, 1399–1407.

**7**   Zhao, Z. bai; An, S. shuang; Xie, H. jiao; Jiang, Y. *Chinese J. Polym. Sci.English Ed.* **2014**, 1*,* 173–183.

**8**   Buwalda, S. J.; Boere, K. W. M.; Dijkstra, P. J.; Feijen, J.; Vermonden, T.; Hennink, W. E. J. *Control. Release* **2014**, *190*, 254–273.

**9**   Hennink, W. E.; van Nostrum, C. F. *Adv. Drug Deliv. Rev.* **2012**, *64*, 223–236.

**10**  Niu, H.; Wang, F.; Weiss, R. A. *Macromolecules* **2015**, *48*, 645–654.

**11**  Bayley, G. M.; Mallon, P. E. *Polym.* **2012**, *53*, 5523–5539.

**12**  Maeda, S.; Kato, T.; Kogure, H.; Hosoya, N. *Appl. Phys. Lett.* **2015**, *106*, 171909.

**13**  Sundar, S. S.; Sangeetha, D. *J. Mater. Sci. Mater. Med.* **2012**, *23*, 1421–1430.

**14**  Sebe, I.; Szabó, P.; Kállai-Szabó, B.; Zelkó, R. *Int. J. Pharm.* **2015**, *494*, 516–530.

**15**  Ravikumar, R.; Peng, M. M.; Abidov, A.; Babu, C. M.; Vinodh, R.; Palanichamy, M.; Choi, E. Y.; Jang, H. *Int. J. Bio-Sci. & Bio-Tech.* **2016**, *8*, 295–306.

# Chapter 2: Literature Review

## 2.1 Introduction to hydrogels

Hydrogels are defined as hydrophilic polymers that can absorb in excess of 20% of their own weight in water, or alternatively, as three dimensional hydrophilic polymeric networks that absorb water but do not dissolve.[1,2,40,65] Common examples of synthetic hydrogels include the poly acrylamides, poly (2-hydroxy ethyl methacrylate) (PHEMA), poly(acrylic acid) (PAA), poly(ethylene glycol) (PEG) and poly(vinyl alcohol) (PVA). Many biological polymers are hydrogels, with the some prominent examples being chitosan and cellulose. Due to their high water content, hydrogel properties resemble biological tissue, thus giving them good biocompatibility. Additionally, due to the relatively soft nature of these materials, they cause little mechanical damage or irritation to surrounding biological tissue,[65] making them suitable for *in-vitro* applications. The first successful commercial use for these materials was in contact lenses, and they were later employed in drug release and delivery systems.[11] Hydrogels have been examined for use in other fields such as tissue engineering scaffolds, wound dressings, drug delivery systems, catalysis, separation, biosensors and actuators.[4,5,12,41] Significant research and commercial interest in hydrogels has led to large scale advances in this technology over the last few decades. A more detailed discussion of several key topics relating to hydrogels will follow.

### 2.1.1 Amphiphilic Cone Networks

Amphiphilic Cone Networks (APCNs) are hydrogels that swell in both polar and non-polar solvents. This is usually brought about by the presence of covalently linked hydrophilic and hydrophobic segments, i.e by the combination of a hydrogel polymer with a hydrophobic moiety.[1,3,6] As with normal hydrogels, these systems may either be physically or chemically crosslinked. A particularly useful property of such systems is their ability to simultaneously allow permeation of both oxygen and water. APCNs are more mechanically stable than pure homopolymer hydrogels, have improved biocompatibility, and swell with little to no dependence on solvent polarity.[6] Siloxanes are commonly used in the hydrophobic segment due to their biocompatibility, oxygen permeability and low surface energies.[4,6] Due to their rubber-like nature and low glass transition temperature, siloxanes  also have the added benefit of improved physical properties. Other commonly used hydrophobic segments include poly(isobutylene) (PIB), polystyrene and stearyl acrylate. When crosslinked, such systems may also be classified as Interpenetrating Polymer Networks (IPNs).[12] Because of their amphiphilic nature, these networks are of particular interest for drug delivery as they are able to transport less polar drug molecules more easily.[71] He *et al.*[3] showed simultaneous swelling of PEG-conet-PDMS systems in water and n-heptane; interestingly the simultaneous and separate swelling studies yielded similar results, indicating that the hydrophobic/hydrophilic domains were well separated. Kali *et al.*[6] synthesized thermally responsive PNIPAAM-co-PIB networks, and tracked their thermal response and swelling behaviour as a function of composition. It was found that at a 50/50 composition, the gels could swell to approximately equal amounts in both water and n-hexane. The networks exhibited two glass transition temperatures that differed from those of the hompolymers, indicating that the two

polymers were not miscible. Xu *et al.*[4] synthesized a PNIPAM-co-siloxane APCN with controlled pore sizes by means of ATRP chemistry. Because of the finely controlled microstructure, the material had greatly improved oxygen permeability and physical properties, while maintaining high water uptake and good biocompatibility.

## 2.1.2 Crosslinking in hydrogels

Since most pure hydrogel polymers will disperse or dissolve in water, these materials necessarily have to be crosslinked. When bound together by chemical crosslinks, they are referred to as 'chemical' or 'permanent' hydrogels.[1] Alternatively, hydrogels may be termed 'reversible' or 'physical' when they are not covalently crosslinked, but are held together instead by other non-covalent interactions. The crosslinking density of a hydrogel system is a key parameter that governs a number of structural characteristics,[69] as increasing the crosslinking density will result in an overall reduction in the equilibrium swelling and drug diffusivity of the gels.[54,70]

A large number of reported chemical crosslinking processes exist, with some commonly applied examples being the addition of agents such N,N'-methylenebisacrylamide (BIS) and gluteraldehyde, or the formation of siloxane crosslinks (in APCNs) using compounds such as Kerstadt's catalyst to facilitate hydrosilation reactions.[4,11] Figure 2-1 illustrates the effect of gluteraldehyde as a crosslinker with poly(acrylamide). Other methods include the use of click chemistry, photo crosslinking, condensation/addition reactions and even enzymatic crosslinking.[13] Chemical crosslinking is often preferred, since physically crosslinked hydrogel systems often lack mechanical strength. However, this approach frequently requires the use of toxic compounds or harsh reaction conditions,[64] potentially making the materials unsuitable for biological applications. The use of enzymes and other biomolecules for crosslinking is one possible alternative that can be used to negate this issue. In thermoresponsive gels, chemical crosslinking can significantly retard the response time of the gels due to collective diffusion of the polymer network and osmosis of the solvent molecules.[7] A gelation period is generally required to allow for crosslinking to occur. In this regard, the use of physically crosslinked networks is advantageous, since no additional reactions are required to facilitate network formation, therefore eliminating the need for a gelation period. Combined approaches, utilizing physical crosslinking for initial network formation, followed by an *in-situ* gelling reaction, have also been explored.[67]
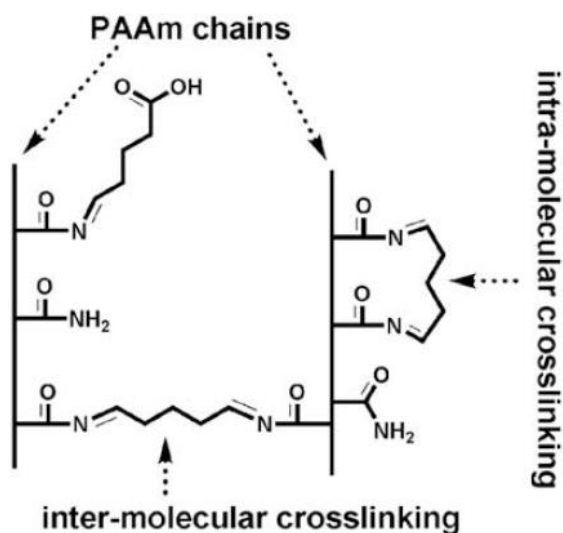
**Figure 2-1:** Intra- and inter molecular crosslinks formed by the addition of glutaraldehyde to poly(acrylamide).[35]

Physical crosslinking may be accomplished through the use of ionic groups, bundling of hydrophobic domains (i.e in graft or block copolymer APCN systems containing hydrophobic segments), hydrogen bonding in systems such as PAA blended with PEG, stereo complex formation in mixed enantiomeric systems of D- and L-lactic acid, and via crystallization in systems of PVA.[11,13] Interestingly, ionic crosslinking may even take place in some hydrogels lacking ionic side groups, such as dextran upon the addition of potassium ions.[68] A related molecule, cyclodextrin, possesses a hydrophobic cavity that can be used to accommodate other hydrophobic molecules. The addition of a polymer that is able to "thread through" the cyclodextrin can thus be used to produce a supermolecular hydrogel.[66]

As illustrated in Figure 2-2, segregation of the hydrophilic and hydrophobic segments of a block copolymer can lead to the formation of hydrophobic domains. Since this area is insoluble in water, it will not dissociate, thereby acting as a physical crosslink. In our study, this type of crosslinking is induced by hydrophobic poly(dimethyl siloxane) side chains in the graft copolymers.

_____
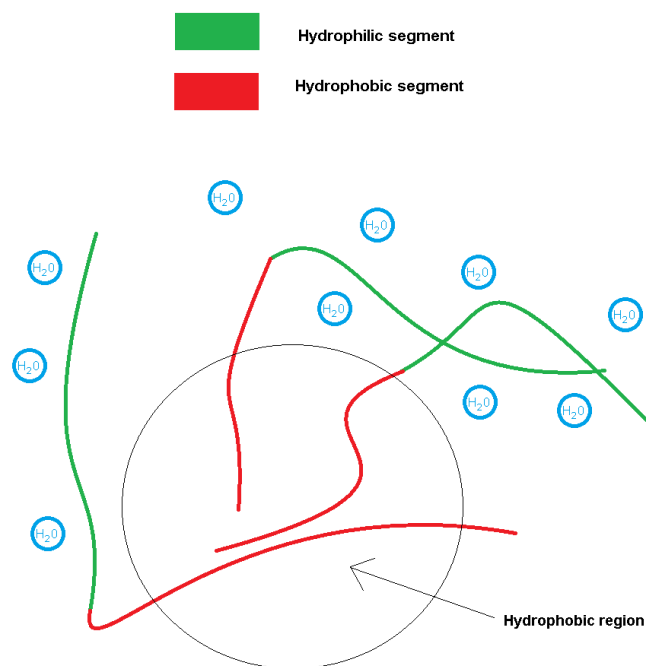


**Figure 2-2:** Physical crosslinking in an amphiphilic block copolymer induced by the clustering of hydrophobic segments.

## 2.1.3 Water structure in hydrogels

Studies have shown that the internal water structure in hydrogels may have a significant impact on the biocompatibility of such materials.[14-16,19] The water content of hydrogel systems is directly related to the drug loading capacity,[17] thus making the overall equilibrium swelling ratio and relative amounts of each type of imbibed water important parameters in the development of biomedical hydrogels.

The water contained within hydrogels can be classified according to sets of criteria, based on either the mobility or the thermal behaviour.  *Primary bound* water refers to the water that is immobile and bound directly with hydrophilic moiety, *secondary bound* water is the fraction that is bound by the hydrophobic components of the gel, and *free water* is additional water imbibed by osmosis as the system tends toward infinite dilution. Figure 2-3 illustrates the position of these water fractions around the polymer chains. If the polymer is crosslinked, this osmotic swelling will be counteracted by the network until an equilibrium swelling is achieved. The amount of water contained within the gel at this point is referred to as the Equillibrium Water Content (EWC). At the EWC, no further water uptake is possible without breaking the crosslinks. For the purposes of thermal analysis of swollen hydrogels, the water may, alternatively, be classified as *non-freezing water*, *freezing bound water*, and *free water*.[1,14,16,19,29] These fractions correlate to the aforementioned categories, but are defined differently. Non-freezing water, as the name implies, has been shown to remain unfrozen at temperatures of -100˚C.[14,29] Freezing bound water remains in close proximity to the non-freezing water, but does not undergo strong hydrogen bonding to the monomer, and consequently is still able to form ice crystals.
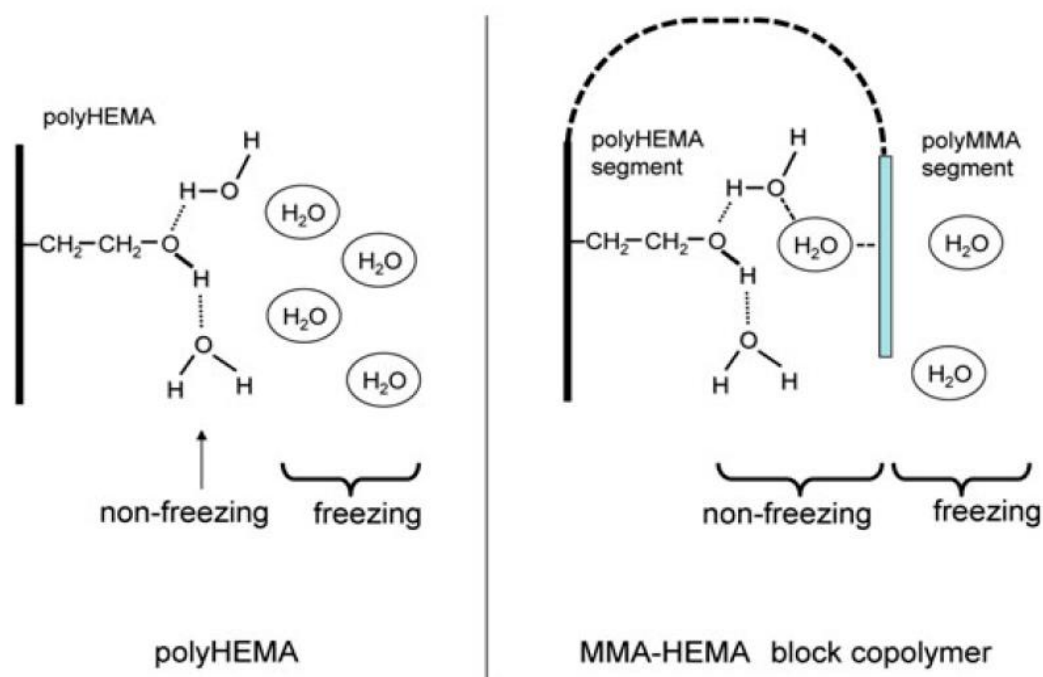
**Figure 2-3:** Schematic of freezing and non-freezing water fractions in a hydrogel.[15]

As the water content in a hydrogel is decreased, the average strength of the hydrogen bonds will increase, since a larger portion of the remaining water is directly bound to the hydrophilic moiety. Consequently, the melting point of water in a hydrogel may shift based on the water content of the gel, since the hydrogen bonding effects will inhibit freezing and melting of the freezing bound water. The polymer species itself has a significant effect on the freezing and melting point suppression of imbibed water,[28,29] as indicated by the presence of multiple peaks in the thermograms of gels containing significant fractions of free water and freezing bound water.[32] It follows that polymers that are able to undergo strong hydrogen bonding to water will show larger shifts in the melting point of their imbibed water, compared to that of pure water or free water, in comparison to species exhibiting weak hydrogen bonding.

At equilibrium swelling, primary, secondary and free water all exist within the hydrogel. As the gel is dehydrated, free water is lost first, followed by the secondary bound water and finally the primary bound water. As the secondary water is lost, the physical properties of the hydrogel change from gel-like to glassy.[28] Conversely, during hydration of dry gels, the initially absorbed water is primary bound or non-freezing water, with freezing-bound or secondary water and free water only being observed at higher levels of saturation. The fraction of non-freezing water can be determined from calorimetric calculations based on the enthalpies of melting and freezing of pure water, if the water content of the gel is known:

$$w_c = w_{fb} + w_{nf} + w_f \tag{2-1}$$

_____

Where $w_c$ is the water content of the swollen hydrogel, $w_{fb}$ is the freezing bound water, $w_{nf}$ is the non-freezing water, and $w_f$ is the free water.[16] The combined free water and freezing bound water fractions can be determined from:

$$Wfb + Wf = \frac{\Delta H_m}{\Delta H} \qquad \text{or} \qquad 1 - Wnf = \frac{\Delta H_m}{\Delta H} \qquad (2\text{-}2)$$

Where $\Delta H$ is the enthalpy of fusion for water and $\Delta H_m$ is the measured enthalpy of freezing within the sample. Distinguishing the freezing bound and free water fractions is not possible in all cases, although overlapping freezing peaks are sometimes observed, with the free water undergoing its melt transition closest to that of pure bulk water.[32] In this case, the relative fractions may be determined by peak deconvolution.

A notable phenomenon in some systems is the cold crystallization of imbibed water that occurs due to the transition of amorphous ice to crystalline ice upon re-heating of the system, as illustrated by simultaneous DSC-WAXD studies.[15] This event is attributed to the freezing bound water and often occurs at or near the glass transition temperature of the polymer system.

With the introduction of chemical heterogeneities into a hydrogel system, the average number of affixed water molecules per monomer unit provides insights into the hydrogel's behaviour. The average number of water molecules per monomer unit can be calculated using the equation:

$$n = \frac{M}{18}\left[Q\left(f_H - \frac{\Delta H_m}{\Delta H}\right)\right] \qquad (2\text{-}3)$$

$$\text{Where} \quad f_H = \frac{Q-1}{Q} \qquad \text{and} \qquad Q = \frac{W_S}{W_D} \qquad (2\text{-}4)$$

Where $n$ is the average number of water molecules, $M$ is the molecular weight of the repeat unit, $\Delta H$ is the enthalpy of fusion for water, $\Delta H_m$ is the measured enthalpy of freezing within the sample, $W_s$ is the weight of the swollen sample and $W_D$ is the weight of the dry sample.[32] The enthalpy of fusion may be determined by DSC analysis on swollen samples.

Another important variable in crosslinked polymer networks is the crosslink density, which may be calculated from the Mooney-Rivlin or Flory Rhehner methods. In the Flory Rhehner equation:

$$-\left[\ln\left(1 - v_p\right) + v_p + \chi v_p^2\right] = NV_S\left[v_p^{\frac{1}{3}} - \frac{v_p}{2}\right] \qquad (2\text{-}5)$$

$N$ is the crosslinking density (mol.m$^{-3}$), $\chi$ is the polymer solvent interaction parameter, $v_p$ is the volume fraction of the polymer in the swollen gel, and $V_S$ is the molar volume of the solvent. The equation

_____

provides a correlation between the degree of swelling and the crosslink density, with the implication that networks with large numbers of crosslinks will undergo less swelling due to these constraints on the network structure. This method has been noted to provide larger values than that of the Mooney-Rivlin equation, and this is believed to be because the Flory-Rhehner equation also accounts for some of the physical crosslinks formed between chains from entanglements.[33] In cases where $\chi$ is less than 0.5, the polymer system is considered to be water soluble, and in cases where it is above 0.5, the system will swell but not dissolve.

## 2.1.4 "Smart" hydrogels

Hydrogel systems that are able to react to external stimuli, such as changes in pH, temperature, light or electrical stimuli etc. are classified as stimuli-responsive or "smart" hydrogels.[10,17] Such systems undergo conformational changes and/or substantial alteration of their physical properties in response to changes in their environment. Thermoresponsive systems have garnered the most attention due to the importance of temperature in biomedical systems.[41]

Poly(N-isopropyl acrylamide) (PNIPAAM) has been extensively studied due to its unique thermo sensitive behaviour, as it undergoes a phase transition at its lower critical solution temperature (LCST) of around 32˚C, at which point it will transition from hydrophilic to hydrophobic behaviour.[6,7] Figure 2-4 illustrates this process. This occurs due to a balance between the hydrophilic amide group and the hydrophobic isopropyl segment. At the LCST, the hydrophobic interactions of the isopropyl group become stronger than the hydrophilic interactions from the amide, leading to a sudden transition from hydrophilicity to hydrophobicity.[8] Consequently, the polymer will undergo a volume phase transition as the imbibed water is expelled.

This behaviour is potentially useful in drug delivery systems, since the LCST temperature of PNIPAAM is between room temperature and that of the human body.[11] Copolymerization with other monomers may be used to alter the LCST in PNIPAAM, or to tweak the thermal response.[8,9] Poly(dimethyl acrylamide) (PDMAA) is a related acrylamide monomer with similar biocompatibility and swelling behaviour, however it does not show the LCST phenomenon found in PNIPAAM. Recently, Ida *et al.*[8] showed how copolymerization of PDMAA with a series of more hydrophobic acrylamide monomers could induce thermal responsiveness similar to that of PNIPAAM. Micic *et al.*[41] synthesized a library of poly(oligo(propylene glycol)methacrylate)-co-(hydroxy ethyl methacrylate) polymers utilizing gamma radiation, and successfully tuned the volume phase transition temperatures by varying the composition.

Pastoriza *et al.*[21] synthesized macroporous solvent responsive PDMAA, showing sharp volume phase transitions when exposed to organic solvents such as dioxane and acetone. A pH responsive hydrogel, composed of chitosan grafted with crosslinked poly acrylamides and poly(acrylic acid), was designed by Mahdavinia *et al.*[22] The presence or absence of aqeous salts could be used to control the swelling response in a reversible manner, due to the presence of cations blocking the hydrophilic

_____

sites of the acrylic acetate group formed from the alkaline hydrolysis of acrylic acid. Saha *et al.*[10] illustrated the use of an electrically conductive hydrogel system in which drug release from a poly(acrylamide-co-pyrrole) hydrogel could be actualized by the application of an electrical field. Haider *et al.*[17] showed the successful synthesis of mechanically tough acrylamide hydrogels loaded with magnetic nanoparticles, and illustrated their potential as an actuator for soft robotics.
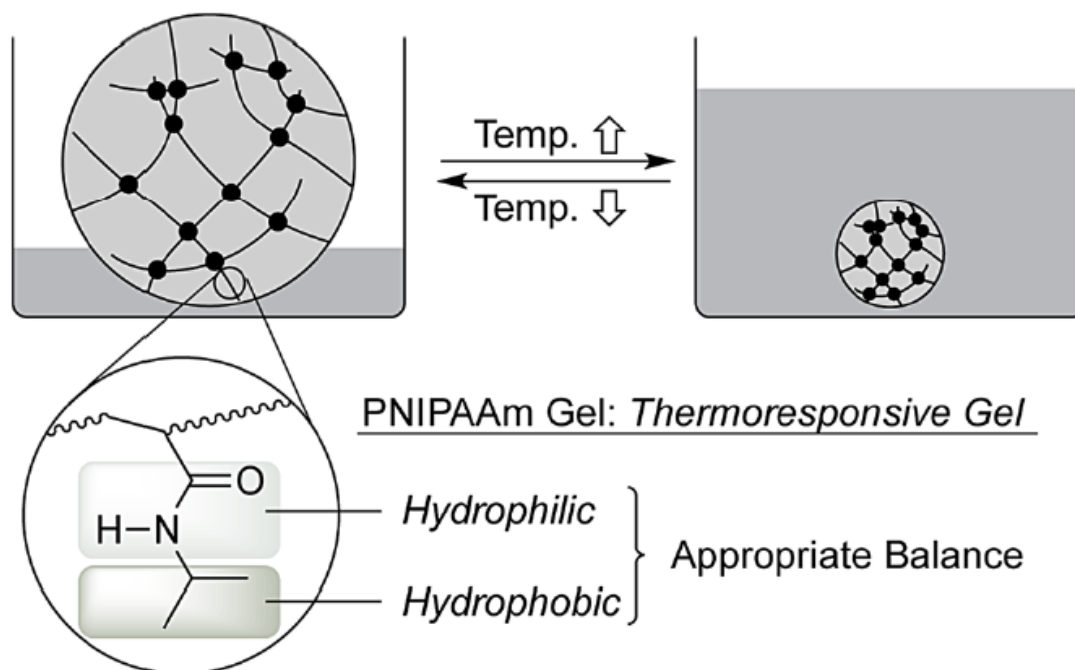


**Figure 2-4:** Thermoresponsive behaviour in PNIPAAM.[8]

---

## 2.1.5 Nanofibre hydrogels

With the rising interest in electrospinning and other nanofibre techniques, hydrogel nanofibres have been developed and studied in recent years.[7,23-25] Due to their high surface to volume ratios, such materials are able to swell more rapidly since solvent saturation of the fibres occurs far more quickly than in the bulk materials; this also allows for faster response times in stimuli-sensitive materials. Maeda et al.[7] synthesized porous PNIPAAM nanofibres which showed thermal response times up to 100 times more rapidly than normal gels. The porous structure further enhances the surface to volume ratio of the fibres, allowing for significant improvement over the typical response times of crosslinked systems. Nanofibre hydrogels have also been shown to have lower toxicity and improved ease of use and therapeutic effects.[24] Okuzaki et al.[23] synthesized poly(NIPAAM-co-stearyl acrylate) nanofibre mats which remained stable in water due to the presence of physical crosslinking by the aliphatic chains, and showed rapid thermal response around the LCST temperature. Through use of Atomic Force Microscopy (AFM) in a temperature controlled solution cell, the behaviour of an individual nanofibre could be observed. The high surface to volume ratios also allow for improved drug loading capacity and efficiency of release. Sundar et al.[24] studied the drug release kinetics of PNIPAAM-chitosan nanofibre hydrogels and found that both the pH and the drug loading affected the release kinetics. Kim et al.[25] synthesized temperature responsive nanofibres with a switchable "on-off" drug release response. The fibres were produced from a physically crosslinked copolymer of NIPAAM and N-hydroxymethylacrylamide (NHMAam), and loaded by blending fluorescein isothiocyanate (FITC)-dextran into the electrospinning mixture. Subsequent heating and cooling cycles trigger the release of the drug into a buffered saline medium. Kim et al.[39] illustrated the simultaneous crosslinking and polymerization of PHEMA hydrogels. This was accomplished via the formation of oligomers prior to the electrospinning process, during which the fibres were exposed to strong UV radiation to complete the polymerization and simultaneously induce crosslinking through the added ethylene glycol dimethacrylate (EGDMA) crosslinker.

One challenge in the production of nanofibre hydrogels is that crosslinked hydrogels are generally insoluble, and as such they cannot be electrospun. This issue is commonly circumvented by conducting the crosslinking process after fibre formation, often by the use of agents such as glutaraldehyde.  In the study by Maeda et al.[7], β-cyclodextrin was added to the electrospinning mixture as a thermal crosslinker, and the fibres subsequently crosslinked by thermal curing. In the study by Lu and Husieh,[35] fibres were crosslinked by immersion in an ethanol glutaraldehyde mixture, and thermally cured before washing with ethanol and water to remove byproducts from the reaction. In some cases, the hydrogel fibres may be too soluble in the glutaraldehyde solutions, and crosslinking through the use of glutaraldehyde vapours may be necessary instead. Alternatively, thermally- or UV activated crosslinkers may be added to the electrospinning mixture and the fibres subsequently crosslinked by heating or irradiation.[39]

## 2.1.6 N,N'-dimethyl acrylamide – poly(dimethyl siloxane) grafts as a system of interest

Although somewhat similar to PNIPAAM, PDMAA has been less extensively studied as it does not exhibit a LCST, even when heated to above 200°C.[53] However, it remains an interesting monomer due to its low cost, high biocompatibility and resistance to oxidative degradation in physiological applications, where it has been examined as a replacement for PEG.[18,50]

Because PDMAA is less hydrophobic than PNIPAAM, it does not show a LCST phenomenon since the hydrophobic interactions need to become dominant for a transition to occur. However, the copolymerization with hydrophobic monomers has been previously shown to induce the LCST phenomenon, where Ida et al.[8] showed such behaviour in PDMAA-co-PIB hydrogels by regulating the amount of added hydrophobic monomer to produce a tuneable thermal response.

Although there are numerous studies on various crosslinked networks of PDMAA,[8,18,20,29,50,60] there are far fewer publications regarding physical crosslinking in PDMAA gels,[61] and none to our knowledge specifically on the use of grafted siloxanes as physical crosslinker. Erdodi and Kennedy[50] synthesized amphiphilic cone networks of PDMAA grafted with PDMS, which were then crosslinked through the use of Kerstadt's catalyst and the addition of hydrosilanes. In another study, Kwon et al.[56] prepared DMAA and HEMA hydrogels containing TRIS, α- and α,ω-methacrylate siloxanes, with EGDMA as added crosslinker.  Pavlovic et al.[52] synthesized multi block copolymers of PDMAA and PDMS by utilizing raft polymerization techniques, however they did not address the potential formation of physical crosslinks or study the swelling of these compounds in water, noting however that the synthesized polymers were highly amphiphilic and dissolved in a range of solvents. Yamamoto et al.[20] prepared PDMAA-co-PDMS cone networks by radical copolymerization of the DMAA monomer with telechelic acrylate terminated PDMS (~ 6500 g/mol). The resultant networks were thus crosslinked by the inclusion of the acrylate PDMS chain ends bridging the polymer chains. TEM images of the resultant polymer showed a periodic, bicontinuous structure. Hodorog et al.[55] prepared polysiloxanes grafted with NIPAAM and DMAA through the use of controlled living radical polymerization, however their study focused primarily on the rheological behaviour of the prepared polymers and no swelling studies indicative of the presence of physical crosslinks were presented. Niu et al.[61] synthesized triblock copolymers of DMAA with poly(2-(N-ethylperfluorooctanesulfonamido) ethylmethyl acrylate) via RAFT mediated polymerization which showcased pure physical crosslinking, swelling on average to around 200%.

_____

## 2.2 Electrospinning

Electrospinning is a facile and widely used technique for the production of polymer fibres with diameters ranging from tens of nanometers to several microns. The process was first patented in 1934, but only found widespread popularity in the 1990's when it was shown that a wide variety of polymers could be electrospun using this method.[34,47] Electrospun fibre mats have found application in tissue scaffolds, filtration, drug delivery, wound dressings, catalysis, artificial blood vessels, nanocomposites and the general production of non-woven textiles.[25,26,34] Fibres produced by this method show higher mechanical strength, flexibility and larger surface to volume ratios than fibres produced by conventional methods.[45,47] Though electrospinning is widely studied throughout literature, it is not the only technique available for the formation of nanofibres, but is often preferred for academic use due to its relatively low cost and ease of use.[38,46]

The electrospinning process is illustrated in Figure 2-5. A polymer solution is typically extruded through a capillary or a needle, placed opposite a collector plate. A large voltage is then applied to both the solution and the collector plate. As charged ions are formed in the solution due to the electric field, the internal charge repulsion counteracts the solution's surface tension, forming a hemispherical tip known as a Taylor cone.[26,44] With a sufficiently strong electric field, the solution will be ejected from the Taylor cone and undergo rapid elongation and drying as it travels toward the collector plate which is oppositely charged. If the polymer chains are of sufficient molecular weight such that entanglement occurs, fibres are formed in the process, leading to a randomly oriented fibre mat.[26,27,47] In the absence of sufficient entanglement, fine droplets of the solution will be ejected in a process known as electrospraying.[48] As the jet travels from the Taylor cone to the collector plate, the internal charge densities increase due to the decrease in fibre diameters caused by both the stretching of the fibres and the evaporation of the solvent. Ultimately, this will split the jet into smaller jets carrying some sideways velocity. This process is called splaying, and will often occur numerous times, thus leading to the formation of small diameter fibres.[26,44,47] This process is thought to be the main reason for very small diameters of fibres obtainable from electrospinning.[44] However, this process does not occur in all cases, and is largely affected by the experimental parameters employed. The fibres do not travel in a straight line, but rather in a spiral
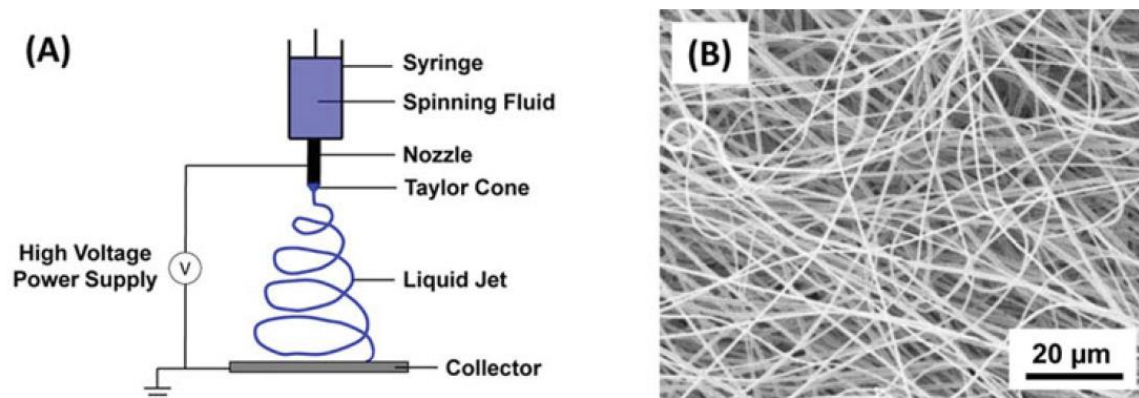
**Figure 2-5:** Schematic of an electrospinning setup (A) and (B) SEM image of electrospun nanofibres.[38]

formation as shown in Figure 2-5, undergoing whipping and stretching as they travel.[47]

Several configurations of electrospinning setups exist, with the vertical (Figure 2-5) and horizontally aligned setups most commonly employed. Additionally, setups that make use of ball spinnerets and revolving drums that act as collector plates also exist.[44,47] In the revolving drum set up, the fibres are aligned due to the rotation of the drum.[47] Co-axial setups, where two polymers are spun simultaneously to produce fibres with chemically distinct core and sheath arrangements, have also been explored in recent years.[25,42,46]

## 2.2.1 Variables in the electrospinning process

A large number of variables affect the electrospinning process, including but not limited to: the molecular weight, type and structure of the polymer, viscoelasticity, conductivity and concentration of the solution, the applied voltage of the electrical field, the distance between the solution tip and the collector, the solution feed rate, as well as the temperature and atmospheric humidity.[26,44,47] A brief discussion of these parameters and their effect on the process is given below.

### 2.2.1.1 Solution viscosity effects

The solvent type, and subsequently the solvent interaction parameters, will determine the overall solution viscosity and surface tension of the solution, in addition to the molecular weight, concentration and architecture of the molecules in question.[44] Higher molecular weight polymers will lead to increased solution viscosity, whereas branched systems will have a lower solution viscosity at the same concentration and molecular weight than their linear counter parts.[30,31] Altering the overall solution viscosity will change the amount of energy required to overcome the surface tension. If the solution viscosity is too low, droplets are formed and electrospraying is likely to occur. Conversely, at high solution viscosity the electrostatic repulsion may not be sufficient to overcome the surface tension and flow instabilities are likely to occur.[47] Generally, at higher viscosity higher voltages are required to initiate the electrospinning process.[44] Between these extremes, increased solution viscosity will generally lead to increases in the fibre diameters.[47] Solution volatility needs to be

selected for optimal drying rates of the fibres in flight. Wet fibres on the collector plate may undergo amalgamation and collapse to form film like structures rather than fibres. Rapid drying of fibres, however, may lead to fibre breakage as they lose most of their elasticity and ability to stretch during the drying process.

### 2.2.1.2 Applied voltage and solution conductivity

Typical electrospinning voltages vary between 5 – 20 kV. Higher voltages lead to increased electrostatic repulsion between both the polymer and solvent molecules. At very high voltage, electrospray is likely to occur, and conversely at low voltage the electrostatic repulsion may not be sufficient to overcome the surface tension of the solution and induce fibre formation. An increase in applied voltage may lead to larger fibre diameters due to the more rapid evaporation of solvent. An increase in the amount of beading with increasing voltage has been reported, and this effect should be considered when conducting electrospinning at high voltage since it may lead to the formation of undesirable morphologies.[47,48]

The overall conductivity of the polymer and the solvent will greatly affect the fibre diameters and required voltage. Highly non-conductive solutions such as toluene are unlikely to allow electrospinning to occur, usually requiring a co-solvent to improve the solution conductivity. Solvent systems such as DMF/chloroform are often employed due to its ability to solvate both polar and non-polar molecules while maintaining good conductivity due to DMF's relatively high dielectric constant.

The addition of electrically conductive additives to the mixture, for instance carbon nanotubes or silver nano particles, will greatly alter the solution conductivity and may even change the overall conditions required for fibre formation entirely. In solvents with low conductivity, this behaviour can be exploited to improve the solution conductivity.[47]

### 2.2.1.3 Tip to collector distance, solution flow rate, ambient conditions

Ideally, the flow rate of the solution into the capillary should be matched to the rate at which the solution is ejected from the capillary tip by the electrical field. Non-optimal flow rates will lead to the formation of polymer beads as the excess solution is ejected toward the collector plate, whereas slower flow rates will result in short bursts of fibres rather than a stable continuous spinning process. It should be noted that the electrical current itself will affect the rate of fibre formation, with high voltage, and consequently high current, increasing the rate of mass transfer.[47]

A longer tip to collector distance, provided the electrical field is sufficient, will generally lead to smaller fibre diameters because the polymer jet undergoes more whipping and elongation. A non-linear decrease in diameter is encountered with increasing tip to collector distance.[26] This effect is counter balanced to some extent by the rate of drying of the fibres, since very little further elongation can occur once the fibres have dried. The atmospheric humidity and temperature will also play a role in this process, with high temperatures and low humidity leading to more rapid solvent evaporation, ultimately resulting in thicker fibres. Fast solvent evaporation also leads to reduced viscoelasticity of the polymer jet, thereby slowing the overall mass transfer velocity.[26] Generally, electrospinning should be conducted in a low humidity environment to prevent undesirable amalgamation and build up of fibre webs on the collector plate.

## 2.2.2 Common problems in the electrospinning process

Due to its relatively low throughput, single needle electrospinning is not ideal for large scale fibre production, and has primarily been limited to use in academic settings, although some industrial scale electrospinning systems are in use. [38,44,47]

Dissolving the polymer of interest in an appropriate solvent may not be feasible in all cases, such as in the case of highly non-polar polymers that may not dissolve in conductive solvents. Chemically crosslinked polymers cannot be electrospun because they are, by nature, insoluble.

Figure 2-6 shows the formation of polymer beads and the relatively uneven fibre diameter distribution caused by the splaying process, which remains problematic. In some cases, porous structures may arise, which can lead to weak fibres. Polymer samples with large dispersities can lead to beading as some of the chain lengths in the sample may fall below the minimum molecular weight.
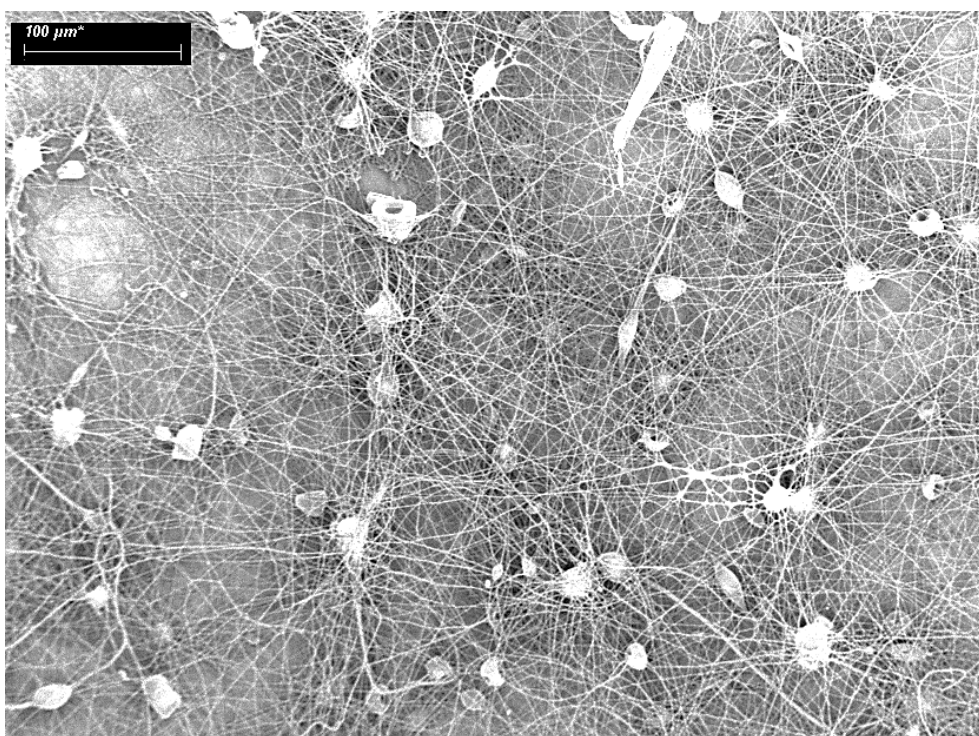


**Figure 2-6:** SEM micrograph (from the present study) of a PDMAA-graft-PDMS fibre mat produced under non-optimal conditions showing beading.

_____

## 2.3 Graft copolymers

Graft copolymers consist of a polymer backbone with numerous side chains. These side chains are usually, but not always, chemically distinct from the polymer backbone. Due to this branched topology, graft copolymer properties differ from that of linear polymers, and they generally have lower solution and melt viscosities than linear polymers of the same molecular weight.[30,31] As with block copolymers, they may undergo self assembly in solution and form ordered morphologies, although the nature of this behaviour has been much less extensively researched in comparison to block copolymers. This will be discussed further in Section 2.3.2.

### 2.3.1 Graft copolymer synthesis

Graft copolymers can be synthesized by a variety of polymerization methods, including anionic, RAFT, ATRP, SET-LRP and free radical polymerization.[36] Several strategies exist for the assembly of graft copolymers, namely grafting onto, grafting from and grafting through.[30,31,36,37] These are presented schematically in Figure 2-7.
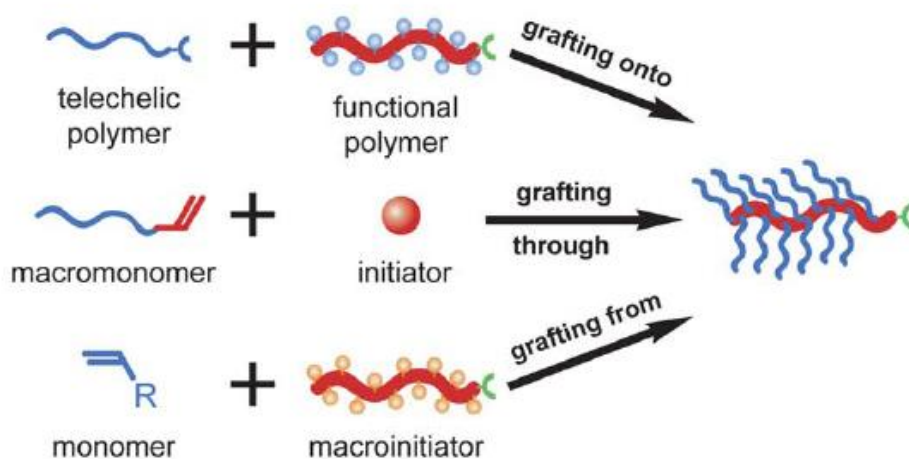


**Figure 2-7:** Graft copolymer synthesis strategies.[30]

_____

### 2.3.1.1 Grafting onto

In this process, the backbone and pendant chains are prepared separately and then coupled to form the graft polymer. Side chains are attached to a backbone structure via coupling reactions, such as esterifications, hydrosilation or the use of click-chemistry. This method has the advantage that both segments can be synthesized separately to form well defined grafts, however the coupling reactions of macromolecular molecules tends to occur more slowly. Additionally, lower coupling efficiency is encountered with this method.[36,37] Due to steric effects, the attainable graft densities in such systems is also lower.

### 2.3.1.2 Grafting from

In the grafting from strategy, a polymer backbone that is able to act as an initiator at various points is synthesized first, and monomers are added to grow the pendant groups from the backbone. This strategy has become increasingly popular with the improvements made in the field of controlled radical polymerization, particularly ATRP. Generally, the initiator is formed via a reaction with the pendant groups of the homopolymer chain first and the new polymer chains subsequently initiated from these groups. Because the side chains are grown *in-situ*, steric effects such as those encountered in the grafting onto strategy are less prominent and allow for greater obtainable side chain densities.[30] However, a general issue with this method is the formation of homopolymers from the added monomers, which can weaken the physical properties of the formed graft polymer. Pure grafts with well controlled structures can only be formed by this method if the starting polymer is well defined, and the subsequent grafting reaction proceeds to completion. [31]

### 2.3.1.3 Grafting through

In this methodology, pendant group chains having a polymerizable end group are first prepared. The macromoners may be polymerized directly with each other by addition of an initiator, or other monomers may be added to form the backbone and copolymerize with the macromonomer, resulting in a graft copolymer. Advantages of this method include good control of the side chain lengths (since they are presynthesised to the desired length) and the ability to form relatively dense grafts. However, grafts prepared in this manner tend to have relatively broad chain length distributions and lower molecular weight. Both the "grafting through" and "-from" methods have an inherent draw back due to the high likelihood of homopolymer formation, leading to poor physical properties.[31] Fractionation of such polymers may be required to obtain chemically homogenous fractions. Differences in reactivity ratios of the monomers, as well as the initial monomers concentrations, need to be taken into account in order to prepare well distributed grafts by this method. The monomer with a higher reactivity ratio is likely to undergo some degree of homopolymerization, until a sufficient amount is consumed, before inclusion of the second monomer will begin to occur in larger amounts. This may lead to enrichment in the chain ends in one type of monomer. Other factors that need to be considered are diffusion effects due to macromonomer's size relative to that of the other monomer(s). Repulsion between monomers and the growing polymer chains may lead to undesirable reaction kinetics, as in the case of

combinations of moieties that are thermodynamically incompatible,[43] such as strongly polar and non-polar mixtures.

## 2.3.2 Self assembly and morphology of graft copolymers

The self assembly of block copolymers is a well known phenomenon. A variety of possible configurations for such polymers exist in solution, including spheres, rods, vesicles and lamellae.[34,57,58] When a polymer containing two chemically distinct segments is subjected to a solvent or environment which only interacts favourably with one segment, the molecule will undergo a change in conformation so as to minimize the number of unfavourable interactions. For instance, if block A consists of a hydrophilic monomer and block B consists of a hydrophobic monomer, the chains may self assemble in aqeous media so as to segregate the B block toward the interior, away from contact with the solvent. This results in the formation of various ordered nanoscale structures. This behaviour is common in amphiphilic copolymers, but can occur with any immiscible combination of blocks or segments along the polymer chain. The formation of these structures can be controlled by altering the relative length of each block, altering the solvent composition, or by the addition of additives.[57,58] Figure 2-8 illustrates the variables of the critical packing parameter ($p$), which can be used to predict the morphology in amphiphilic blocks:

$$p = \frac{v}{a_0 l_c}$$
(2-6)

Where $v$ is the volume of the hydrocarbon chains, $a_0$ is the optimal area of the hydrophilic head, and and $l_c$ is the critical chain length of the hydrophobic group.[72] Values of around 1/3 result in spherical micelles; between ½ to 1/3 result in cylinders, and for values between ½ and 1, bilayers and vesicles are formed.[57,72] Various more complex morphologies are also possible.

In graft copolymers, this behaviour is more complex since the graft densities and distribution are additional variables that have a significant impact on the types of structures formed. Unlike block copolymers, the morphologies cannot be readily predicted from simple equations. However, the morphology of graft copolymers is often approximated by extrapolation from block copolymer behaviour.

_____
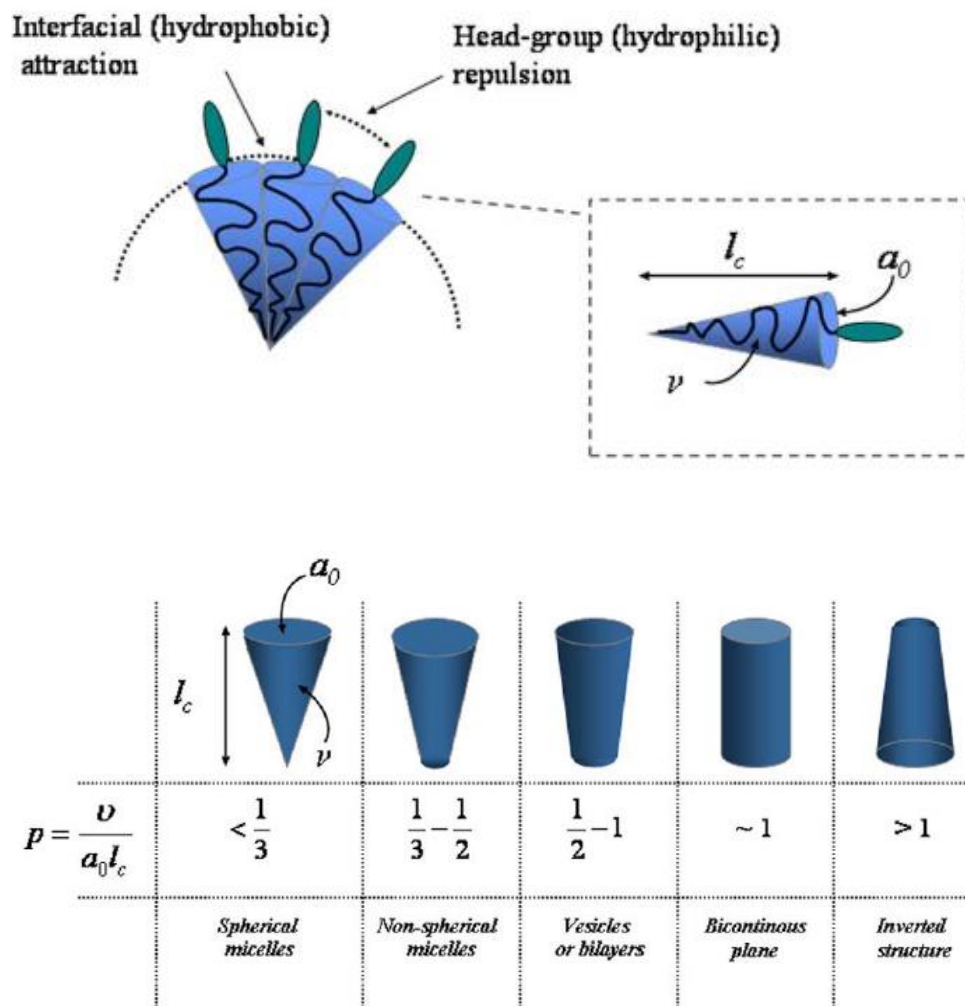


**Figure 2-8:** Schematic representation of the variables in the critical packing parameter equation, and the resultant arrangement for various values of packing parameter for block copolymers.[72]

## 2.3.2.1 Self assembly of grafts in solution

Figure 2-9 shows the possible conformations of a graft copolymer in solution with a low, even graft density. As the solvent quality is gradually altered from neutral toward favouring only the backbone (Line B, region 2), a string of "flower" like micelles is formed as a single polymer chain undergoes coiling to segregate the grafts toward the interior. As this process continues, the number of flowers decreases until each chain forms a single micelle.[59] In the opposing scenario (Line A, region 1), where the solvent favours the grafts but not the backbone, coils of chains are first encountered which gradually transition to cylindrical micelles, and eventually form spheres where the backbone is segregated toward the interior. Figure 2-10 shows how increasing the graft density, while maintaining a constant solvent composition, leads to smaller micelles in solution when the solvent favours the backbone.[62,63] It is also found that when the solvent favours the graft, and the graft density is increased across a series, less aggregation of micelles occurs.[63] In most models, the graft density is assumed to be homogenous throughout the chain, but this is unlikely to occur in practice. As outlined in Section 2.3.1.3, enrichment of the chain ends in one monomer relative to the other can occur due to differences in reactivity; this may potentially form chains that are "block-like", with highly asymmetrical structures.
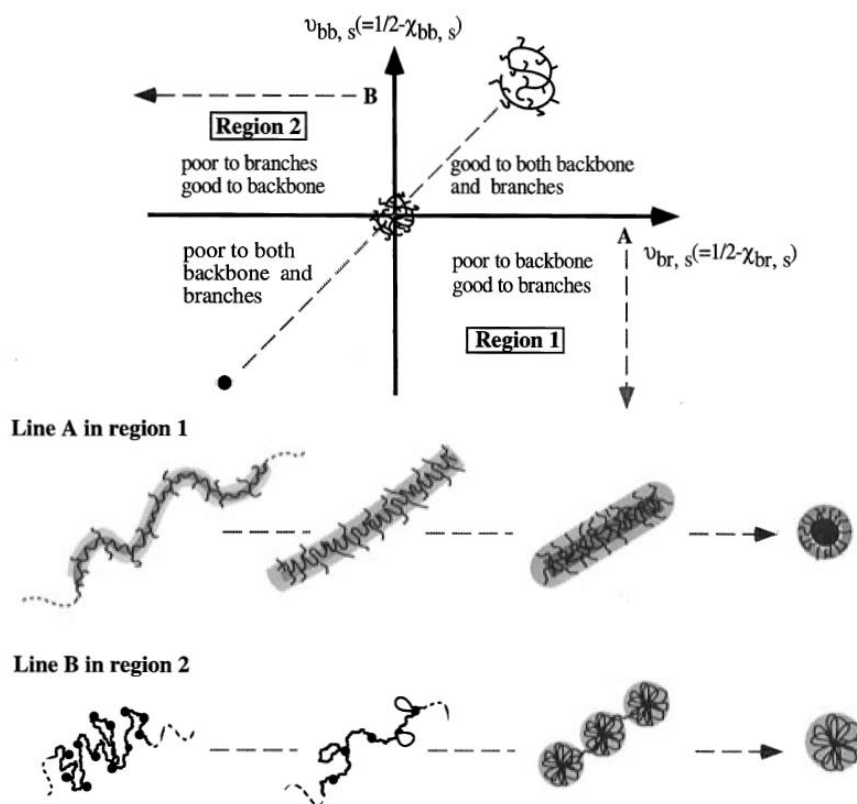


**Figure 2-9:** Possible self assembled structures in graft copolymers having low graft densities.[59]

_____
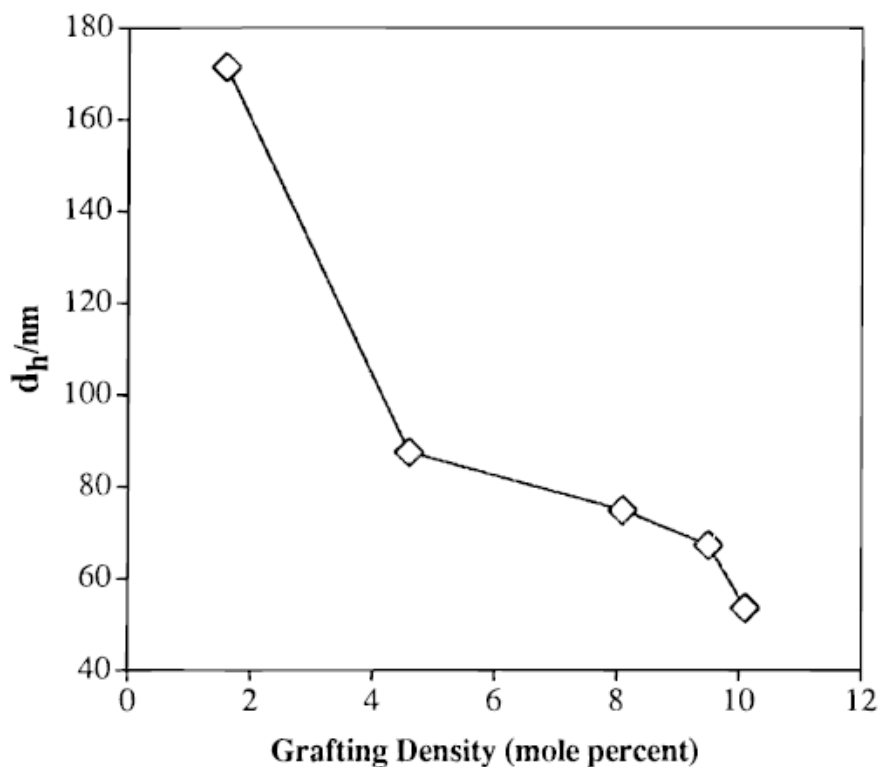


**Figure 2-10:** Effect of graft density on the hydrodynamic diameter of poly(acrylic acid)-graft-poly(styrene) micelles in aqeous solution.[63]

## 2.3.2.2 Self assembly of blocks and grafts in the solid state

The self assembly of block copolymers in the solid state has garnered a great deal of attention due to their use as a precursor material for the production of nanoporous membranes with applications in ultrafiltration technologies.[73] Such membranes are prepared by alignment of the ordered nanoscale morphologies through solvent annealing, electric fields or shearing forces to create long range ordered structures. Various etching processes have also been applied to selectively remove one component of the blocks, resulting in nanoporous membranes.[74]

Solid state self assembly of block copolymers has thus been extensively researched, and well ordered structures can readily be produced. Graft copolymers have also been applied to membrane filtration technology,[74] however, such developments have often been focused on chemioselective interactions for the permeation of gases, although some reports of systems with homogenous pore sizes do exist.[75,76] However, the solid state morphology of these systems is not clearly defined in terms of the chain coil conformations, although the interdomain sizes can be determined from Small Angle X-ray Scattering (SAXS) and Small Angle Neutron Scattering (SANS) studies.[63,77]

The solid state morphologies in graft copolymers, corresponding to those observed in diblock copolymers, are generally observed at larger volume fractions of the second component than would be expected in the equivalent block copolymer.[78] Figure 2-11 shows how increasing graft densities result in smaller domain sizes in the solid state, as determined from SAXS and DLS measurements. This effect is presumably due to disentanglement of the backbone chains.[63]

In the context of physically crosslinked hydrogels, where crosslinks exist as large hydrophobic domains, the distribution, position and size of these domains is likely to play a key role in the overall performance of the material.
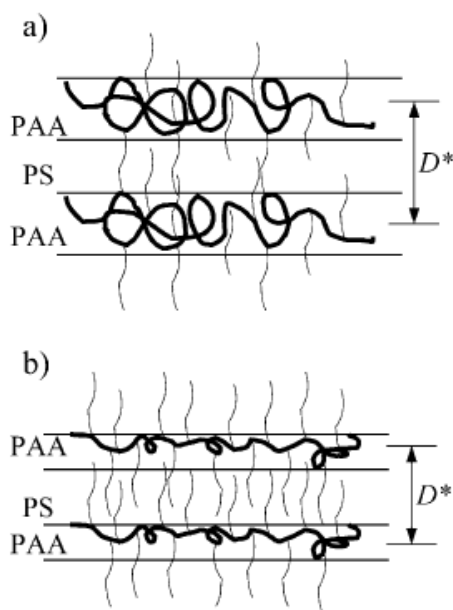


**Figure 2-11:** Effect of graft density on the interdomain sizes of poly(acrylic acid)-graft-poly(styrene) in the solid state.[63]

## 2.4 Solid state NMR in the determination of morphology

Solid state NMR is a powerful technique in the study of morphology and orientation dependant interactions in both crystalline and amorphous materials, as well as complex graft and block copolymer materials.[79,80] Unlike solution state NMR, where the rapid tumbling of molecules in solution leads to averaging of orientation dependant spin-spin and spin-lattice interactions, such rapid molecular motion in the solid state is not possible. Therefore, the orientation of the molecules and the differing rates of movement lead to peaks in the NMR spectrum with unique characteristics. In other words, the position and shape of peaks in solid state NMR spectra are determined not only by chemical shift, but also by the 3D structure of the molecules. This makes it possible to distinguish between crystalline and amorphous domains based on their chemical shift, as well as rigid and mobile domains.[83] Further information can also be obtained by way of relaxation experiments. The various

relaxation times in a sample can be measured by conducting T1, T2, and T1ρ experiments. T1 refers to the spin-lattice relaxation time of a signal in an NMR spectrum, and is observed as a loss of peak intensity over time. Signals from different chemical groups in a sample that show differing T1 values indicate phase separation on a scale of 30 nm and larger. T1ρ relaxation experiments, where the measurements are performed in a rotating reference frame, probe smaller scale heterogeneities in structure on a scale below 30 nm. Phase separated regions can be detected by analysing the relaxation times stemming from different signals in the spectrum. Figure 2-12 illustrates this process, where both the T1 and T1ρ relaxation times were determined for so-called "hard" and "soft" segments, referring to the diisocyanate and polyol segments, in a poly(urethane) system.[82] The large differences in the T1ρ relaxation times are indicative of a phase separated system, with the degree of phase separation varying based on the composition of the polymers. When plotted as a function of time, the nature of the T1 and T1ρ data curve obtained can provide further information, depending on the number of components that it can be separated into,[79,80,82] where a single component indicates a homogenous system, and two or more components show that the system is phase segregated, assuming that the rate of spin diffusion is sufficient.[84]



$^{13}$C CP/MAS spectrum of sample 3 with peak assignments.
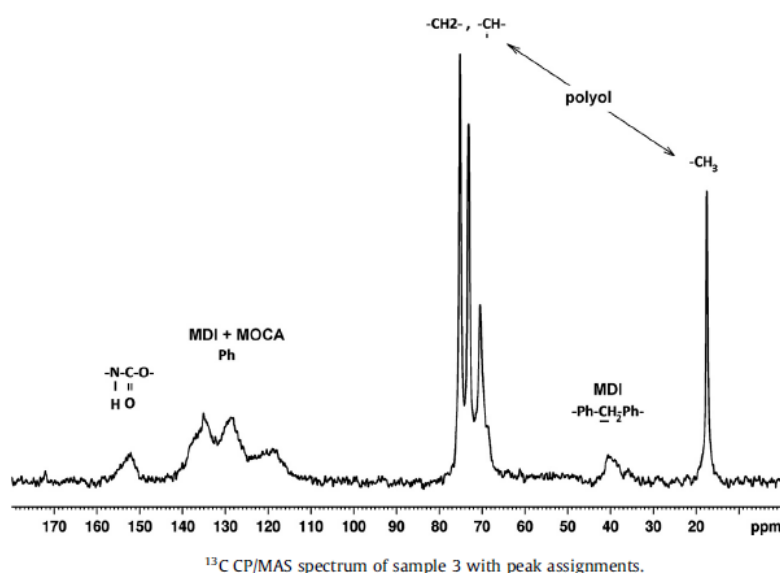
$^1$H $T_1$ and $T_{1\rho}$ values determined for hard and soft segments of the PU samples at 293 K (averaged values for peaks corresponding to the protons in hard and soft segments of the polymer, see details in Supplementary Information).

| Sample | $T_1$, s Hard segment | $T_1$, s Soft segment | $T_{1\rho}$, ms Hard segment | $T_{1\rho}$, ms Soft segment |
|---|---|---|---|---|
| 1 | 1.0 | 0.7 | 2.0 | 7.0 |
| 2 | 0.8 | 0.6 | 2.5 | 7.4 |
| 3 | 0.9 | 0.8 | 3.2 | 5.8 |
| 4 | 1.1 | 1.0 | 3.3 | 2.7 |
| 5 | 1.3 | 1.1 | 2.7 | 1.5 |
| 6 | 1.2 | 1.1 | 2.9 | 1.8 |

**Figure 2-12:** T1 and T1ρ values showing phase segregation in a poly(urethane) sample.[82]

Severe broadening of signals is encountered in solid state NMR spectra due to the orientation dependent interactions. Magic angle spinning (MAS) is commonly employed to reduce the spectral line widths by cancelling out nuclear dipole-dipole coupling interactions to yield higher resolution

spectra.[81] In this process, samples are spun at an angle of 54.75° relative to the magnetic field, usually at a rate of several thousand hertz. Without MAS, severe peak overlap would lead to spectra in which specific peaks cannot be readily distinguished. Although useful to improve the resolution, MAS leads to the formation of spinning side bands in the spectra, which occur at distances proportional to the rate of MAS on either side of the main peaks. Line widths in $^1$H MAS NMR spectra generally remain very broad and significant overlap of peaks can occur. $^{13}$C NMR is more useful due to the larger spectral width, however some signal enhancement is usually required due to the relatively low abundance of $^{13}$C nuclei. This is traditionally accomplished by cross polarization (CP) in which the protons in the sample are excited so that they transfer part of their magnetization to the carbon nuclei, thus improving the signal to noise ratio significantly. Although this process is commonly employed in $^{13}$C solid state NMR as it greatly reduces the amount of time needed to acquire a spectrum, it leads to distortions of the peak intensities, making it unsuitable for quantitative analysis. Single Pulse (SP) experiments, where only the $^{13}$C channel is excited, provide spectra free from these distortions, but take much longer to acquire.

In $^1$H wide line spectra, the presence of sharp peaks is indicative of amorphous or mobile regions, while broad peaks indicate crystalline or rigid areas.[80,84] This relatively simple experiment is conducted without the use of MAS, and consequently gives severely broadened peaks. In the work by Wagler *et al.*,[84] a complex version of this experiment was employed where mixing of the $^{13}$C and $^1$H signals is allowed to occur via transverse magnetization and the phase domain sizes could be determined.

Solid state NMR can thus be used efficiently to probe the morphology and nanostructures of polymeric materials. Although the relatively high cost and long analysis times have limited this technique to being used less frequently than some other analytical techniques, it is able to provide insights into the morphology of both crystalline and amorphous materials that cannot be readily achieved otherwise.

_____

## 2.5 References

**1**    Hoffman, A. S. *Adv. Drug Deliv. Rev.* **2012**, *64*, 18–23.

**2**    Mullarney, M. P.; Seery, T. A. P.; Weiss, R. A. *Polymer* **2006**, *47*, 3845–3855.

**3**    He, C.; Erdodi, G.; Kennedy, J. P. *J. Polym. Sci. Part B Polym. Phys.* **2006**, *44*, 1474–1481.

**4**    Xu, J.; Qiu, M.; Ma, B.; He, C. *ACS Appl. Mater. Interfaces* **2014**, *6*, 15283–15290.

**5**    Bennour, S.; Louzri, F. *Adv. In Chem.* **2014**, *2014,* 10.

**6**    Kali, G.; Vavra, S.; László, K.; Iván, B. *Macromolecules* **2013**, *46*, 5337–5344.

**7**    Maeda, S.; Kato, T.; Kogure, H.; Hosoya, N. *Appl. Phys. Lett.* **2015**, *106*, 171909.

**8**    Ida, S.; Kawahara, T.; Fujita, Y.; Tanimoto, S.; Hirokawa, Y. *Macromol. Symp.* **2015**, *350*, 14–21.

**9**    Guo, P.; Li, H.; Ren, W.; Zhu, J.; Xiao, F.; Xu, S.; Wang, J. *Mater. Lett.* **2015**, *143*, 24–26.

**10**   Saha, S.; Sarkar, P.; Sarkar, M.; Giri, B. *RSC Adv.* **2015**, *5*, 27665–27673.

**11**   Buwalda, S. J.; Boere, K. W. M.; Dijkstra, P. J.; Feijen, J.; Vermonden, T.; Hennink, W. E. *J. Control. Release* **2014**, *190*, 254–273.

**12**   Zhao, Z.; An, S.; Xie, H.; Jiang, Y. *Chinese J. Polym. Sci.* **2014**, *33*, 173–183.

**13**   Hennink, W. E.; van Nostrum, C. F. *Adv. Drug Deliv. Rev.* **2012**, *64,* 223–236.

**14**   Tanaka, M.; Mochizuki, A.; Ishii, N.; Motomura, T. *Biomacromolecules* **2002**, *3*, 36–41.

**15**   Mochizuki, A.; Namiki, T.; Nishimori, Y.; Ogawa, H. *J. Biomater. Sci. Polym. Ed.* **2015**, *26*, 750–765.

**16**   Tanaka, M.; Motomura, T.; Ishii, N.; Shimura, K.; Onishi, M.; Mochizuki, A.; Hatakeyama, T. *Polym. Int.* **2000**, *49*, 1709–1713.

**17**   Haider, H.; Yang, C.H.; Zheng, W.J.; Yang, J.H.; Wang, M.X.; Yang, S.; Osada, Y.; Suo, Z.; Zhang, Q.; Zhou, J.; Chen, Y.M. *Soft Matter* **2015**, *11*, 8253-8261.

**18**   Jewrajka, S. K.; Erdodi, G.; Kennedy, J. P.; Ely, D.; Dunphy, G.; Boehme, S.; Popescu, F. *J. Biomed. Mater. Res. Part A* **2008**, *87*, 69–77.

**19**   Miwa, Y.; Ishida, H.; Tanaka, M.; Mochizuki, A. *J. Biomater. Sci. Polym. Ed.* **2010**, *21*, 1911–1924.

**20**   Yamamoto, K.; Ito, E.; Fukaya, S.; Takagi, H. *Macromolecules* **2009**, *42*, 9561–9567.

**21**   Pastoriza, A.; Pacios, I. E.; Piérola, I. F. *Polym. Int.* **2005**, *54*, 1205–1211.

**22**   Mahdavinia, G. R.; Pourjavadi, A.; Hosseinzadeh, H.; Zohuriaan, M. J. *Eur. Polym. J.* **2004**, *40*, 1399–1407.

**23**   Okuzaki, H.; Kobayashi, K.; Yan, H. *Macromolecules* **2009**, *42*, 5916–5918.

**24**   Sundar, S. S.; Sangeetha, D. *J. Mater. Sci. Mater. Med.* **2012**, *23*, 1421–1430.

**25**   Kim, Y.-J.; Ebara, M.; Aoyagi, T. *Sci. Technol. Adv. Mater.* **2012**, *13*, 1-9.

**26**   Doshi, J.; Reneker, D. H. *Conf. Rec. 1993 IEEE Ind. Appl. Conf. Twenty-Eighth IAS Annu. Meet.*

_____

**1993**, *35*, 151–160.

**27**   Zhang, B.; Lalani, R.; Cheng, F.; Liu, Q.; Liu, L. *J. Biomed. Mater. Res. Part A* **2011**, *99*, 455–466.

**28**   Sekine, Y.; Takagi, H.; Sudo, S.; Kajiwara, Y.; Fukazawa, H.; Ikeda-fukazawa, T. *Polymer* **2014**, *55*, 6320–6324.

**29**   Ikeda-Fukazawa, T.; Ikeda, N.; Tabata, M.; Hattori, M.; Aizawa, M.; Yunoki, S.; Sekine, Y. *J. Polym. Sci. Part B Polym. Phys.* **2013**, *51*, 1017–1027.

**30**   Deng, Y.; Zhang, S.; Lu, G.; Huang, X. *Polym. Chem.* **2013**, *4*, 1289.

**31**   Kawakami, Y. *Prog. Polym. Sci.* **1994**, *19*, 203–232.

**32**   Li, W.; Xue, F.; Cheng, R. *Polymer* **2005**, *46*, 12026–12031.

**33**   Xia, Z.; Patchan, M.; Maranchi, J.; Elisseeff, J.; Trexler, M. *J. Appl. Polym. Sci.* **2013**, *127*, 4537–4541.

**34**   Bayley, G. M.; Mallon, P. E. *Polym.* **2012**, *53*, 5523–5539.

**35**   Lu, P.; Hsieh, Y. Lo. *Polymer* **2009**, *50*, 3670–3679.

**36**   Song, C.; Yu, S.; Liu, C.; Deng, Y.; Xu, Y.; Chen, X.; Dai, L. *Mater. Sci. Eng. C* **2016**, *62*, 45–52.

**37**   Gao, H.; Matyjaszewski, K. *Structure* **2007**, *17*, 6633–6639.

**38**   Zhang, X.; Lu, Y. *Polym. Rev.* **2014**, *54*, 677–701.

**39**   Kim, S. H.; Kim, S. H.; Nair, S.; Moore, E. *Macromolecules* **2005**, *38*, 3719–3723.

**40**   Abraham, A. A.; Sen, A. K. *J. Appl. Polym. Sci.* **2010**, *117*, 2795 - 2802.

**41**   Micic, M.; Rogic Miladinovic, Z.; Suljovrujic, E. *Int. J. Polym. Mater. Polym. Biomater.* **2016**, *65*, 18–27.

**42**   Han, X.-J.; Cheng, B.-J.; Li, Y.-J.; Huang, Z.-M.; Huang, C.; Du, Z.-F.; Wang, J. *Fibres Polym.* **2015**, *16*, 2237–2243.

**43**   Shinoda, H.; Matyjaszewski, K.; Okrasa, L.; Mierzwa, M.; Pakula, T. *Macromolecules* **2003**, *25*, 4772–4778.

**44**   Frenot, A.; Chronakis, I. S. *Curr. Opin. Colloid Interface Sci.* **2003**, *8*, 64–75.

**45**   Chuang, W.-J.; Chiu, W.-Y. *Polymer.* **2012**, *53*, 2829–2838.

**46**   Chen, M.; Dong, M.; Havelund, R.; Regina, V. R.; Meyer, R. L.; Besenbacher, F.; Kingshott, P. *Chem. Mater.* **2010**, *22*, 4214–4221.

**47**   Huang, Z. M.; Zhang, Y. Z.; Kotaki, M.; Ramakrishna, S. *Compos. Sci. Technol.* **2003**, *63*, 2223–2253.

**48**   Deitzel, J. .; Kleinmeyer, J.; Harris, D.; Beck Tan, N. *Polymer* **2001**, *42*, 261–272.

**49**   Kabir, M. H.; Ahmed, K.; Furukawa, H. *Microelectron. Eng.* **2016**, *150*, 43–46.

**50**   Erdodi, G.; Kennedy, J. P. *J. Polym. Sci. Part A Polym. Chem.* **2007**, *45*, 295–307.

**51**   Rivas, B. L.; Pooley, S. A.; Soto, M.; Maturana, H. A.; Geckeler, K. E. *J. Appl. Polym. Sci.* **1998**, *67*, 93–100.

_____

**52**  Pavlović, D.; Linhardt, J. G.; Künzler, J. F.; Shipp, D. A. *J. Polym. Sci. Part A Polym. Chem.* **2008**, *46*, 7033–7048.

**53**  El-Ejmi, A. A. S.; Huglin, M. B. *Eur. Polym. J.* **1997**, *33*, 1281–1284.

**54**  Peppas, N.A.; Keys, K.B.; Torres-Lugo, M.; Lowman A.M. *J.Controlled Release* **1999**, *62*, 81–87.

**55**  Hodorog, A. D. R.; Ibanescu, C.; Danu, M.; Simionescu, B. C.; Rocha, L.; Hurduc, N. *Polym. Bull.* **2012**, *69*, 579–595.

**56**  Kwon, Y.; Song, M.; Hwang, Y. G.; Chang, S. H.; Hong, W. J. *Curr. Appl. Phys.* **2008**, *8*, 486–489.

**57**  Soo, P. L. I. M.; Eisenberg, a D. I. *J. Polym. Sci. Part B Polym. Phys.* **2004**, *42*, 923–938.

**58**  Bordallo, E.; Rieumont, J.; Tiera, M. J.; Gómez, M.; Lazzari, M. *Carbohydr. Polym.* **2015**, *124*, 43–49.

**59**  Kikuchi, A.; Nose, T. *Macromolecules* **1996**, *9297*, 6770–6777.

**60**  Isayeva, I. S.; Kasibhatla, B. T.; Rosenthal, K. S.; Kennedy, J. P. *Biomaterials* **2003**, *24*, 3483–3491.

**61**  Niu, H.; Wang, F.; Weiss, R. A. *Macromolecules* **2015**, *48*, 645–654.

**62**  De La Fuente, J. L.; Wilhelm, M.; Spiess, H. W.; Madruga, E. L.; Fernandez-Garcia, M.; Cerrada, M. L. *Polymer* **2005**, *46*, 4544–4553.

**63**  Ma, Y.; Cao, T.; Webber, S. E. *Macromolecules* **1998**, *9297*, 1773–1778.

**64**  Chung, H. J.; Lee, Y.; Park, T. G. *J. Control. Release* **2008**, *127*, 22–30.

**65**  Nguyen, K. T.; West, J. L. *Biomaterials* **2002**, *23*, 4307–4314.

**66**  Li, J.; Li, X.; Ni, X.; Wang, X.; Li, H.; Leong, K. W. *Biomaterials* **2006**, *27*, 4132–4140.

**67**  Liang-chang, D.; Qi, Y.; Hoffman, A. S. *J. Control. Release* **1992**, *19*, 171–177.

**68**  Watanabe, T.; Ohtsuka, A.; Murase, N.; Barth, P.; Gersonde, K.; *Magn. Reson. Med.* **1996**, *35*, 697-705.

**69**  Klinger, D.; Landfester, K. *Polymer* **2012**, *53*, 5209–5231.

**70**  Kirschner, C.M.; Anseth, K.S. *Acta Mater.* **2013**, *61*, 931–944.

**71**  McKenzie, M.; Betts, D.; Suh, A.; Bui, K.; Kim, L. D.; Cho, H. *Molecules* **2015**, *20*, 20397–20408.

**72**  Rodriguez-Hernandez, J.; Checot, F.; Gnanou, Y.; Lecommandoux, S. *Prog. Polym. Sci.* **2005**, *30*, 691–724.

**73**  Querelle, S. E.; Jackson, E. A.; Cussler, E. L.; Hillmyer, M. A. *ACS Appl. Mater. Interfaces* **2013**, *5*, 5044–5050.

**74**  Leiston-Belanger, J. M.; Russell, T. P.; Drockenmuller, E.; Hawker, C. J. *Macromolecules* **2005**, *38*, 7676–7683.

**75**  Taniguchi, I.; Kinugasa, K.; Egashira, S.; Higa, M. *J. Memb. Sci.* **2016**, *502*, 124–132.

**76**  Tao, G., Wei, L., Xia, Y., Wei, X. *Polym. Mat. Sci. Eng.* **2016**, *32*, 134-140.

_____

**77**   Trapa, P. E.; Won, Y.; Mui, S. C.; Olivetti, E. A.; Huang, B.; Sadoway, D. R.; Mayes, A. M.; Dallek, S. *J. Electrochem. Soc.* **2005**, *152*, A1–A5.

**78**   Milner, S. T. *Macromolecules* **1994**, *27*, 2333–2335.

**79**   Elhrari, W.; Assumption, H.; Mallon, P. E. *Polymer* **2015**, *77*, 95–101.

**80**   Solid State NMR Application Notes, University of Durham Solid State NMR Service, **2007.**

**81**   Maricq, M.M.; Waugh, J.S.  *J. Chem. Phys.* **1979**, *70*, 3300-3316.

**82**   Mokeev, M. V; Zuev, V. V. *Eur. Polym. J.* **2015**, *71*, 372–379.

**83**   Botha, L.; Sinha, P.; Duveskog, H.; van Reenen, A. J. *Macromol. React. Eng.* **2015**, 9, 313–324.

**84**   Wagler, T.; Rinaldi, P. L.; Han, C. D.; Chun, H. *Macromolecules* **2000**, *33*, 1778–1789.

# Chapter 3: Experimental

## 3.1 Material used

N,N'-dimethyl acrylamide (Sigma-Aldrich, South-Africa) was stirred for 24 hours over $CaCl_2$ (Merck) to remove inhibitors and then distilled under high vacuum. The purified monomer was stored under inert atmosphere in a schlenk tube at -10°C. 2-hydroxy ethyl methacrylate and acrylic acid (Sigma-Aldrich, South-Africa), were prepared by passing them through inhibitor removers twice. Toluene (Sigma-Aldrich, South-Africa) was dried by refluxing over sodium/benzophenone and distilled prior to use. Methacryloxypropyl terminated poly(dimethyl siloxane) in varying chain lengths, 1 000 g/mol (MCR-11), 5 000 g/mol (MCR-220), 10 000 g/mol (MCR-41), was used as received from Gelest, USA.

2,2'-azobisisobutyronitrile (AIBN) (ChemLab) was purified via recrystallization from distilled dry methanol (Sigma-Aldrich, South-Africa). An excess amount of AIBN was added to 40 ml of methanol heated to 50°C to form a saturated solution. The methanol was then rapidly decanted and filtered before being cooled in an ice bath to precipitate the crystals. The supernatant was then decanted and the precipitate dried under vacuum at room temperature.

Chromatography grade N,N'-dimethyl formamide (DMF), tetrahydrofuran (THF) and dimethyl acetamide (DMAC) were obtained from Sigma-Aldrich and used as received. MilliQ Millipore deionized water was used for swelling measurements. Chloroform-d ($CDCl_3$ 99.8% atom D), was obtained from Sigma-Aldrich. N,N'-methylenebisacrylamide was obtained from Merck-Schuchardt.

## 3.2 Synthesis of polymers

*Basic procedure:* 3.0 ml of DMAA (0.962 g/ml), and 1.0 – 3.0 ml of PDMS (0.955 g/ml for 900 g/mol) was dissolved in 15 ml of toluene and degassed with dry nitrogen for 15 minutes in a schlenk tube with stirrer bar. 10 mg of AIBN was then added and the solution degassed for a further 10 minutes before it was sealed and allowed to react for 24 hours at 65°C. The samples were cast into aluminium pans, and the solvent was then evaporated under ambient conditions until dry, before being dried further under vacuum at 60°C to remove all residual volatiles. Samples were extracted for 2 days in 2 x 600 ml of hexane to remove unreacted silicone monomers and dried, followed by extraction with 2 x 600 ml distilled water for 2 days to remove any PDMAA homopolymer.

*Crosslinked homopolymer:* To prepare chemically crosslinked PDMAA, the basic procedure was followed but the PDMS was replaced with 90 mg of N,N'-methylenebisacrylamide (2 mol.%).

*Composition studies:* For the study of compositional drift, the basic procedure was followed, but the reactions were halted after 50 minutes by removing the samples from the oil bath, exposing them to atmospheric oxygen and cooling them to prevent evaporation of monomers. NMR samples were then prepared of each sample by mixing an aliquot of the reaction mixture with $CDCl_3$.

_____

## 3.3 Swelling studies

To create high humidity environments (75 and 99% relative humidity), saturated aqeous solutions of sodium chloride and potassium sulphate, respectively, were prepared and placed in dessicators.

60 mg film samples were redissolved in hot toluene (60°C) and cast into discs (2 cm in diameter) and then dried. Samples were left for 1 week to obtain maximum equilibrium swelling. Samples were then removed from solution, dabbed with tissue paper to remove any excess water droplets from the surfaces and quickly weighed. For deswelling studies, the fully swollen samples were placed in a 40% relative humidity environment and weighed at regular intervals after being equilibrated in DDI water for several days. For the DSC measurements, samples were immersed in DDI water for a several days to ensure complete swelling.

To measure swelling of the fibres, they were first removed from the aluminium foil surfaces by soaking them in water; once wetted the fibre mats can be readily removed. Samples were then equilibrated at 40% relative humidity, weighed and placed in a small funnel. Water was added dropwise until the mat became saturated. The water exiting the funnel was collected, weighed and this weight subtracted from the amount of water added to obtain swelling measurements.

To create superswollen gels, 5 ml polymer solutions (5 wt.% in ethanol) were prepared and placed in dialysis tubing (Sigma-Aldrich, MWCO 3000 g/mol). The tubing was then placed in 2 x 600 ml of DDI water for a period of 24 hours. The gels were then removed and analysed.

## 3.4 Electrospinning

Electrospinning was conducted on an in-house built setup, consisting of a Genie Plus Model Kent Scientific syringe pump, and a custom built voltage supply able to produce electrical potentials in the range of 1 - 30kV. Heavy duty aluminium foil was wrapped over a petri dish to form the collector plate. The positive electrode was attached to the syringe needle, and the negative electrode to the collector plate.

18% w/v solutions of polymer samples in ethanol were loaded into standard 3 ml plastic syringes. Fibre formation was accomplished at a flow rate of 0.03 ml/minute, a tip-to-collector distance of 25 cm and a voltage of 15 kV. An ambient temperature of 23°C and an ambient humidity of 40% was maintained during the process. Thereafter, samples were dried under vacuum to remove residual ethanol and any excess water before analysis.

_____

## 3.5 Analysis

### 3.5.1 Differential Scanning Calorimetry (DSC)

DSC analysis was performed on a TA Instruments Model Q100 equipped with flanger unit, and TA Universal Analysis software was used for data analysis.

Bulk samples were prepared for DSC analysis by extensive drying under vacuum at 60°C to remove all moisture. 10 mg samples were then placed in hermetically sealed aluminium pans. Under nitrogen, at a flow rate of 50 ml/min, the samples were first heated to 160°C and held isothermally for 30 minutes. Samples were then cooled to -80°C and heated at 2°C/min to 200°C, held isothermally at this temperature for 10 minutes, and then cooled to -80°C again at a rate of 2°C/min. Data was collected in -80 to 200°C range.

Gel samples of 4 - 8 mg each were frozen in liquid nitrogen and weighed, before being rapidly loaded for analysis. No gas flow was used during analysis so as to avoid evaporation of the imbibed water. Samples were equilibrated at 10°C, and then cooled to -40°C at a rate of 2°C/min, allowed to equilibrate, and then heated to 15°C at 2°C/min.

### 3.5.2 Thermogravimetric analysis

Samples were analysed on a TA instruments TGA Q500. 5 mg samples (stored under 30% R.H) were loaded into hermetically sealed aluminium pans and equilibrated at 25°C before being heated to 600°C at 10°C/min. A nitrogen flow of 50 ml/min was used throughout. Data analysis was performed on TA Universal Analysis software.

### 3.5.3 Fourier Transform Infrared spectroscopy (FTIR)

Infrared spectroscopy was done on polymer films using a Thermo Scientific Niclolet iS10 Smart iTR, utilizing 64 scans over the wavelength of 600 – 4000 $cm^{-1}$. Attenuated total reflectance (ATR) was used.

### 3.5.4.1 Liquid state Nuclear Magnetic Resonance (NMR)

For qualitative analysis, 20 mg samples were dissolved in 0.7 ml of deuterated chloroform ($CDCl_3$) and analysed on a Varian VXR-Unity 400 MHz at 25°C to obtain $^1H$ and $^{13}C$ spectra.

For in-situ NMR, 50 μL of DMAA and 50 μL of PDMS were dissolved in 0.6 ml of deuterated toluene (Sigma-Aldrich, Germany), with 25 μL of N,N'-dimethyl formamide as internal reference, and 2 mg of AIBN as initiator. The sample was then degassed by 7 cycles of freeze pump thaw until no more bubbles were observed. Dry argon gas was added to normalize the pressure. One spectrum was obtained at the starting temperature of 20°C, and thereafter one spectrum, comprising of 64 scans, was obtained every 7 minutes at the reaction temperature of 65°C over 14 hours.

_____

### 3.5.4.2 Solid state NMR

Solid state NMR was performed on a Varian VNMRS 500 MHz instrument, equipped with a 2 channel spectrometer, 6 mm zirconium rotors and a T3 HX probe. In all experiments, with the exception of the static $^1$H wideline, magic angle spinning at 5 000 Hz was used.

For CP experiments, a 6 μs 90° pulse ($^1$H channel), recycle delay of 5 s and a total of 20 000 scans was used with a 7 ms polarization transfer time and a 4 μs delay before acquisition from the $^{13}$C channel. For SP experiments, a 6.0 μs 90°C pulse was used, followed by a 4 μs delay before acquisition. For the CP T1ρ experiments, a t-locked array was constructed with 30 elements and the delay time before polarization transfer varied between 0 – 50 000 μs. A 1 μs polarization transfer time was used followed by a 4 μs delay before acquisition. A 1.5 s recycle delay was used. Proton decoupling was used for all three experiments. Finally, for $^1$H static wideline, the same sequence timings were used as in SP, but without MAS and with detection exclusively on the $^1$H channel.

Samples were equilibrated at 30% relative humidity in a dessicator with dried silica gel before analysis, to avoid interference by the presence of moisture on relaxation experiments.

### 3.5.5 Field Emission Scanning Electron Microscopy (FE-SEM)

A Merlin Field Emission Gun (FEG) SEM with an inlens detector (Oxford Instruments) set to depth mode at a working distance of around 4 mm, spot size of 150 pA and an EHT around 5.00 kV was used for analysis of the fibres. For film samples, an EHT of 0.5 kV and a spot size of 120pA at a working distance of approximately 3.5 mm was used. Samples were dried for several hours under vacuum to remove all residual ethanol and/or moisture. All samples were gold coated before analysis.

Nanofibre diameter analysis was performed manually on Zeiss AxioVision LE software. Calibration was done using the image scale bars. Only fibres in the foreground of the images were measured to ensure that measurements remained unaffected by the distance. A minimum of 50 measurements were taken per image to obtain a mean and standard deviation for each sample.

### 3.5.6 Static contact angle measurements

1 μL of distilled deionized water was placed on a level fibre surface using a micro syringe and photographed using a Nikon VCC 250C microscope equipped with a digital camera. A magnification of approximately 6x was used. In static contact angle measurements, the experiment was repeated 5 times for each sample. For time based experiments, images were recorded every 2 minutes and the experiment was repeated 3 times for each sample. The contact angles were then measured digitally with Zeiss AxioVision LE software by applying the equation: $= 2 \cdot \tan^{-1}(\frac{R}{H})$ , where $R$ is the maximum radius and $H$ is the height.

_____

### 3.5.7 Tensile Strength Testing

A Lloyd Instruments LRX tensile tester equipped with rubber clamps was used. Samples were extended at a rate of 50 mm/min and measured until break. Each measurement was repeated 3 times; breakages occurring inside of the clamps were disqualified. Samples of approximately 25 x 5 mm, with a thickness of around 0.8 mm were used for tensile testing.

### 3.5.8 Size Exclusion Chromatography (SEC)

SEC was performed with HPLC grade DMAC as solvent on a Breeze system equipped with a Waters 1515 Isocratic pump, Waters AF degasser, a Waters 717 Plus auto-sampler and a Waters 600E system controller. An 8 x 50 mm PSS GRAM precolumn with 10 μm particles and an 8 x 300 mm, 100 Å pore size PSS GRAM analytical column was used. Detection was done on Waters 410 Refractive Index and Waters 2487 dual wavelength UV detectors. Breeze SPA software (v3.3) was used for instrumentation handling. The system was calibrated using poly(methyl methacrylate) (PMAA) standards. The molecular weights are reported relative to these standards.

### 3.5.9 High Performance Liquid Chromatogrphy (HPLC)

HPLC was performed on a Waters 2690 Separations Module with a Polymer Labs ELS1000 evaporative light scattering detector, interfaced with PSS WinGPC software for data recording. A Walters C300 symmetry C18 column was used, with dimensions of 4.6 x 250 mm and a 5 μm internal diameter. The column was held isothermally at 30°C during analysis. Samples were thoroughly dried under vacuum and prepared at a concentration of 5 mg/ml in THF.

Figure 3-1 below shows the gradient elution program used. Starting with 100% DMF for 5 minutes, the mobile phase was then linearly altered over 20 minutes to 100% THF.  After data capture, the column was flushed with pure THF for 10 minutes at 1 ml/min and reconditioned with 10 column volumes of 100% DMF before the next sample was analysed.
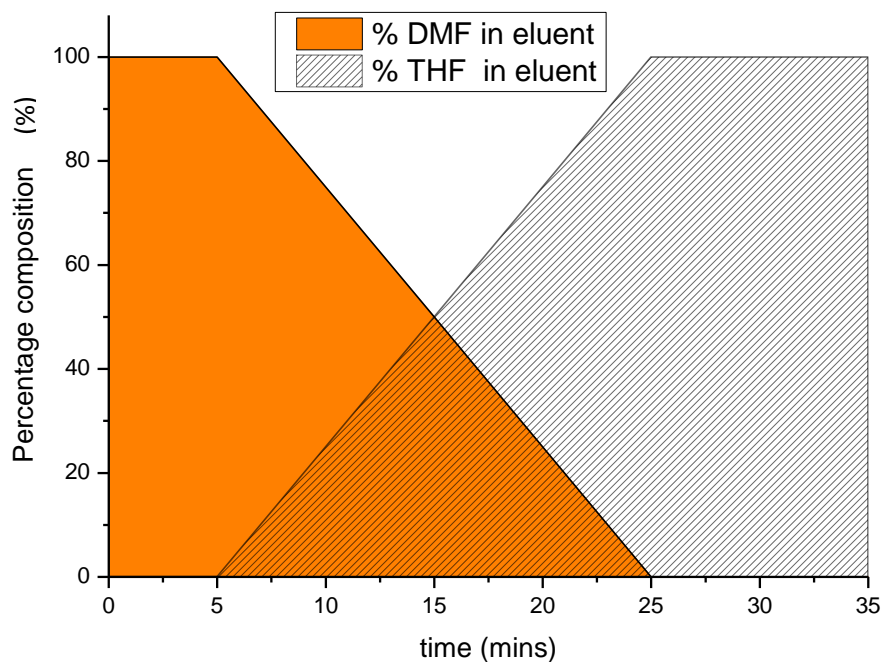
**Figure 3-1:** HPLC gradient elution profile

## 3.5.10 Wide Angle X-ray Diffraction (WAXD)

X-ray diffraction was performed on films and nanofibres using a Bruker AXS D2 Phaser with Copper K-α radiation (λ = 0.154 nm) and a Lynxeye detector. Samples were scanned using the Coupled Two Theta/Theta scan type and Continuous PSD Fast mode in the range of 4 – 40 2θ.

# Chapter 4: Results

## 4.1 Synthesis

The polymerization of hydrogels is generally performed under aqueous conditions, or in polar protic solvents. Due to the large differences in hydrophilicity and polarity in amphiphilic monomer systems, selecting solvents that will dissolve all of the reaction components is often challenging.  In some cases, the product itself may not be miscible in the polymerization medium, leading to loss of control over the reaction. Graft copolymerization, specifically the grafting through methodology, substantially simplifies the synthetic process in this regard as it allows for a one-step, one-pot procedure to be used, as opposed to block copolymerization or other methods of graft polymerization which may require several synthetic steps and a number of reagents in order to control the reaction, all of which need to be simultaneously soluble. Silicones are readily soluble in solvents of low polarity such as toluene, THF, chloroform, and pure aliphatics such as pentane and hexane. N,N'-dimethyl acrylamide (DMAA), acrylic acid (AA) and 2-hydroxy ethyl methacrylate (HEMA) are strongly hydrophilic, however they remain soluble in less polar solvents such as toluene and THF, thus making them natural candidates in the design of amphiphilic copolymers due to the simplistic synthesis reactions.

The aforementioned monomers were tested in the copolymerization with methacryloxy propyl terminated PDMS. The results are summarized in Table 4-1. The nominal chain length of the PDMS graft was varied between 1 000 g/mol and 10 000 g/mol. Of the monomers tested, N,N'-dimethyl acrylamide (DMAA) was the only one found to form hydrogels with the silicone copolymer. Surprisingly, acrylic acid did not form hydrogels, even though it is known from previous studies that methacrylic acid, a structurally similar monomer, is able to form stable hydrogels with PDMS.[1]

Since the novel hydrophobically crosslinked PDMAA-g-PDMS (S1-S5) with 1 000 g/mol PDMS grafts showed several interesting properties, this system was chosen as the focus of this study. Preliminary swelling studies showed that below a threshold PDMS content of around 2-3%, the materials dissolved and broke apart when immersed in water, whereas above 12 wt.% PDMS content, the degree of swelling was not high enough for the material to be considered useful as a hydrogel, absorbing less than 30 wt.% of water. Subsequently, the array within this desired range was selected for further analysis.

The PDMAA-g-PDMS copolymers were prepared by a method adapted from the work of Erdodi *et al.*[2] The reaction scheme is presented in Figure 4-1 and was performed using a simple one pot synthesis with AIBN as free radical initiator. The amount of DMAA present in each sample was held constant relative to the amount of initiator used, while the amount of PDMS macromonomer was varied, with the intention of maintaining a relatively constant backbone chain length. Reactions were run for 24 hours. Samples were cast into films, and allowed to dry under ambient conditions before extraction with hexane, followed by distilled water, to remove unreacted monomers and homopolymer fractions. Less than 1.5 wt.% of extractables was recorded in all cases, indicating a high degree of conversion.

**Table 4-1:** Summary of tested monomers and resulting materials

| Sample | Hydrophilic monomer | Appearance and physical properties | Mol.% PDMS in feed | PDMS graft weight (g/mol) | Swelling in water |
|--------|--------------------|-----------------------------------|-------------------|--------------------------|-------------------|
| S0 | DMAA | Cloudy, wax-like | -- | -- | Very good[a] |
| SL | DMAA | Clear, transparent, waxy | 2.8% | ~1000 | Soluble |
| S1 | DMAA | Clear, transparent, tough | 3.5% | ~1000 | Good |
| S2 | DMAA | Clear, transparent, tough | 5.2% | ~1000 | Good |
| S3 | DMAA | Clear, transparent, tough | 6.8% | ~1000 | Good |
| S4 | DMAA | Clear, transparent, tough | 8.4% | ~1000 | Good |
| S5 | DMAA | Clear, transparent, tough | 9.8% | ~1000 | Good |
| S6 | DMAA | Yellow, transparent, rubbery | 12.7% | ~1000 | Minor |
| G1 | DMAA | Cloudy, soft, weak | 2.0% | ~5000 | Minor |
| G2 | DMAA | White flakes | 5.0% | ~5000 | Minor |
| G3 | DMAA | Cloudy, wax-like | 2.0% | ~10 000 | None |
| G4 | DMAA | Cloudy, wax-like | 5.0% | ~10 000 | None |
| H1 | HEMA | White, powdery | 0.5% | ~1000 | None |
| H2 | HEMA | White, powdery | 5.0% | ~1000 | None |
| H3 | HEMA | White, powdery | 10.0% | ~1000 | None |
| A1 | AA | White, powdery | 0.50% | ~1000 | Minor |
| A2 | AA | White, powdery | 5.0% | ~1000 | Minor |
| A3 | AA | White, powdery | 10.0% | ~1000 | Minor |

*a: When chemically crosslinked with BIS; without crosslinker this sample would be highly water soluble.*
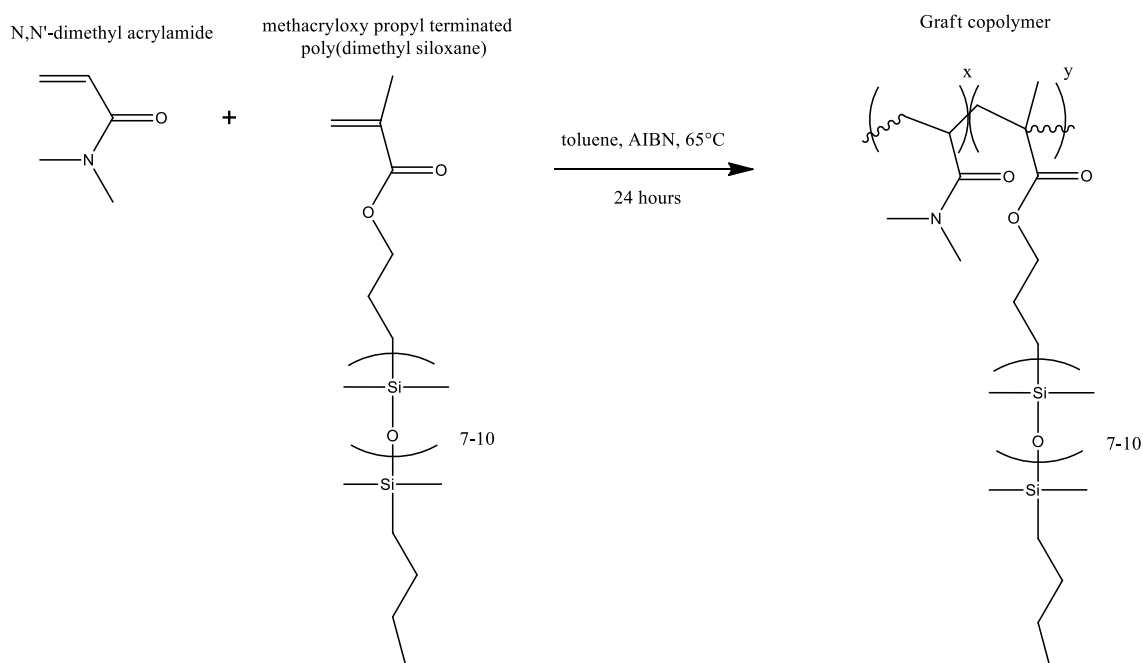


**Figure 4-1:** Reaction scheme for the synthesis of PDMAA-g-PDMS

Samples were obtained as transparent films. The physical properties were noted to be rubber like, provided that the material was stored above a humidity of 30-40%. The copolymer was soluble in most polar organic solvents, as well as halogenated solvents such as chloroform. The copolymer could not be redissolved in toluene at room temperature, but did dissolve when heated to 60°C while stirring for at least 1 hour.

In some cases the newly prepared samples showed a yellow-brown hue which dissipated after extraction with hexane; this was found to occur predominantly in films with high PDMS content, and may potentially be due to small fractions of unreacted PDMS macromonomers. Figure 4-2 shows a comparison between a newly prepared film and a film stored in deionized water for around 6 months, and it is noted that similar discolouration occurs. This is theorized to be due to the slow extraction and solvation of PDMS deficient polymer chains; consequently the remaining polymer is enriched in PDMS and undergoes phase separation, resulting in the scattering of incident light and the observed discolouration. The presence of optical discolouration is evidence of phase segregated domains on the order of > 400 nm.[6] The yellowing observed in high PDMS content samples likely stems from the same phenomenon.
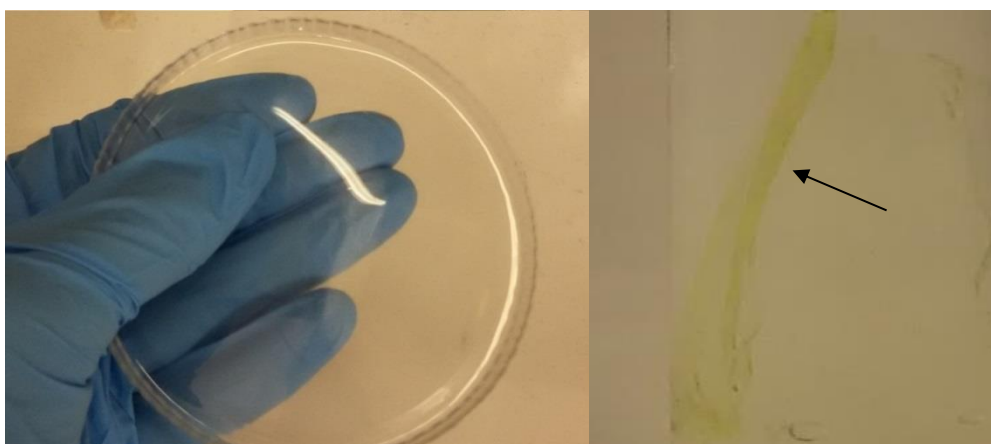


**Figure 4-2:** New 7.9 mol.% PDMS  film (left) vs. film aged for 6 months in water (right)

Table 4-2 summarizes the molecular weight, dispersities, feed ratios and PDMS content determined from $^1$H NMR. The average molecular weight increases across the series due to the incorporation of larger amounts of PDMS macromonomer. The dispersity values observed are typical of free radical polymerizations. Feed ratios and $^1$H NMR measurements were found to correlate relatively well, although a significant deviation is seen in sample 1. This is likely because the relatively low PDMS content in the reaction mixture leads to the formation of a significant amount of PDMAA homopolymer which is lost during extraction. Therefore, the sample becomes indirectly enriched in PDMS.

_____

**Table 4-2:** Sample compositions and general information

| Sample | Molecular weight (x10³ g/mol) | Dispersity (Đ) | Mol.% PDMS monomer in feed | Mol.% PDMS as determined from ¹H NMRª |
|--------|------------------------------|----------------|---------------------------|-------------------------------------|
| S1 | 46.7 | 2.93 | 3.5 % | 4.2% |
| S2 | 53.2 | 2.91 | 5.2 % | 4.9% |
| S3 | 56.3 | 2.90 | 6.8 % | 6.7% |
| S4 | 69.4 | 2.87 | 8.4 % | 7.9% |
| S5 | 83.5 | 2.31 | 9.8 % | 10.5% |

*a: See Appendix A for calculations*

$^1$H NMR and FTIR analysis was conducted to confirm the successful synthesis of the copolymer system. Figure 4-3 shows the obtained FTIR spectra of the prepared samples and homopolymer. The inset shows a magnified image of the Si-C region. The peak intensity in this region increases with increasing PDMS feed ratio, and is absent in the homopolymer, thus indicating successful incorporation of the macromonomer.
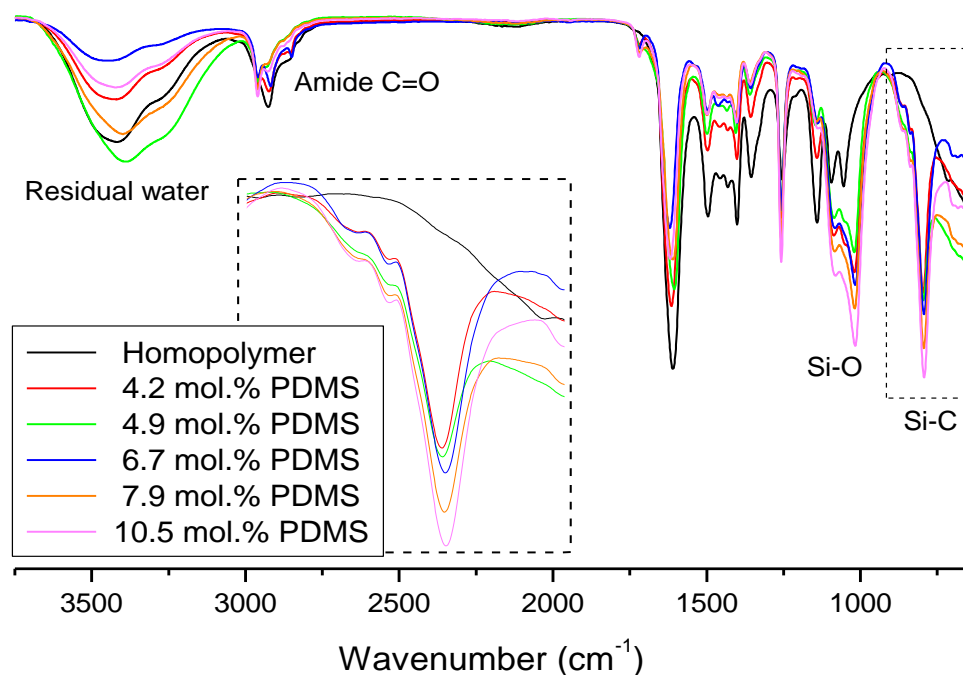


**Figure 4-3:** FTIR spectrum of PDMAA and PDMAA-g-PDMS samples

_____

Figure 4-4 shows the ^{1}H NMR spectra of DMAA and the PDMS macromonomer. In the DMAA spectrum, the methyl groups (**d**) attached to the amide appear as a strong doublet around 2.9 ppm. The single proton (**c**) on the tertiary carbon appears as a quartet around 6.5 ppm. The vinyl protons (**a**) and (**b**) appear as doublets with fine splitting around 5.5 and 6.2 ppm, respectively.

In the spectrum of the macromonomer, the downfield region from 0 – 2 ppm contains the majority of the signals, and some overlap occurs for the propyl and butyl chains attached to the siloxane segment. The strong cluster of signals (**e**) from the methyl groups attached to the siloxanes leads to a distinctive peak at 0 ppm. The vinyl protons appear far upfield (**a**,**b**).
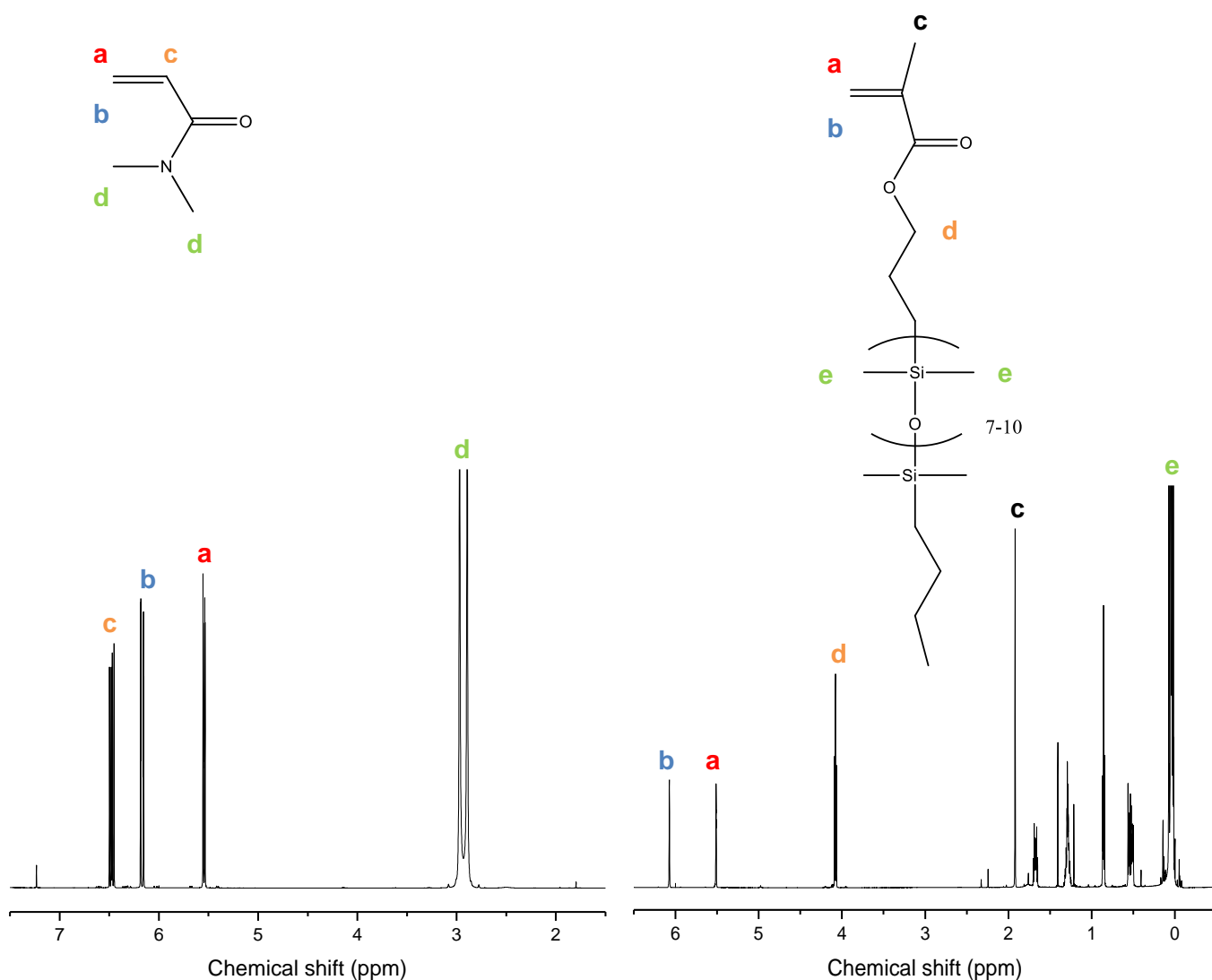


**Figure 4-4:** ^{1}H NMR assignments of N,N-dimethyl acrylamide (left) and methacryloxy propyl terminated PDMS (1 000 g/mol) (right) in deuterated chloroform

Figure 4-5 shows the $^1$H NMR spectrum of the 6.7 mol.% PDMS copolymer as an example. The methyl groups of the acrylamide (**a**) appear as a large peak at around 3 ppm, and the siloxane methyl groups (**b**) near 0 ppm. The upfield region shows no vinyl proton peaks, indicating that virtually all of residual monomers have been successfully extracted. The ratio of monomers in each sample after extraction was determined from the appropriate peak integrals (see Appendix A for details).
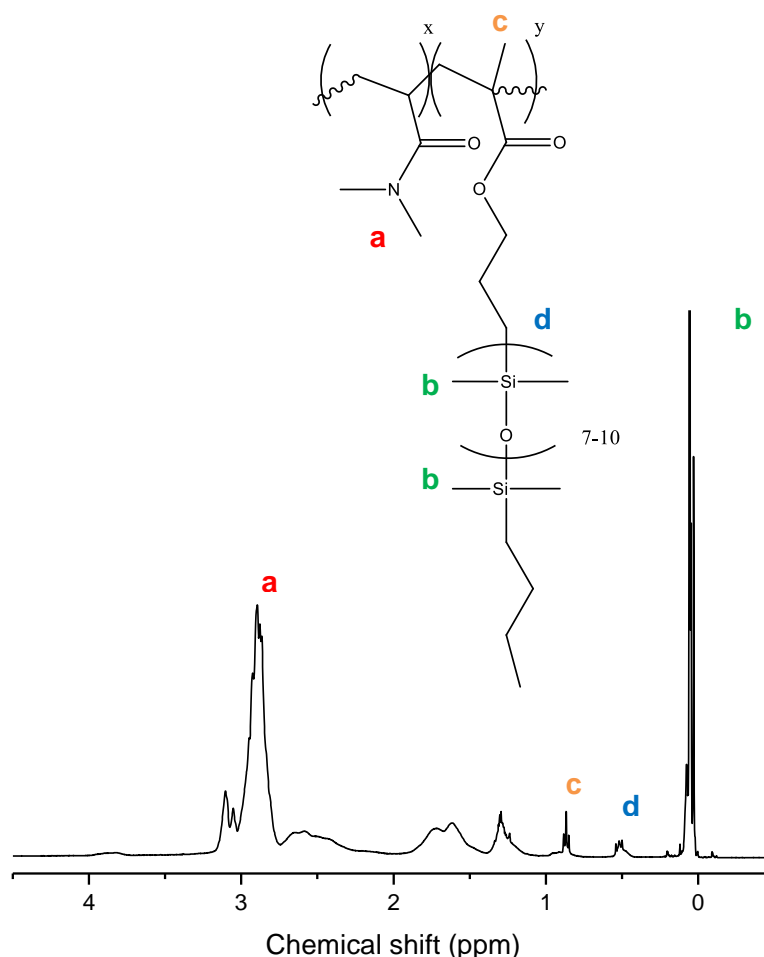


**Figure 4-5:** $^1$H NMR spectrum of PDMAA-g-PDMS (6.7 mol.% PDMS) in deuterated chloroform

Although the feed ratios generally correlate with the copolymer composition, it is of interest to determine how the monomers concentrations change over the course of the reaction. In order to confirm whether the monomers are consumed at the same rate throughout the reaction, *in-situ* NMR was conducted to track the decrease in the monomer concentration over the course of the reaction. The relative integral of the vinyl peaks (**a** in the DMAA spectrum and **b** in the PDMS spectrum in Figure 4-4) from the monomers was tracked using DMF as internal reference standard over the course of a 10 hour reaction at 65°C in deuterated toluene. The results are presented in Figure 4-6. The relative rate of monomer consumption throughout the course of the reaction is almost identical until the last stage of the reaction, when the PDMS becomes depleted and some homopolymerization of the DMAA occurs. Little to no further decrease is observed from *in-situ* NMR after this stage. This

may be due to the relatively insensitive nature of the experiment, rather than total completion of the reaction, since the PDMS macromonomer's vinyl proton signals are far weaker than that of DMAA due to the relative concentrations.
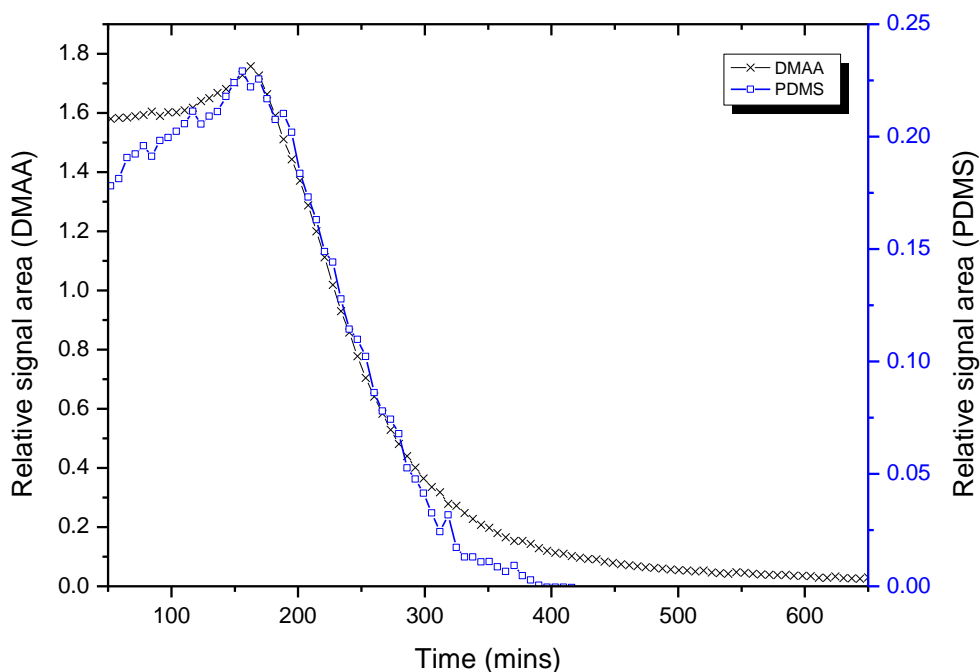


**Figure 4-6:** Reaction kinetics tracked using *in-situ* ^{1}H NMR

In most reactions between comonomers, compositional drift is encountered where the actual amounts of incorporated monomers diverge from the feed ratio over the compositional range. Although *in-situ* NMR gives some insight into the reaction kinetics, from both an academic and practical perspective it is desirable to know the reactivity ratios of a copolymer system as this provides an understanding of how the two monomers react with each other in the reaction medium. Figure 4-7 shows the feed ratios and resulting copolymer composition measured at 10% conversion. Compositional drift is encountered with more PDMS being incorporated relative to the feed ratio. This is also in agreement with the HPLC data, discussed in the next section. Using a Fineman-Ross plot (see Appendix A for details), the reactivity ratios of the monomers were calculated, with r1 determined as 0.926, and r2 = 4.31.[29,30] In this scenario, we expect one monomer (the PDMS) to be favoured during the course of the reaction, but once it is depleted some homopolymerization of the DMAA is likely to occur. Given that the radicals are better stabilized in the PDMS monomer, which has a tertiary carbon alongside the vinyl unit, this result is not surprising.

_____
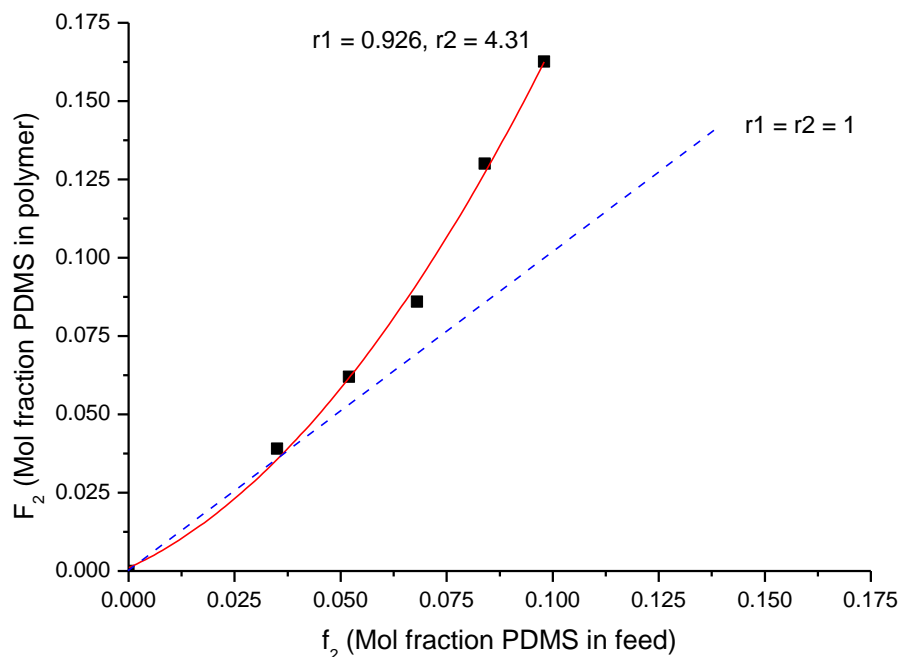


**Figure 4-7:** Compositional drift in samples at 10% conversion.

Figure 4-8 below shows the HPLC chromatograms of the synthesized copolymers after extraction in water and hexane. Separation was done on a C18 column using 100% DMF as the initial solvent composition, which was then followed by a gradient elution profile. The polar homopolymer fraction undergoes little to no interaction with the non-polar column and elutes first, followed much later by the PDMS rich copolymer, which only elutes once the solvent composition begins to exceed 50% THF. Inset A shows an expansion of the homopolymer region. Although NMR and FTIR data showed that the 4.2 and 4.9 mol.% PDMS samples are similar in terms of actual PDMS content, HPLC separation revealed that the 4.2 mol.% PDMS sample contains a much larger fraction of homopolymers relative to the 4.9 mol.% PDMS sample. The sample compositions therefore still differ significantly, in spite of the apparently similar molar amounts of PDMS incorporated during the course of the reaction. This is presumably due to the relatively slow rate of diffusion of the macromonomer, which leads to the formation of more homopolymers. With larger amounts of the macromonomer present, this effect becomes less relevant and the homopolymer fraction diminishes rapidly. Inset B shows the copolymer region. Increased PDMS content leads to a direct corresponding increase in retention time, and the peaks simultaneously become narrower. The 10.5 mol.% PDMS sample shows a small shoulder, and likely contains two separate distributions of PDMS rich fractions. Attempts to resolve the second main peak further were unsuccessful.
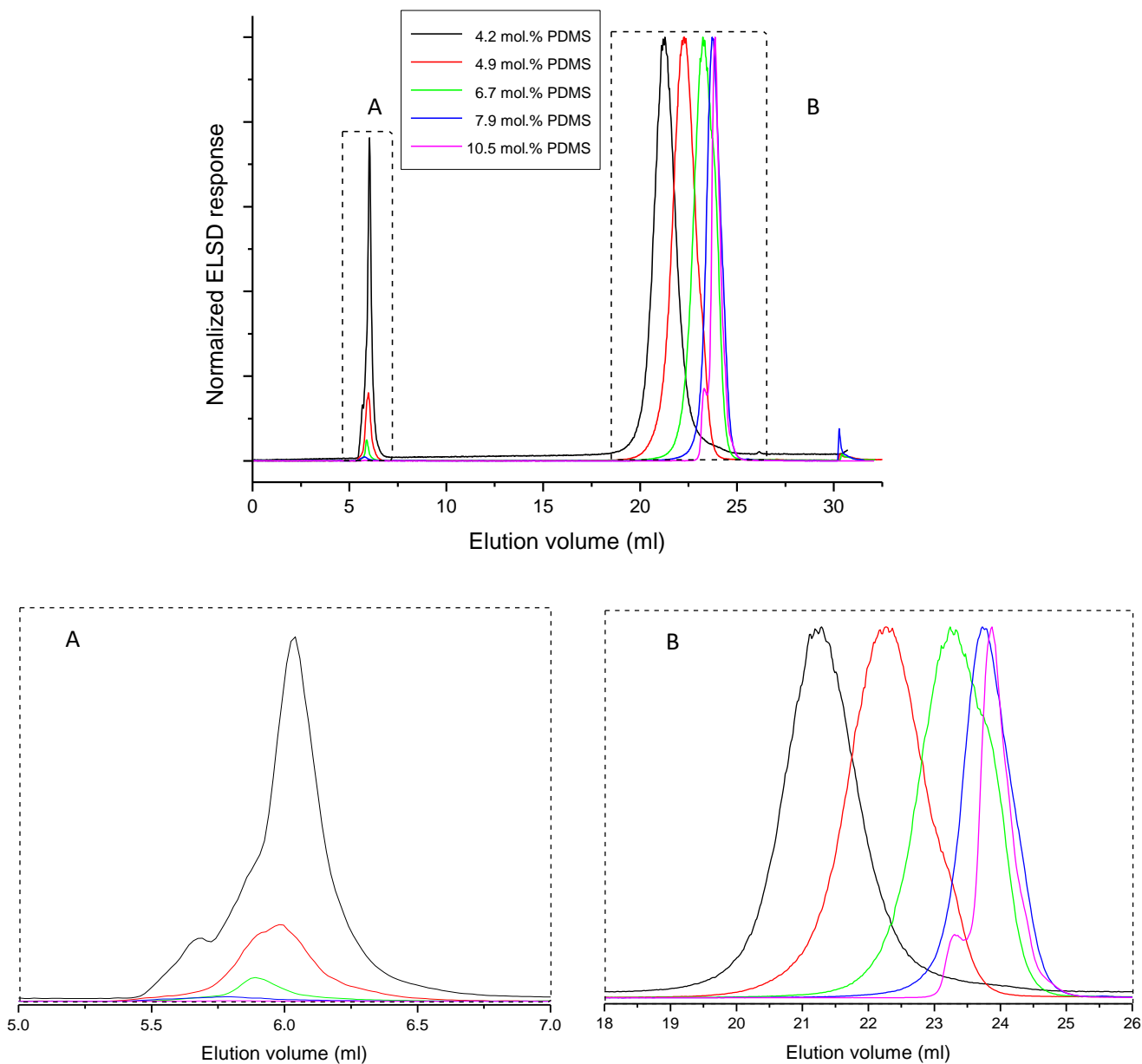
**Figure 4-8:** HPLC chromatograms of the prepared samples, with expansion of regions A (homopolymer fraction) and B (copolymer fraction).

_____

Figure 4-9 below shows thermogravimetric data for the homopolymer and the PDMAA-g-PDMS samples, while Table 4-3 lists the associated data.  Some initial mass loss occurs due to loss of atmospheric moisture; interestingly there is little correlation between the amount of moisture loss and the PDMS content of the samples. First derivative curves of the data reveal that several inflection points occur along the slope, with the right most peak being attributed to the decomposition of the PDMAA as this matches the homopolymer data. Note that the thermal stability of the copolymer diminishes upon the introduction of PDMS, with the main decomposition step occurring around 70 - 90°C lower than in the homopolymer samples. The main decomposition onset temperature increases slightly with increased PDMS content, whereas the PDMAA decomposition onset shifts to a lower temperature. The residual mass above 450°C is attributed to non-volatile silicon oxides.
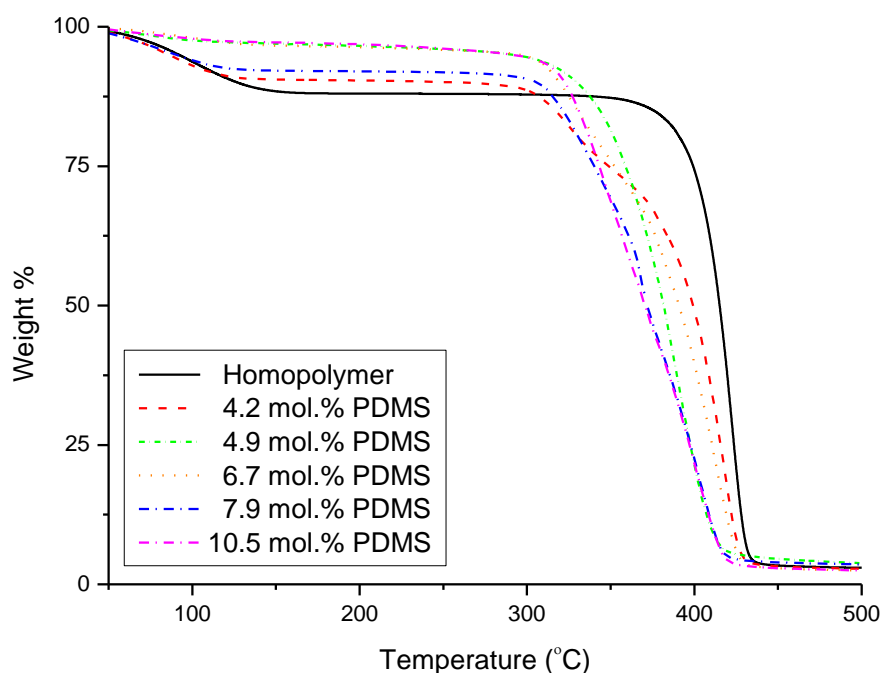


**Figure 4-9:** TGA thermograms of PDMAA homopolymer and PDMAA-g-PDMS samples

**Table 4-3:** Summary of TGA data

| Mol.% PDMS | Main decomposition onset point (°C) | PDMAA decomposition onset point (°C)[a] | Wt.% PDMS in polymer |
|---|---|---|---|
| 0 | 393.8 | 422.4°C | 0.0% |
| 4.2 | 303.6 | 417.2°C | 30.6% |
| 4.9 | 305.8 | 414.2°C | 34.2% |
| 6.7 | 308.3 | 412.2°C | 42.0% |
| 7.9 | 312.3 | 403.1°C | 46.4% |
| 10.5 | 322.3 | 399.7°C | 54.2% |

*a: Determined from the peak maxima of the first derivative (temperature) curve*

_____

## 4.2 Swelling behaviour

The ability of a material to swell in water not only serves to define whether or not it can be considered a hydrogel, but also showcases a number of important physical properties of the material. For example, in in the field of drug release, the degree of swelling can affect the cytotoxicity of the material and will impose a limit on the maximum drug loading capacity.[3]

Swelling may be defined either by the weight percentage of water uptake, or by the Q value, which is the swollen wet mass divided by the initial dry mass. Since most equations surrounding hydrogels make use of Q values, this measure will be used to present swelling results, where a Q value of 1 means that no swelling occurs. Swelling in non-polar solvents will be denoted as Z. A covalently crosslinked homopolymer sample, denoted as S0, was also prepared by the addition of 2 mol.% N,N'-methylenebisacrylamide as reference sample, for comparative purposes.

### 4.2.1 General swelling behaviour

Table 4-4 shows a summary of the composition, swelling and estimated "crosslink density" of the synthesized films (this crosslink density will be discussed in more detail in the next section). The tabulated data shows how the addition of PDMS leads to a dramatic reduction in the equilibrium swelling of the material, when compared with the swelling of the crosslinked homopolymer. This is shown visually in Figure 4-10. The overall swelling for the first three samples is relatively consistent, but a more notable reduction occurs when the PDMS content is increased up to 7.9% and beyond.

**Table 4-4:** Swelling data as a function of PDMS content

| Sample | Mol. % PDMS | Swelling (Q) | Q of swellables $(Q_S)^a$ | Estimated crosslink density in DMAA domains $(mol.m^{-3})^b$ | Swelling in hexane (Z) | Z of swellables $(Z_S)^a$ |
|---|---|---|---|---|---|---|
| **S0** | 0.0 % | 14.2 | 14.2 | 0.0192 | 1.03 | -- |
| **S1** | 4.2 % | 2.54 | 3.04 | 1.49 | 1.08 | 1.31 |
| **S2** | 4.9 % | 2.60 | 3.40 | 1.05 | 1.05 | 1.15 |
| **S3** | 6.7 % | 2.63 | 3.71 | 0.800 | 1.38 | 1.95 |
| **S4** | 7.9 % | 2.09 | 2.99 | 1.57 | 1.77 | 2.70 |
| **S5** | 10.5 % | 1.74 | 2.47 | 2.95 | 2.45 | 3.91 |

*a: See Appendix A*
*b: See Section 4.2.2 for details*

It is important to take into account that the PDMS segments undergo virtually no swelling in water. Therefore, as the weight percentage of PDMS is increased, a decrease in equilibrium swelling would be expected, however it is observed that after the initial sharp decrease in swellability relative to the reference sample, there is only a small change in the swellability up to 7.9 mol.% PDMS. This implies

_____

that other factors beyond just the "quantity" of PDMS must also play a role in determining the equilibrium water content.

Because the imbibed water is almost exclusively contained in the PDMAA fraction, considering these segments in isolation provides important insights into the possible morphology of the samples. To this end, the swelling of the PDMAA segments was calculated independently, and denoted as $Q_S$, thus representing the true swelling in water of PDMAA domains. In other words, the total weight of absorbed water was used to determine the real swelling of the fraction of PDMAA in the copolymer. Analogously, swelling of the PDMS domains in hexane was denoted as $Z_S$, as it can be assumed that the PDMAA segments swell negligibly in hexane. Surprisingly, $Q_S$ initially increases with increasing PDMS content.   This suggests that the increasing quantities of PDMS as "crosslinker" show diminishing returns, until some morphological transition occurs between 6.7 and 7.9 mol.% PDMS content.

When swollen in hexane, the addition of PDMS provides no immediate improvement in the ability of the material to swell in a non-polar solvent, potentially due to "blocking" by the surrounding hydrophilic material. However, with increased PDMS content, significant swelling in hexane begins to take place, as illustrated in Figure 4-10.
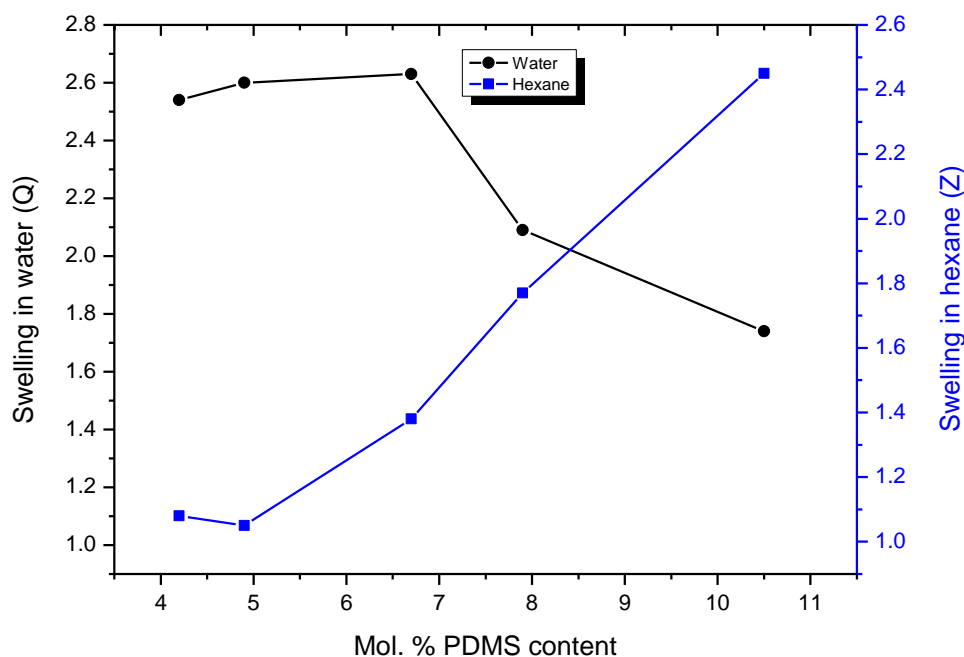


**Figure 4-10:** Effect of PDMS content on swelling in water and hexane

By contrast, He *et al.*[6] showed that networks of PEG-b-PDMS (6000 g/mol PDMS chain lengths) underwent distinct linear increases in the degree of swelling for both hexane and water when the amount of the appropriate component was increased, as illustrated in Figure 4-11 below. Similarly, Guan *et al.*[21] illustrated relatively linear behaviour in networks of PNIPAAm-*l*-PTHF. Because of the large number of differing variables between these systems and the one presented here, no single

cause for the difference in behaviour can be immediately deduced; however the primary difference between PDMAA-g-PDMS and these other systems (in addition to the method of crosslinking) is that this is a graft copolymer system, which likely leads to a distinct morphology that will in turn affect the crosslinking density.
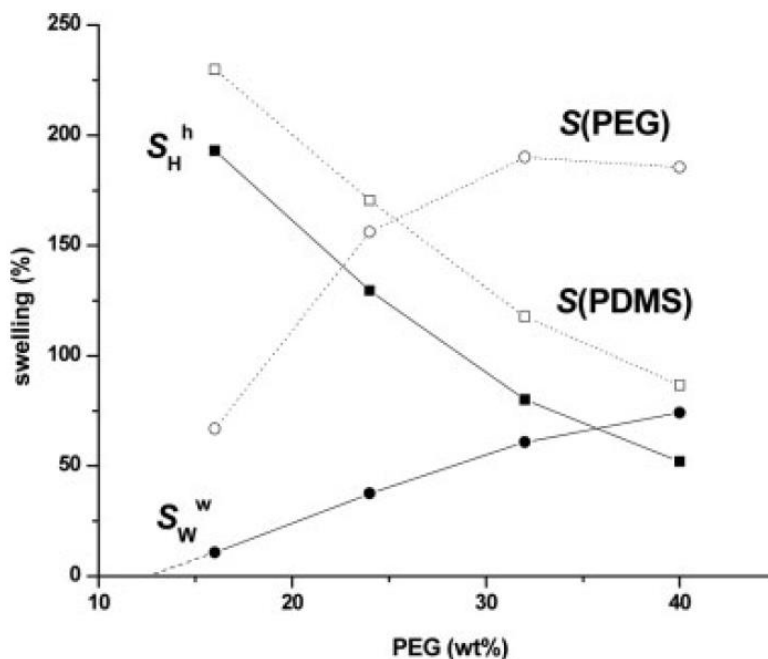


**Figure 4-11:** Effect of PEG content on the degree of swelling of crosslinked PEG-*b*-PDMS networks in hexane and water.[6]

The rate of swelling was determined in the thin film samples and the results are shown in Figure 4-12. Film samples were found to reach as much as 90% saturation within 5 minutes of immersion in water. Compared to other literature studies, the rate of swelling is extremely fast, since most other gels take several hours or even days to reach equilibrium swelling.[21-23] Similarly, the samples deswell rapidly (Figure 4-13), losing half of their water content in under 50 minutes. Exponential decay functions were fitted to the deswelling data and the half-life for each of the curves was determined. The results are shown in Table 4-5. It is noted that the half-life decreases with increasing PDMS content, even though the first 3 samples do not show significant differences in equilibrium swelling due to PDMS content. However, the larger weight percentage of PDMS clearly has an effect on the deswelling kinetics.

**Table 4-5:** Half lives of function fitted deswelling curves

| Sample (Mol. % PDMS) | Half-life (minutes) | $R^2$ value of fit |
|---|---|---|
| 4.2 | 61.0 | 0.9947 |
| 4.9 | 49.7 | 0.9953 |
| 6.7 | 40.9 | 0.9954 |
| 7.9 | 42.5 | 0.9897 |
| 10.5 | 29.1 | 0.9866 |
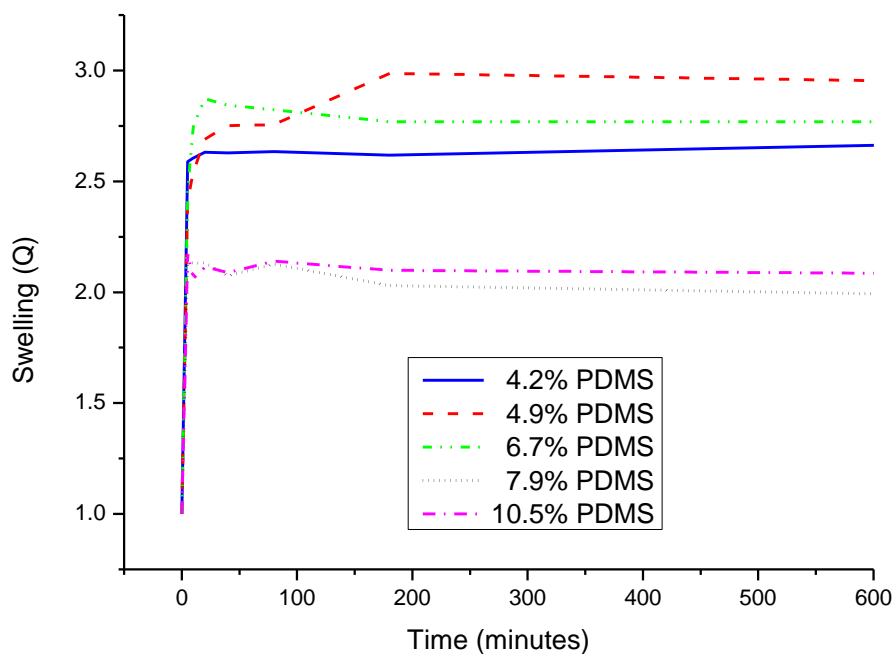
**Figure 4-12:** Swelling of thin film samples in water
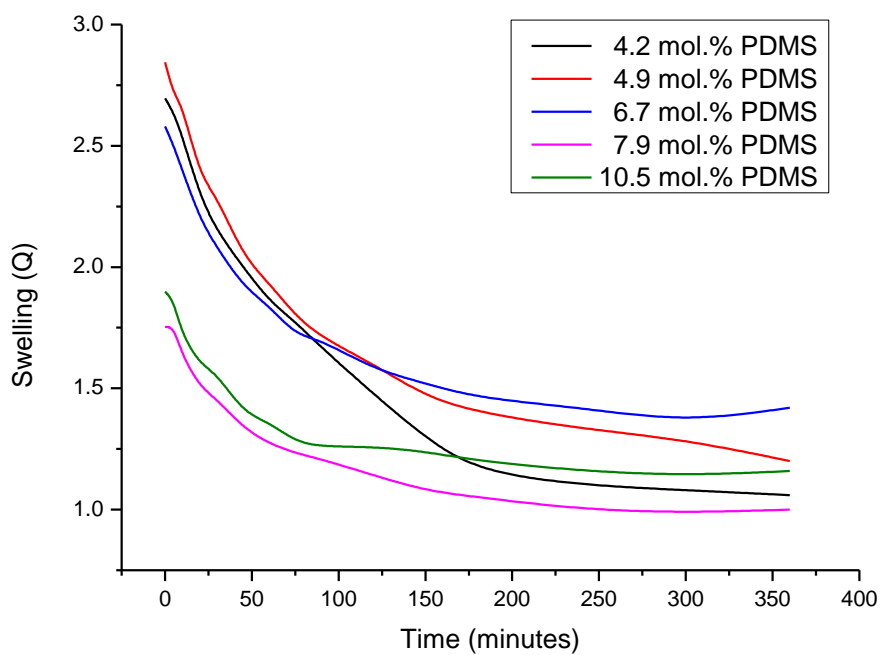


**Figure 4-13:** Deswelling of fully swollen samples under 40% R.H at 25°C.

_____

## 4.2.2 Crosslink density

The swelling of a pure hydrogel is primarily determined by the crosslink density, where an increasing number of crosslinks leads to a decrease in the degree of swelling. As more crosslinking points are added, the ability of the material to expand and absorb water is reduced exponentially, as shown in Figure 4-14.
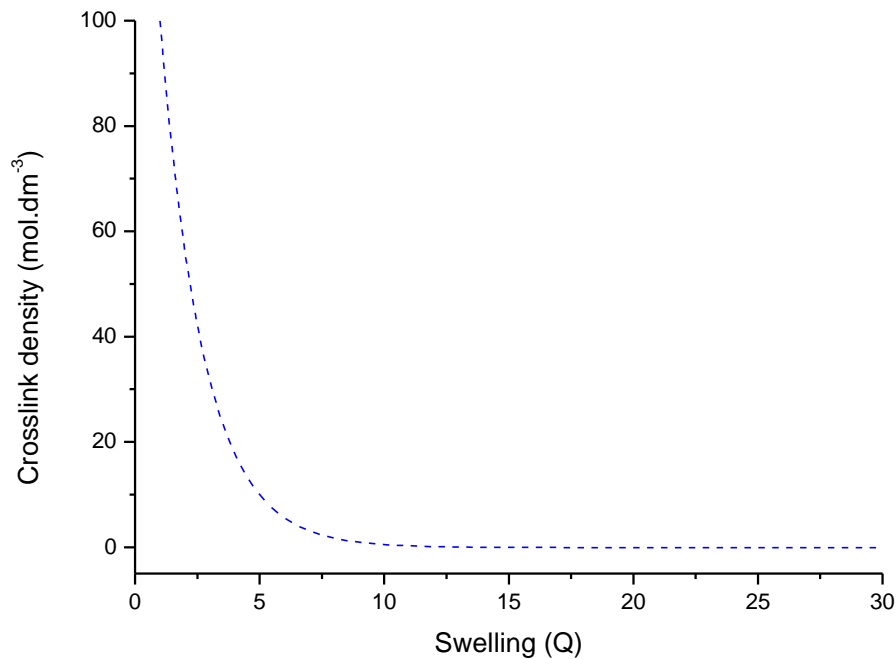


**Figure 4-14:** Crosslinking density vs. swelling, as described by Flory-Rhehner.

Because the system in the current study has physical crosslinks induced by hydrophobic crosslinking, rather than traditional covalent linkages between the polymer chains, the crosslink density for the system determined using the standard models cannot be directly compared against other obtained values in literature. In a traditional crosslinked polymer system, the assumption is that there are randomly distributed inter-chain bonds forming a three dimensional network. In this system, large, periodic domains arise instead due to phase segregation. The results presented here are therefore only for the purpose of showing what effect the PDMS content has on the relative crosslink density of the samples.

Crosslink density may be estimated either through Mooney-Rivlin or the Flory-Rhenher model.[4] The Flory-Rhehner model is used here:

$$-\left[\ln\left(1-v_p\right) + v_p + \chi v_p^2\right] = NV_s\left[v_p^{\frac{1}{3}} - \frac{v_p}{2}\right] \qquad (4\text{-}1)$$

_____

Where $v_p$ is the volume fraction of the polymer in the swollen gel, $\chi$ is the interaction parameter between the polymer and the solvent, $V_s$ is the molar volume of the solvent, and $N$ is the crosslink density in mol.dm$^{-3}$.

The volume fraction of the polymer can be readily determined once the density and degree of swelling of the polymer is known:

$$\text{v}_p = \frac{p_{\text{polymer}}}{[(Q-1).p_{\text{water}}]+p_{\text{polymer}}} \qquad (4\text{-}2)$$

Where $p_{polymer}$ and $p_{water}$ are the densities of the polymer and water under standard conditions, respectively.

Using the Flory-Rehner equation, the listed $Q_s$ values, a $\chi$ value of 0.486 for DMAA as calculated from the work by Gundogan *et. al.*[5] and a density of 1.08 g.ml$^{-1}$, the effective crosslink density of the PDMAA domains was then determined for each sample. These results are visually illustrated in Figure 4-15.
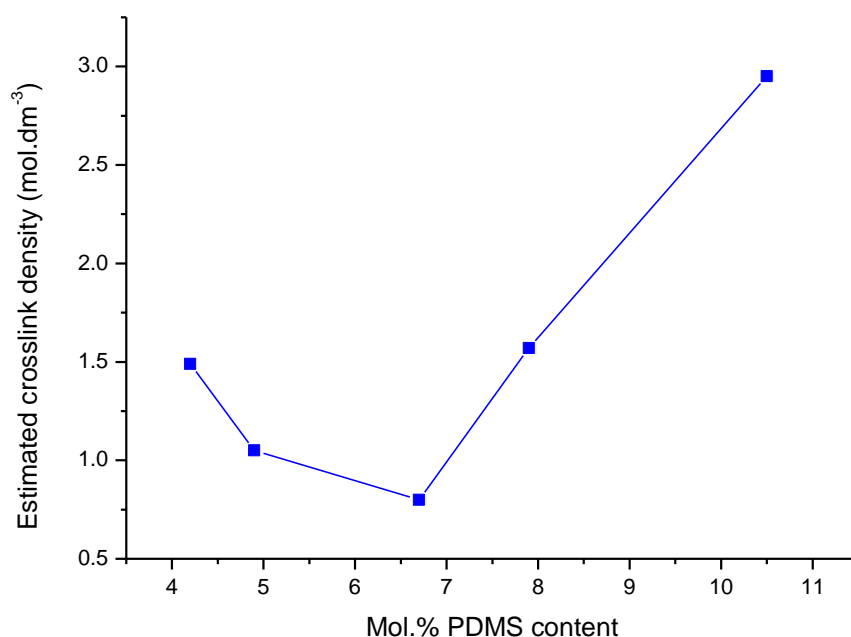


**Figure 4-15:** Effective crosslink density as a function of PDMS content

Less efficient crosslinking is seen in the intermediate PDMS content samples in relation to the amount of PDMS present. Although the 6.7 mol.% PDMS sample contains around 50% more PDMS than the 4.2 mol% PDMS sample, the effective crosslinking density is reduced by nearly half (refer back to Table 4-4). It is worth noting that below a general threshold of 25 wt.% PDMS (3 mol%), the films will break apart when immersed in water; this is presumably because the crosslinking density is not sufficient to prevent dissolution, however because the material is not perfectly homogenous (as will be shown later), some segments remain undissolved.

_____

## 4.3 Preparation of hydrogel nanofibres by electrospinning

Hydrogel nanofibres have been regularly reported throughout literature,[7-9] however relatively few reports exist on the production of non-chemically crosslinked hydrogel fibres. Often, crosslinking is performed after fibre formation by thermal curing, by the addition of a crosslinker after polymerization, or by simultaneous *in-situ* polymerization and crosslinking.[10-12]

The major advantage of the system in the current study is that it remains fully soluble in organic solvents, even after electrospinning, but still remains a hydrogel. This makes it simple to prepare samples for electrospinning, and no additional crosslinking procedures during or after electrospinning are required to produce functional hydrogel nanofibres. Fibres could be readily electrospun from a number of solvents, including THF, acetone, dichloromethane and ethanol. Mixtures of DMF/chloroform were also found to be very effective as electrospinning solvents. However, ethanol was selected as solvent of choice due to its relatively low toxicity and its efficacy. The rapid rate of solvent evaporation is also convenient, since the formed fibres are relatively dry.

A solution concentration of 18% w/v, an electric potential of 15 kV, tip-to-collector distance of 25 cm and a flow rate of 0.03 ml/min were selected as the basic parameters for electrospinning. The average fibre diameters and images of each of the samples is shown below in Figure 4-16. The error bars provide an indication of the fibre diameter distribution in each sample. The average fibre diameter decreases slightly across the series with increased PDMS content, but not by a significant degree. This in contrast to the results observed by Meltz[1] and Bayley[13] for poly(methacrylic acid)-graft-PDMS and poly(acrylonitrile)-graft-PDMS copolymers, respectively. However, in these cases electrospinning was done from solvents that are less compatible with PDMS, and the increasing fibre
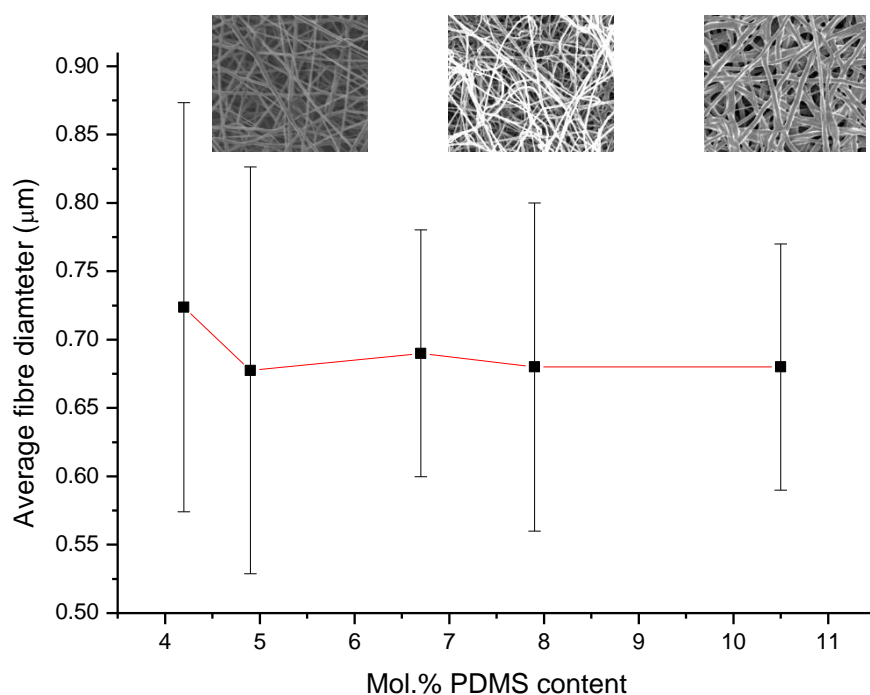


**Figure 4-16:** Average fibre diameter as a function of PDMS content

diameters were ascribed to self assembly of the polymers in the electrospinning solution, which led to an associated viscosity increase with increased PDMS content.

It has previously been noted that porous microstructures can arise in nanofibres made from amphiphilic molecules due to the self-assembly of the molecules in the electrospinning solution.[13] Because the electrospinning process is conducted from ethanol, which is a non-solvent for the PDMS branches, some solution self assembly was likely to occur. However, the reported system with porous morphologies underwent crystallization, whereas PDMAA and PDMS are both amorphous polymers at room temperature. High resolution FE-SEM microscopy (Figure 4-17) showed that the fibre surfaces were smooth, with no morphology or pores visible (note that the grains present are due to the gold coating applied during sample preparation).
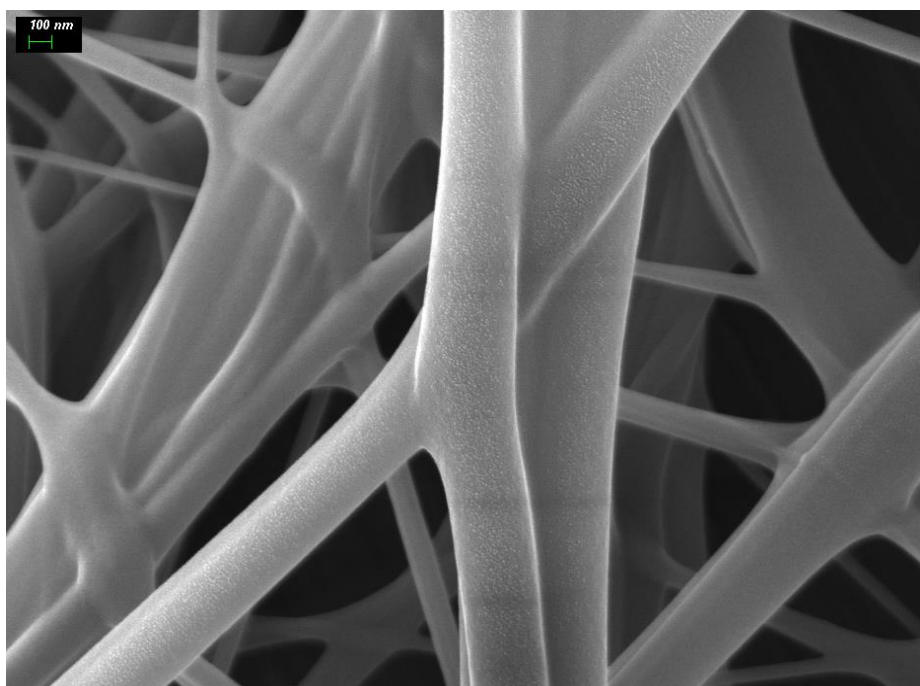


**Figure 4-17:** FE-SEM image of electrospun nanofibre surfaces from the 4.9 mol.% PDMS sample.

To test water stability, the fibres were immersed in water for 1 hour and then dried and imaged. The results are illustrated in Figure 4-18 below. The stability of the fibres is primarily linked to the PDMS content, and the 4.2 mol.% PDMS content sample leaves only amalgamated remnants behind, which shows that the PDMS content is not sufficient to maintain the fibre integrity when swollen.
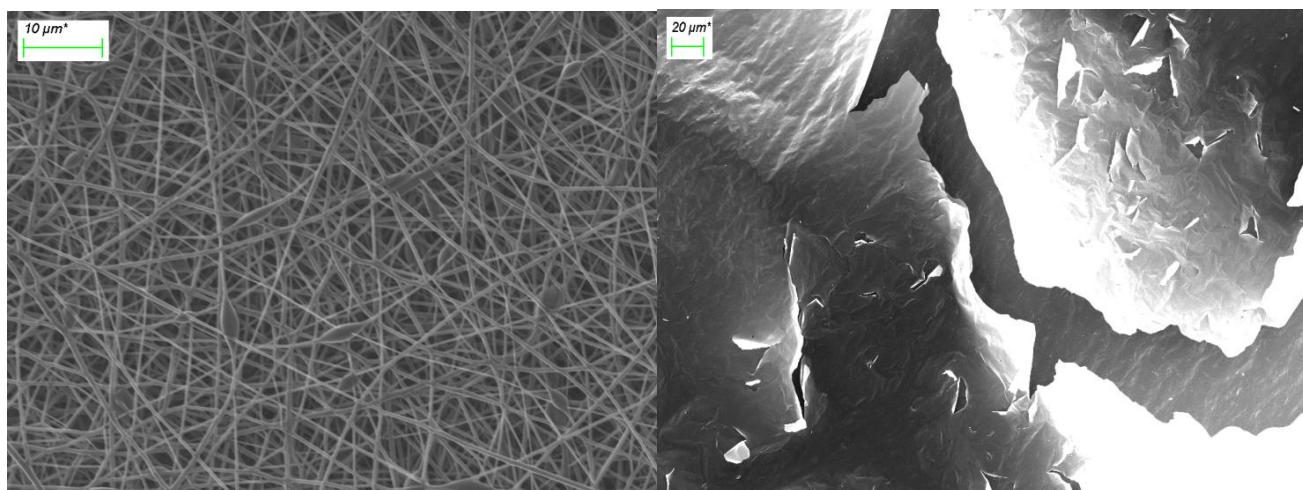
**Figure 4-18**: Nanofibres produced from the 4.2 mol.% PDMS sample before (left) and after (right) 1 hour of water exposure

By comparison, the 6.7 mol.% PDMS nanofibres maintain some integrity, but still tend toward forming a porous film-like surface.
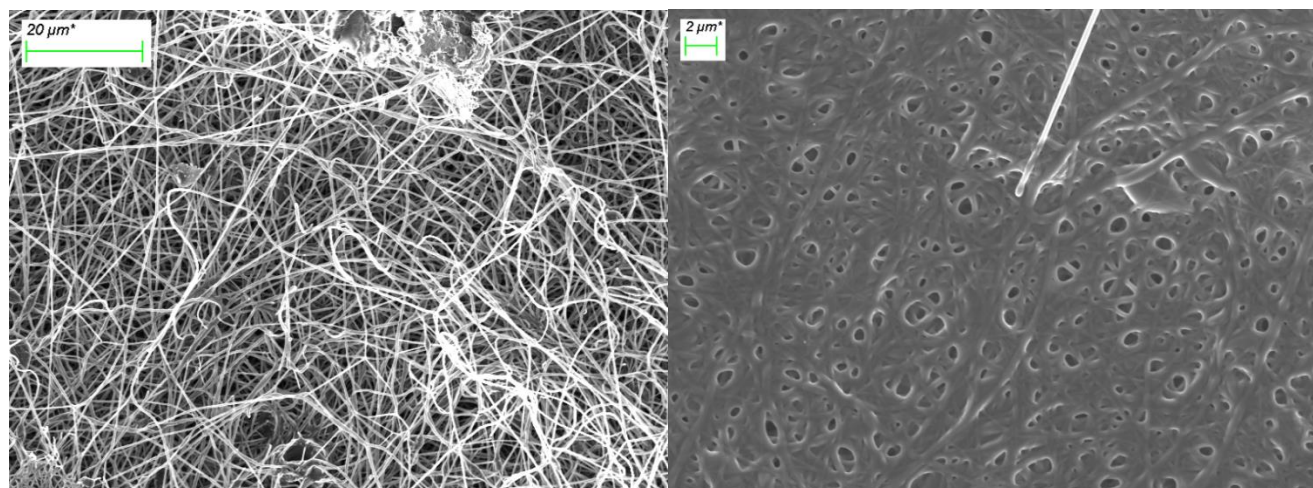


**Figure 4-19:** Nanofibres produced from the 6.7 mol.% PDMS sample before (left) and after (right) 1 hour of water exposure.

The fibre structure is preserved better in the 10.5 mol.% PDMS samples (Figure 4-20), although it is evident that they are still not perfectly stable.

These water stability tests show that although stable hydrogel films can be formed, there is less retention of the fibrous shapes after deswelling due to their high swelling ratios. Simply put, the fibres swell so much that they begin to make contact with each other and fuse together when wet. However, in spite of this, the degree of swelling does not change significantly when they are dried and rehydrated.

_____
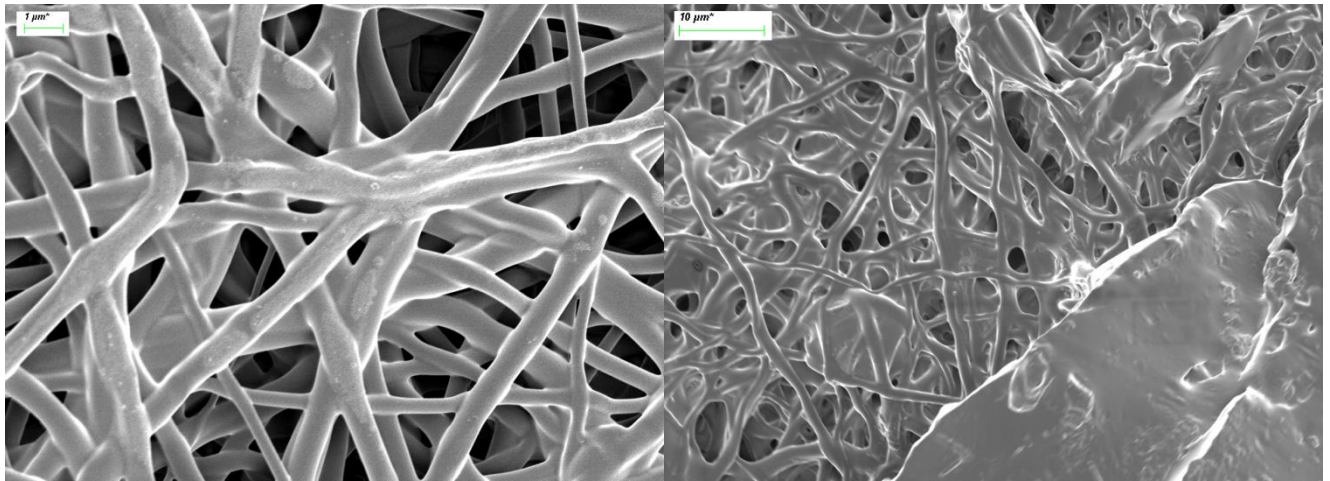


**Figure 4-20:** Nanofibres produced from the 10.5 mol.% PDMS sample before (left) and after (right) 1 hour of water exposure.

_____

## 4.4 DSC analysis

DSC is a useful technique for the detection of various transitions in materials, such as crystallization, melting, glass transitions and other secondary transitions. In addition to routine analysis, the interaction between a material and imbibed solvents can also be elucidated using DSC data.

### 4.4.1 Conventional DSC analysis

Figure 4-21 shows a DSC thermogram of the 4.2 mol.% PDMS sample. PDMAA is expected to exhibit its glass transition at temperatures upwards of 90°C (depending on the molecular weight),[15] while the accepted glass transition temperature of poly(dimethyl siloxane) is known to be at around -120°C.[14] Both of these materials are amorphous at room temperature, since PDMS undergoes its melt transition at around -35°C, and PDMAA is a non-crystalline polymer. The PDMS melting transition is observed in the DSC thermograms as a sharp peak. A weak glass transition can be observed at around 98°C, well within the expected range for PDMAA. A broad, ill-defined peak is seen at around -10°C, and is also present in the thermograms of the homopolymer. In the homopolymer, it is far weaker and less readily observed, and is not addressed in any of the reviewed literature. The origin of this transition remains unclear, but may either be due to the presence of residual moisture in the samples, or due to secondary events such as hydrogen bonding interactions among the amide groups.
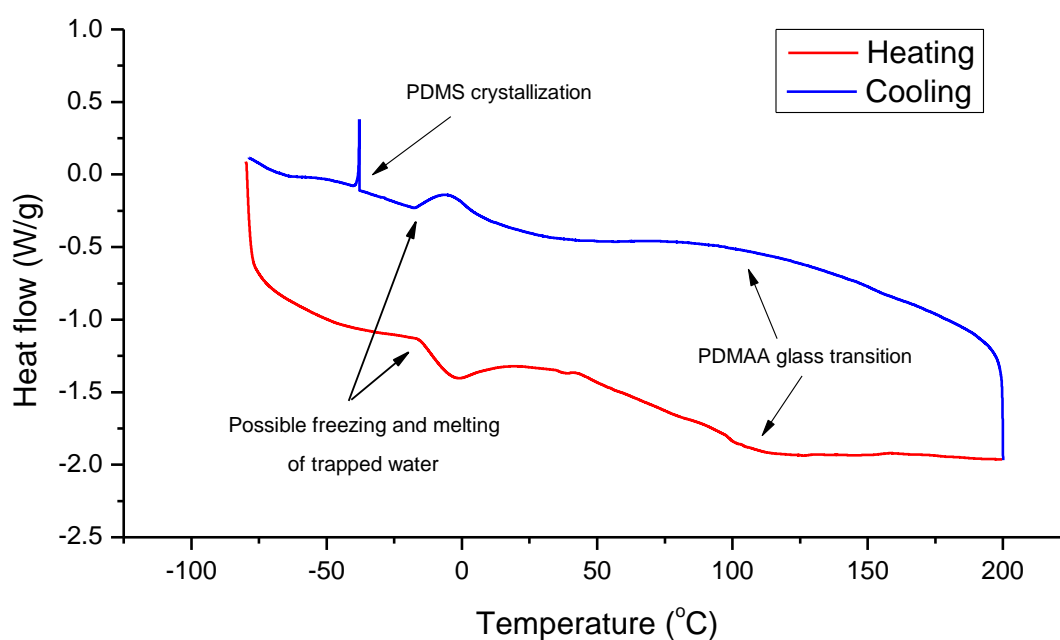


**Figure 4-21:** DSC thermogram of the 4.2 mol.% PDMS sample

_____

### 4.4.2 DSC analysis for water structure determination

Hydrogels generally possess three types of water in their structure: non-freezing water bound directly to the hydrophilic moeities, which remains liquid down to -100°C; freezing bound water, which is loosely bound to the hydrogel but undergoes freezing; and free water, which undergoes freezing and is imbibed primarily through osmosis.[16]  If the fraction of water in the gel is known, the relative amounts of freezing and non-freezing water can be determined from the enthalpy of melting or freezing of the imbibed water:[17]

$$Wfb + Wff = \frac{\Delta H_m}{\Delta H} \qquad \text{or} \qquad 1 - Wnf = \frac{\Delta H_m}{\Delta H} \qquad\qquad (4\text{-}3)$$

Where $Wfb$ is the freezing bound fraction, $Wff$ is the free water, $Wnf$ is the non-freezing fraction, $\Delta H_m$ is the measured enthalpy of melt, and $\Delta H$ is the standard enthalpy of melting of water. Because the melt enthalpy recorded via DSC is determined on a per mass basis, and this inherently includes the weight of the gel as well as the added water; therefore the obtained enthalpy is first divided by the weight fraction of water in the gel, $f_H$, in order to determine the true enthalpy of melt for the imbibed water, where:

$$f_H = \frac{Q-1}{Q} \qquad\qquad (4\text{-}4)$$

$$\text{and} \qquad \Delta H_{actual} = \frac{\Delta H_{DSC}}{f_H} \qquad\qquad (4\text{-}5)$$

A typical DSC thermogram of a gel sample at equilibrium water content (EWC) is presented in Figure 4-22. The exothermic freezing peak does not occur at the expected temperature of 0°C, but rather in the range of -10 to -20°C due to super cooling effects that occur when dealing with small quantities of water.[18] This effect leads to very low reproducibility in terms of temperature based measurements, thus rendering it nearly impossible to determine freezing and/or melting point suppression values of the freezing water fractions interacting with the hydrogel. However, for gels at equilibrium swelling, the enthalpy of melting remains consistent for a given sample. The endothermic melt transition shows two overlapping peaks, one representing the melting of free water near 0°C, and the other at 2.6°C attributed to the melting of freezing bound water. The melt transition of the freezing bound water is shifted upward due to interactions with both the polymer chain and the non-freezing water. In some reports, the cold crystallization of freezing bound water has been found to occur, which provides a convenient method for differentiating between the freezing bound and free water fractions.[31] Such cold crystallization was not observed in these polymers, presumably because the lack of hydroxyl groups leads to weaker interactions between the water and the hydrophilic moieties in DMAA than in the previously reported case citing PHEMA as the system of interest.

_____
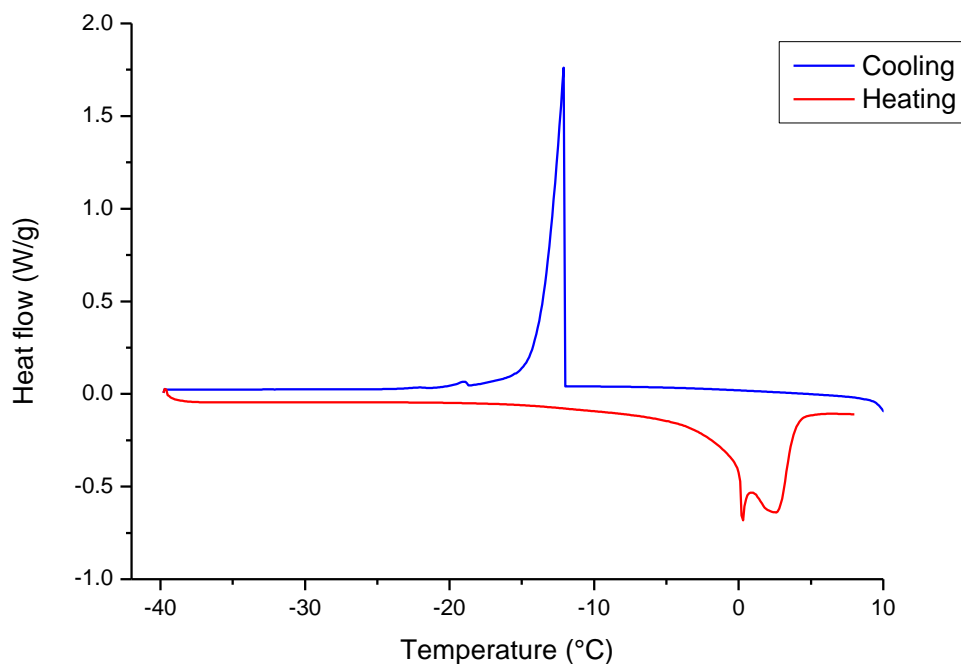


**Figure 4-22:** DSC thermogram of fully swollen 4.9 mol.% PDMS sample.

Because the non-freezing water fraction interacts more strongly with the hydrogel than the free water fraction, it undergoes melting closer to the expected temperature of 0°C, whereas the freezing bound fraction melts at a slightly higher temperature. This results in a bimodal peak structure around the melt transition. In order to differentiate between the freezing bound and free water fractions, peak deconvolution was performed on the endothermic melt peaks. The results of the deconvolution process are summarized in Table 4-6 below.

**Table 4-6:** DSC results and associated data for swollen gels

| Mol.% PDMS | Enthalpy of melt (kJ/mol) | Q of swellable fraction ($Q_S$) | Avg. water molecules per monomer unit | Non-freezing water fraction | W(ff+fb) | Free water as fraction of W(ff+fb) |
|---|---|---|---|---|---|---|
| **0.0** | 196 | 14.2 | 26.8 | 0.37 | 0.63 | -- |
| **4.2** | 112 | 3.81 | 7.35 | 0.45 | 0.55 | 0.740 |
| **4.9** | 106 | 4.41 | 10.8 | 0.50 | 0.50 | 0.697 |
| **6.7** | 84.2 | 4.88 | 14.9 | 0.61 | 0.39 | 0.753 |
| **7.9** | 77.9 | 3.74 | 11.8 | 0.55 | 0.45 | 0.821 |
| **10.5** | 62.3 | 2.99 | 11.3 | 0.56 | 0.44 | 0.788 |

The average number of water molecules bound to each hydrophilic monomer is determined using the equation:[17]

$$n = \frac{99}{18}\left[Q\left(f_H - \frac{\Delta H_m}{\Delta H}\right)\right]$$ (4-6)

Where $n$ is the average number of water molecules. A good correlation in trend is found between $Q_s$ (water in swellable fractions) and the average number of water molecules per monomer unit. Presumably, this indicates a shift in the conformation of the chains that allows for more water molecules to come into direct contact with the acrylamide units.

Figure 4-23 visually illustrates the relationship between the non-freezing water fraction and the PDMS content, and clearly illustrates that a non-linear relationship exists between these two variables due to some change in behaviour that occurs above a threshold PDMS content. This discontinuity has been noted before in the swelling studies.
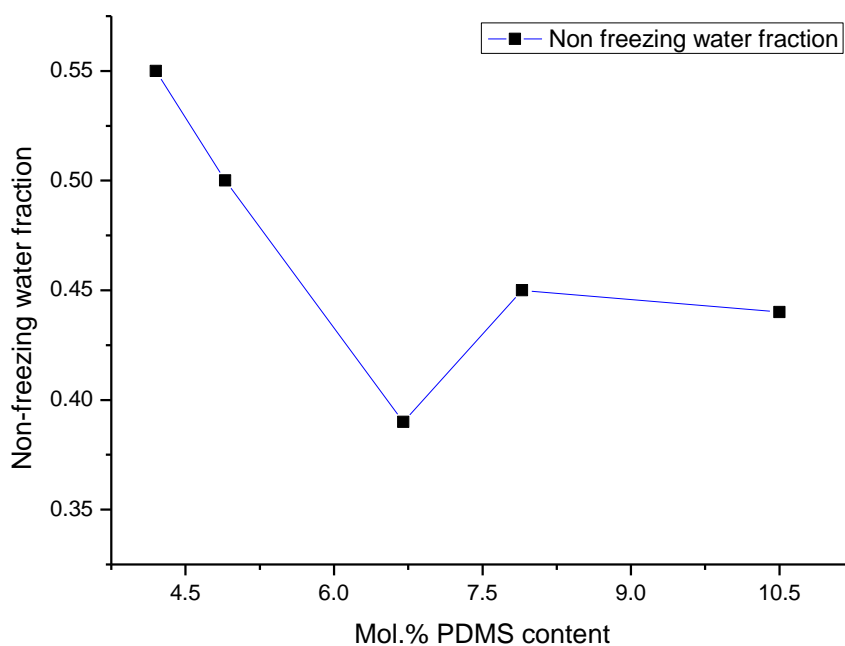


**Figure 4-23:** Variation of non-freezing water fraction with PDMS content.

_____

## 4.5 Effect of the electrospinning process on swelling behaviour

The electrospinning process exposes the polymer solution to large shearing forces in addition to a large electrical current. During casting of films, the slow evaporation of the solvent allows sufficient time for the polymers to reach equilibrium morphology. Electrospinning induces extremely rapid drying of the fibres, and may, therefore, result in the formation of non-equilibrium morphologies that will differ from that of the film state. Films cast directly from ethanol show only very small differences in the degree of swelling, thus providing evidence that it is the process of film (or fibre) formation, rather than the solvent that would induce changes in the morphology. It is thus necessary to investigate the effect of rapid solvent evaporation on the material.

### 4.5.1 Swelling behaviour of nanofibres

Measurements of swelling in the fibre state were conducted under a 75% relative humidity atmosphere and the results are shown in Figure 4-24. In the DSC thermograms of these samples, no peaks were observed, indicating that no freezing (secondary bound) water or free water was present. Therefore, the imbibed water is present only as non-freezing water that interacts directly with the hydrophilic monomer units. The fibres were found to contain marginally more imbibed moisture than the films, but this is expected because of the presence of interstitial spaces in the fibrous structure. Since all of the imbibed water is bound directly to the hydrophilic monomer, the relative fraction of PDMAA primarily determines the degree of swelling under these conditions, and as this is similar in both samples, it is not surprising that the observed difference is relatively small.
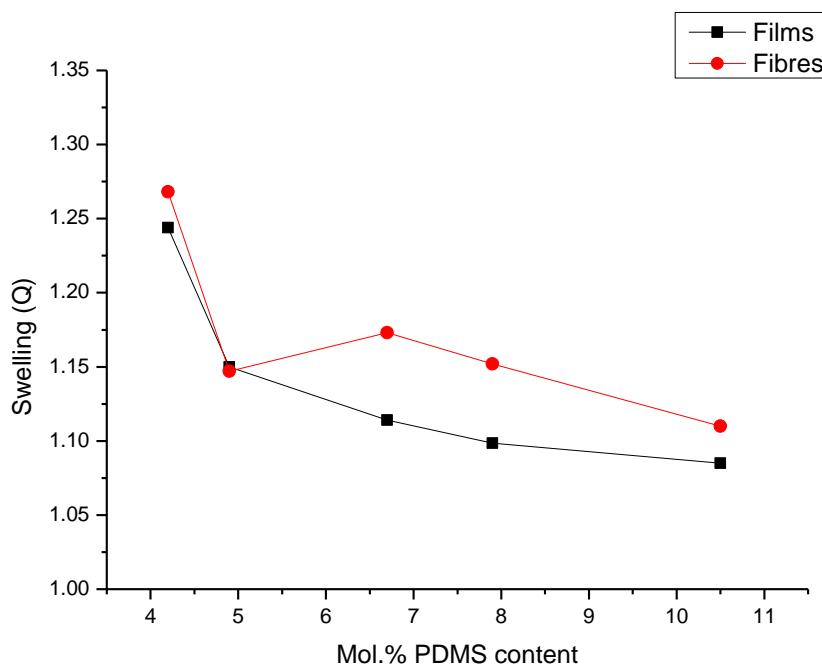


**Figure 4-24:** Comparison of film and fibre swelling at 75% relative humidity

Figure 4-25 shows a comparison between films and nanofibres at equilibrium swelling. Direct measurements of the swelling of the nanofibres using the gravimetric method on equilibrium swollen gels proved to be impractical due to the nature of the swollen gels and the large amount of water trapped in the interstitial spaces between the nanofibres. Thus, to more accurately measure the amount of imbibed water in the fibres, the samples were placed in a small funnel and water was added drop wise until some began to flow out freely. The excess was then allowed to drip off before the fibres were quickly weighed. Large increases in the amount of imbibed water were found, particularly for the samples with the two lowest amounts of PDMS. Because the higher silicone content samples appeared to swell substantially less, it is likely that the majority of the "excess" imbibed water was not simply trapped in the interstitial spaces, but was held in place predominantly by the direct hydrophilic interactions with the monomers. Further evidence for this is provided in the next section.
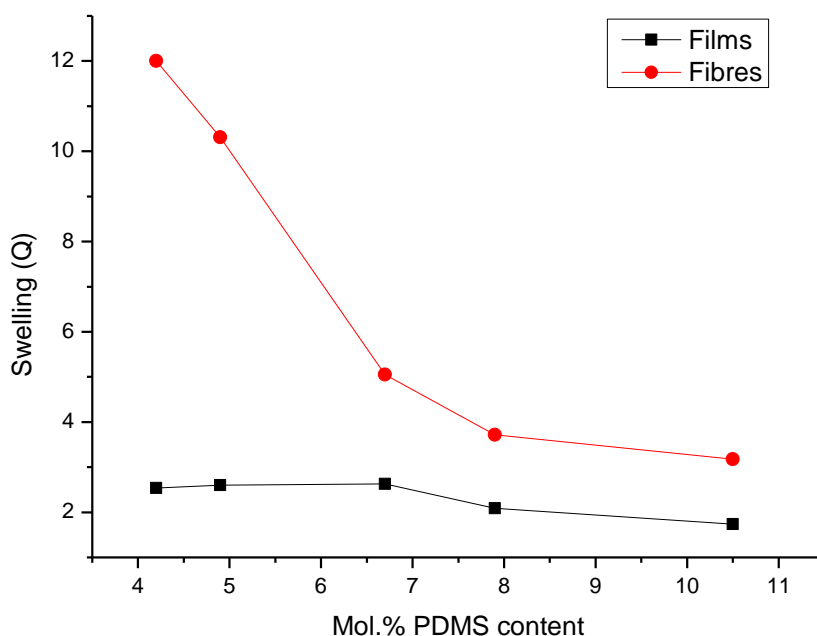


**Figure 4-25:** Swelling in films and fibres at equilibrium water content

As with the films, the fibres underwent very rapid swelling when immersed in water. However, when water droplets were applied to the fibre surfaces in static contact angle studies, the contact angles were surprisingly large and almost resembled that of a hydrophobic surface (Table 4-7). This is due to the trapping of air between the water droplet and the fibre surfaces, but may also be related to surface segregation of the PDMS domains, as suggested by the fact that the PDMS content appears to have no clear correlation to the observed contact angles. The change in the contact angles over time was also determined and this data is presented in Figure 4-26. The fibre surfaces appear to behave in a hydrophobic manner as before, and no clear relationship between the PDMS content and the rate of contact angle decay could be established. This result is somewhat surprising given the high degree of

swelling recorded in the fibre state, however this behaviour appears to be related to the size of the water drops applied to the fibre surfaces, as larger drops are more readily absorbed by the material.

**Table 4-7:** Static contact angles of nanofibre surfaces

| Mol. % PDMS | Contact Angle (θ) | Standard deviation (± θ) |
|:---:|:---:|:---:|
| 4.2 | 114 | 2.5 |
| 4.9 | 124 | 4.6 |
| 6.7 | 125 | 2.0 |
| 7.9 | 112 | 3.4 |
| 10.5 | 116 | 3.5 |
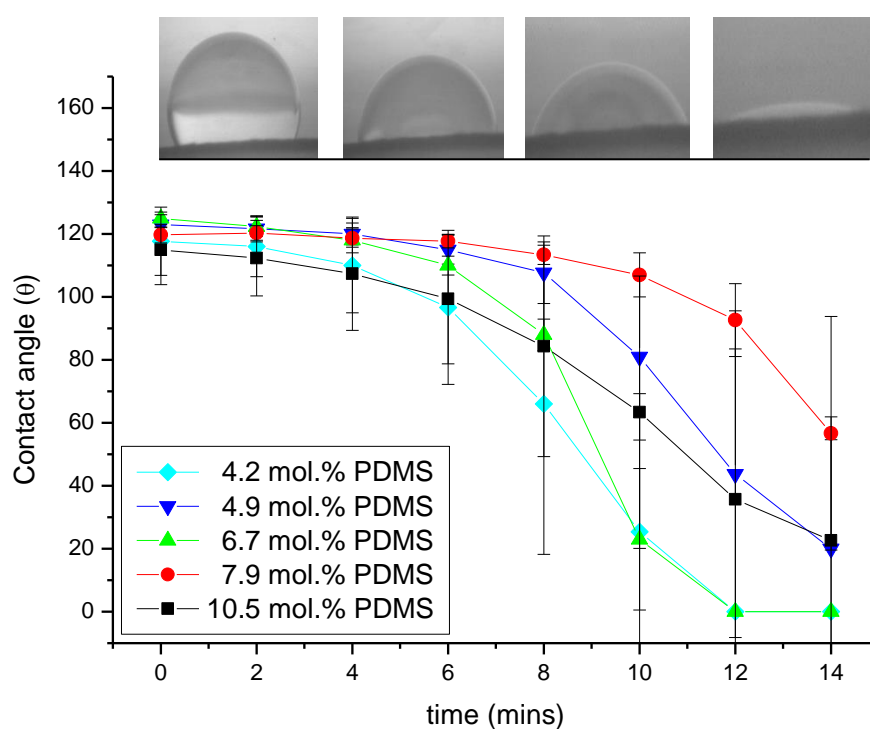


**Figure 4-26:** Change in contact angle over time of water droplets on nanofibre surfaces

## 4.5.2 Water structure in the fibre state

At this point it is necessary to investigate the water structure in the fibres, and how this may differ from that of the films. Comparing the water structure in the film and fibre states can provide insight in to whether there are fundamental differences in the morphology of the films and nanofibres. DSC analysis on fully and partially swollen fibres was used to analyse the relative fractions of freezing and non-freezing water in the fibres. This was then compared to the films.

For both film and fibre samples swollen under 75% R.H, no water related exo- or endothermic peaks are detected by DSC analysis; all of this moisture is thus in the form of non-freezing water. However, the Q values of the fibres are marginally higher than that of the films; this shows that the fibres may be able to hold larger amounts of non-freezing water. In fact, it was found that regardless of how the samples were swollen with water, the fibre samples always contained larger total amounts of non-freezing water. Table 4-8 shows the absolute amounts of non-freezing water in the film and fibre states, as well as the number of water molecules per monomer unit in each material. When the total amount of non-freezing water is calculated for each sample, it is found that the fibres contain more non-freezing water than the films (in absolute terms). Note that non-freezing water can only exist in direct contact with the monomer units, and thus the water in the interstitial spaces will have a negligible effect on this metric. Consequently, the average number of water molecules associated with each monomer must also be higher in the fibre state than in the film state.  It is therefore likely that a significant difference in morphology exists between the films and fibres, and it is concluded that the electrospinning process leads to an enhancement in the swelling of the material. The average number of water molecules associated with each monomer in the 4.2 and 4.9 mol.% PDMS samples is surprisingly high, and appears to exceed even that of the homopolymer. However, direct comparisons between the chemically crosslinked homopolymer and the physically crosslinked graft copolymers should be done with caution.

**Table 4-8:** Comparison of water structure in fibres and films at EWC.

| Mol. % PDMS content | $W_{nf}$ x Q in film state | $W_{nf}$ x Q in fibre state | Water molecules per swellable monomer in films | Water molecules per swellable monomer in fibres |
|:---:|:---:|:---:|:---:|:---:|
| 0.0 | 5.2 | -- | 26.8 | -- |
| 4.2 | 1.3 | 1.5 | 8.42 | 36.9 |
| 4.9 | 1.4 | 3.6 | 11.1 | 34.7 |
| 6.7 | 1.7 | 2.0 | 14.6 | 20.8 |
| 7.9 | 0.97 | 1.1 | 10.3 | 13.6 |
| 10.5 | 0.47 | 1.7 | 7.89 | 13.9 |

## 4.6 Morphology

As previously discussed, the swelling studies show significant discrepancies between the expected behaviour and the actual behaviour of the materials when swollen in water and hexane. The most likely cause for this is the presence of a phase segregated system with morphologies that differ between each sample. It is therefore necessary to explore the structure of the material and how this relates to the observed physical properties. The nature of these domain orderings is particularly relevant in a physically crosslinked system, since aggregation of the secondary domains is the driving force for crosslinking.  Graft copolymers are substantially more complex in their morphology than typical block copolymers, since there are more variables to consider when attempting to predict their morphology. It is not the purpose of this work to fully characterize all of these details, but rather to determine how these configurations affect the material's ability to swell and behave as a hydrogel.

### 4.6.1 Effect of solvent on morphology

Since samples were polymerized and cast from toluene, and electrospinning was done from ethanol, it is necessary to first determine whether any differences in morphology can arise solely due to solvent effects. The first, most obvious approach was the casting of films from ethanol and a subsequent comparison of the degree of swelling. No significant differences in the degree of swelling were observed, indicating that the likely cause for changes in morphology was related more to the kinetics of the drying process than the nature of the solvent used. To prove this, gels were prepared by an alternative method in an attempt to induce a new morphology with superior swelling properties. It was theorized that by precipitating the samples from a polar solvent that mainly favours the hydrophilic backbone, a morphology that allows for a greater degree of swelling in water could be induced.  To this end, samples were dissolved in ethanol and the ethanol was replaced with distilled water by dialysis to slowly precipitate the gels. The results are tabulated below in Table 4-9. The reconditioned gels underwent large increases in their degree of equilibrium swelling, swelling 3 – 10 times more than the normal films. DSC analysis of the superswollen gels showed large increases in the amounts of non-freezing water, indicating that fundamental differences in morphology exist. Although not as striking as the overall increase in swelling, the increase in the non-freezing water fraction again serves to confirm that the morphology of these gels is significantly different to that of

**Table 4-9:** Swelling ratio comparison of normal and reconditioned gels

| Sample | Mol. % PDMS | Q value of reconditioned gel | Normal Q value[a] | Increase in non-freezing water[b] |
|:---:|:---:|:---:|:---:|:---:|
| S1 | 4.2 | 21.5 | 2.54 | 1070 % |
| S2 | 4.9 | 9.93 | 2.75 | 271 % |
| S3 | 6.7 | 9.26 | 2.80 | 264 % |
| S4 | 7.9 | 7.70 | 2.09 | 242 % |
| S5 | 10.5 | 8.55 | 1.74 | 395 % |

a: *Q value of reconditioned gels after drying and rehydration*
b: *Absolute amounts of non-freezing water as determined by DSC for the reconditioned gel compared to normal gels*

_____

the films. Further evidence of this is present when looking at the opacity of the super swollen gels, versus the relative transparency of the dry and rehydrated gels. Figure 4-27 shows photographs of the super swollen, dry and rehydrated reconditioned gels, respectively. After drying, these gels reverted back to normal swelling behaviour, which shows that this morphology is only stable under aqueous conditions, and collapses in the absence of water. To understand how this can occur, it is proposed that these gels should be viewed as a dense emulsion, rather than a solid material. Once the emulsion is dehydrated, the intermolecular distances between the chains decrease rapidly, and the PDMS side chains are able to form new hydrophobic clusters, leading to a rise in the effective crosslink density. Since this conformation is more stable, it will not swell to the same degree when hydrated again. This proves that the solvent itself cannot alter the degree of swelling, but rather that the surrounding environment is responsible, and clearly illustrates that simply dissolving and casting the films from a different solvent under normal conditions will not have an effect on the swelling of the material. Hence, the enhanced degree of swelling of the nanofibres cannot be as a result of the use of ethanol as solvent, but must be related to the rapid drying kinetics of the electrospinning process itself.
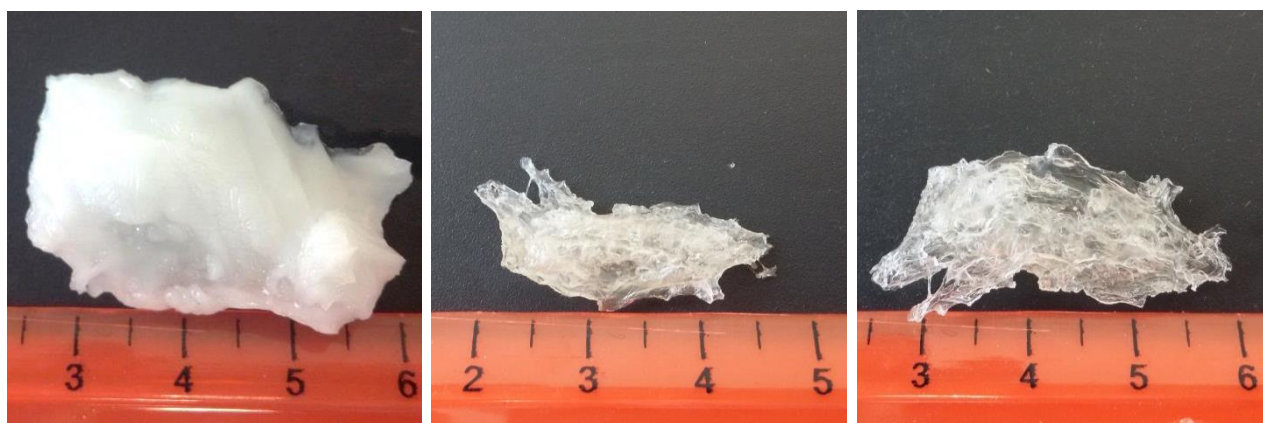


**Figure 4-27:** (From left to right): Reconditioned superswollen 4.9 mol.% PDMS gel; dry reconditioned gel; rehydrated reconditioned gel.

The ability to recondition gels in this manner is particularly interesting, as it shows that under the right conditions, the relatively large amounts of PDMS contained in the samples will not necessarily impede the swelling of the gels. However, unlike the normal swollen gels, the superswollen gels are mechanically weak and difficult to handle without breaking, which is unsurprising given the low crosslinking density of these samples.

_____

## 4.6.2 General deductions from swelling data

It is hypothesized that up to four different morphologies may exist, based on the physical evidence presented up to this point:

- Below ~ 3 mol.% PDMS content, very little crosslinking takes place due to the scarcity of PDMS grafts. This results in weak, water soluble films. Samples are found to break up in water and only small flakes remain undissolved.

- 4.2 – 6.7 mol.% PDMS: The PDMAA domains are sufficiently crosslinked, but the addition of more PDMS results in reduced crosslinking density. The lower crosslink density leads to larger amounts of imbibed water within the swellable domains.

- 7.9 – 10.5 mol.% PDMS: Swelling in the PDMS domains in hexane increases and a large increase in effective crosslinking density is observed in the DMAA domains, leading to reduced swelling in water. The localized swelling in hexane greatly exceeds that of the PDMAA domains in water as the PDMS domains become dominant.

- Fibres prepared by electrospinning: The method of preparation leads to a kinetic morphology with superior swelling properties. PDMS domains are more isolated, and this results in a lower effective crosslinking density. The lower apparent degree of crosslinking means that the materials lose their structural integrity when immersed in water.

It is particularly interesting to note the contrast between the 4.2 and 7.9 mol.% PDMS samples (shown below in Table 4-10), as they have very similar $Q_S$ values (and consequently similar effective crosslinking densities), although the 7.9 mol.% PDMS sample contains substantially more PDMS monomers. This illustrates that domains must be highly separated in the low PDMS content samples, rather than co-continuous. Since the PDMS domains need to permeate the PDMAA to act as crosslinkers, it is likely that most of PDMS is contained inside of isolated domains, and therefore increasing the PDMS content does not lead to an equivalent decrease in swelling. What is also interesting to note is the change in $Z_S$, which is almost negligible for the 4.2 mol.% PDMS sample, but approaches 70 wt.% in the 7.9 mol.% PDMS sample, showing that the PDMS domains undergo a complete morphological rearrangement.

**Table 4-10:** Comparison of 4.2 and 7.9 mol.% PDMS samples

| Sample | Mol.% PDMS | Swelling (Q) | Q of swellables ($Q_S$) | Estimated crosslink density in DMAA domains (mol.m$^{-3}$) | Swelling in hexane (Z) | Z of swellables ($Z_S$) |
|--------|-----------|--------------|-------------------------|-----------------------------------------------------------|------------------------|-------------------------|
| **S1** | 4.2 | 2.54 | 2.99 | 1.49 | 1.08 | 1.31 |
| **S4** | 7.9 | 2.09 | 3.04 | 1.57 | 1.77 | 2.70 |

_____

## 4.6.3 FE-SEM imaging

In an attempt to visually investigate the morphology, freeze fracture experiments were conducted on the swollen gels. In this process, a fully swollen sample is frozen in liquid nitrogen, shattered and then dried. The fracture surface is then analysed by way of electron microscopy. In theory, since the PDMS domains cannot undergo swelling in water, they should thus become visible along the fracture surface as the surrounding PDMAA domains deswell. Due to the hydrogen bonded interactions between water and the hydrogel, the complete removal of water from the material during sample preparation is difficult to accomplish, and this can greatly affect the quality of images obtained via electron microscopy. This effectively limits the maximum resolution to around the 100 nm scale.

Figure 4-28 shows that many distinctive protrusions are observed along the fracture surface of the 4.2 mol.% PDMS sample. This is tentatively associated with clusters of PDMS rich material, and is consistent with previous observations, in that the isolation of the PDMS segments in this manner would lead to very poor swelling in non-polar solvents. However, the interpretation of these images should be treated with some caution as they only represent the "deswollen" collapsed structure after fracture. Nevertheless, the protrusions observed are most likely representative of solvent deficient areas in the microstructure.
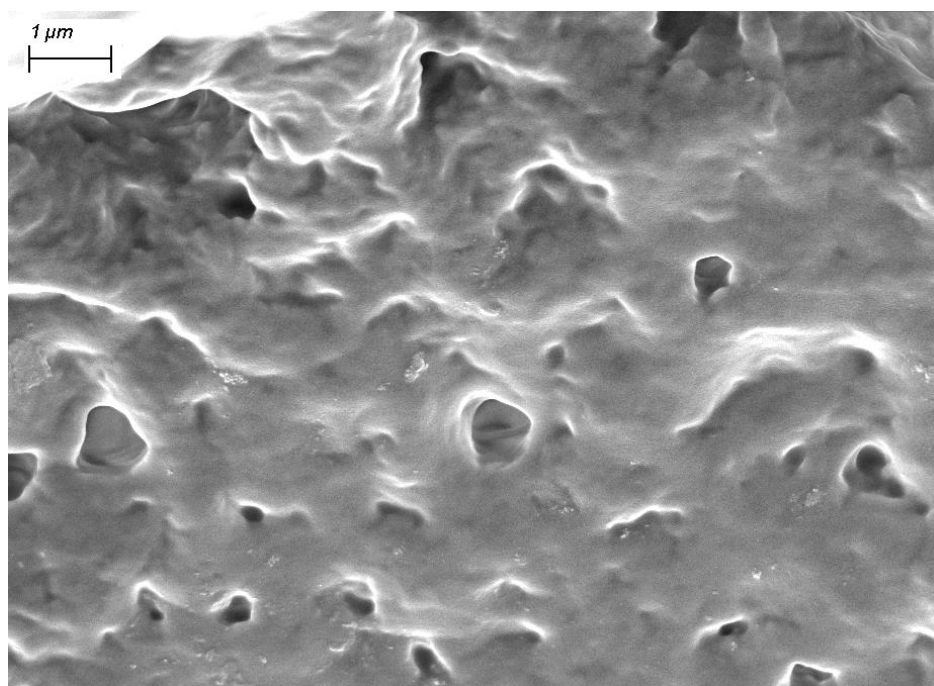


**Figure 4-28:** FE-SEM image of the freeze fractured surface of the 4.2 mol.% PDMS film

In the 6.7 mol.% PDMS sample (Figure 4-29) a similar surface structure is observed, however there are a greater number of protrusions per unit of surface area, which is consistent with the higher PDMS content.
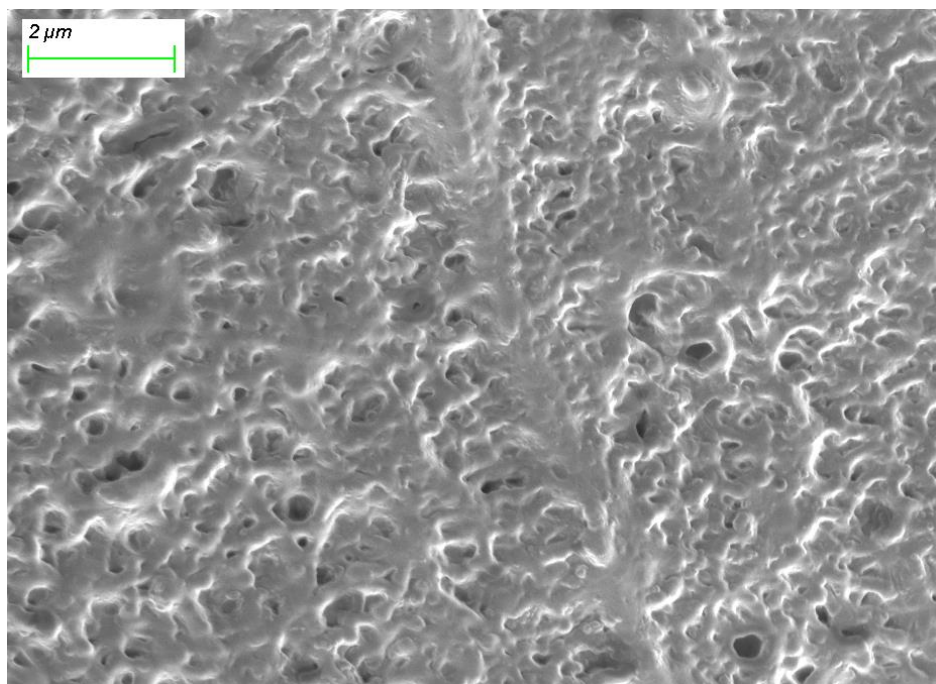
**Figure 4-29:** FE-SEM image of freeze fractured surfaces of the 6.7 mol.% PDMS film

Finally, in the 10.5 mol.% PDMS sample, the surface structure appears smoother and fewer distinct clusters or protrusions are seen. The morphology appears visually different to the preceding samples, and is possibly more homogenous.
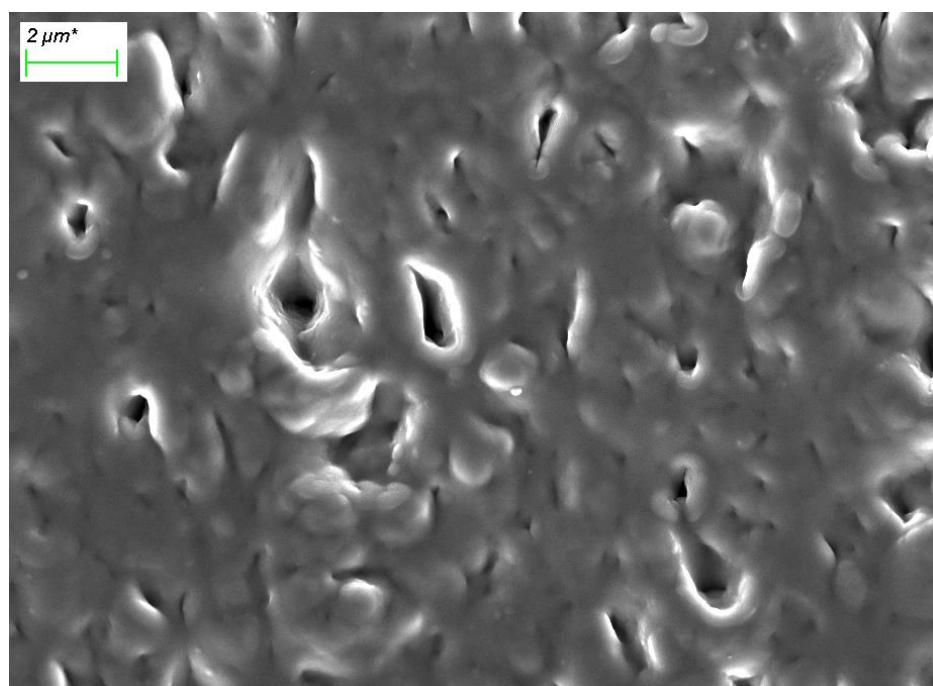


**Figure 4-30:** FE-SEM image of freeze fractured surface of the 10.5 mol.% PDMS film

_____

## 4.6.4 Wide Angle X-Ray Scattering

Although not as useful in its application to polymeric substances as with smaller molecules, WAXD can still provide information regarding the ordering of molecules within a polymeric substrate. Since the copolymer system in question is not crystalline, only broad diffuse amorphous reflections are expected.

Figure 4-31 shows that two distinct XRD peaks can be identified in all of the spectra of the polymers. Only the relative intensities of these peaks are found to vary from sample to sample in the dry state. In a previous study on PDMAA-co-poly(2-(N-ethylperfluorooctanesulfonamido)ethylmethyl acrylate),[22] a physically crosslinked system that also makes use of a hydrophobic copolymer, it was stated that these peaks stem from inter chain correlations among the PDMAA polymer backbone (left peak) and *intra* chain correlations among the PDMAA amide side groups (right peak). Comparing the homopolymer spectrum (black, top) with the copolymer (blue, center), the right peak diminishes in relative intensity. This is presumably due to the presence of the irregularly distributed PDMS grafts that lead to a disruption of the side group structure, reducing the amount of correlation between the amide groups. Most notably, in the nanofibre spectrum (red, bottom), this peak is further suppressed. Considering how rapidly the solvent is removed during the electrospinning process, this result is not unexpected, as the polymer chains have virtually no time to undergo rearrangement, especially given that the glass transition for PDMAA is well above room temperature. No significant differences were observed when the PDMS content was increased. This lower degree of correlation between the amide groups may explain the increased amount of non-freezing water in the nanofibre state, as these groups are potentially free to interact more with the water molecules.
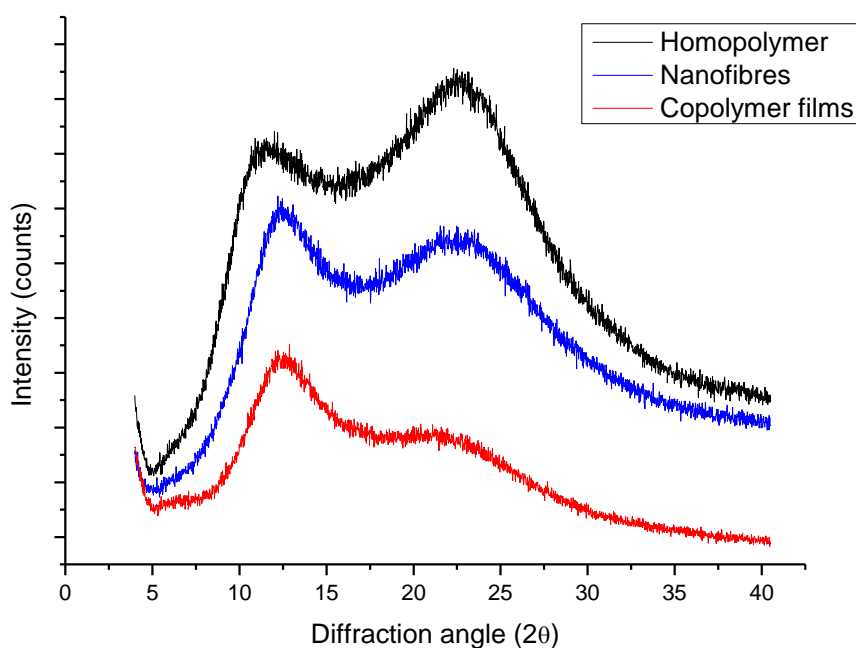


**Figure 4-31:** Wide Angle X-Ray spectra of the homopolymer, film and nanofibres of the 4.9 mol.% PDMS sample.

_____

Wet samples were also analysed in order to determine the effect of imbibed water on the morphology, and the comparisons are shown in Figure 4-32 and Figure 4-33. It is evident that the presence of water in both the films and fibre states leads to some notable changes in the WAXD spectra. The most notable change occurs with regards to the peak associated with the PDMAA backbone, which is suppressed, presumably because the backbone is more hydrophobic and the surrounding water molecules therefore inhibit inter chain interactions.[22] Additionally, the second peak shifts to a higher theta value. Using Bragg's Law, the distance between the groups before and after water absorption can be estimated:

$$2d \, \sin\theta = n\lambda \tag{4-7}$$

Where $d$ is the distance, $n$ is some integer value, and $\lambda$ is the incident wavelength.[24] Before water absorption, this distance in the film state is 0.395 nm, and in the swollen state it is reduced to around 0.331 nm. Niu *et al.*[22] drew similar conclusions, but they were unable to definitively resolve whether the shift in scattering angle stemmed from changes in the backbone correlation, the amide groups or the comonomer used in their study, due to the high degree of swelling in their system which led to the total extinction of the peaks normally seen in the dry copolymer. This apparent decrease in the distance between amide groups is unexpected. We propose that in the swollen state, some of the water molecules may hydrogen bond to more than one amide group, which makes it energetically favourable for the polymer to adopt a more coiled conformation in which the amide groups are closer to one another, at the expense of the polymer backbone.
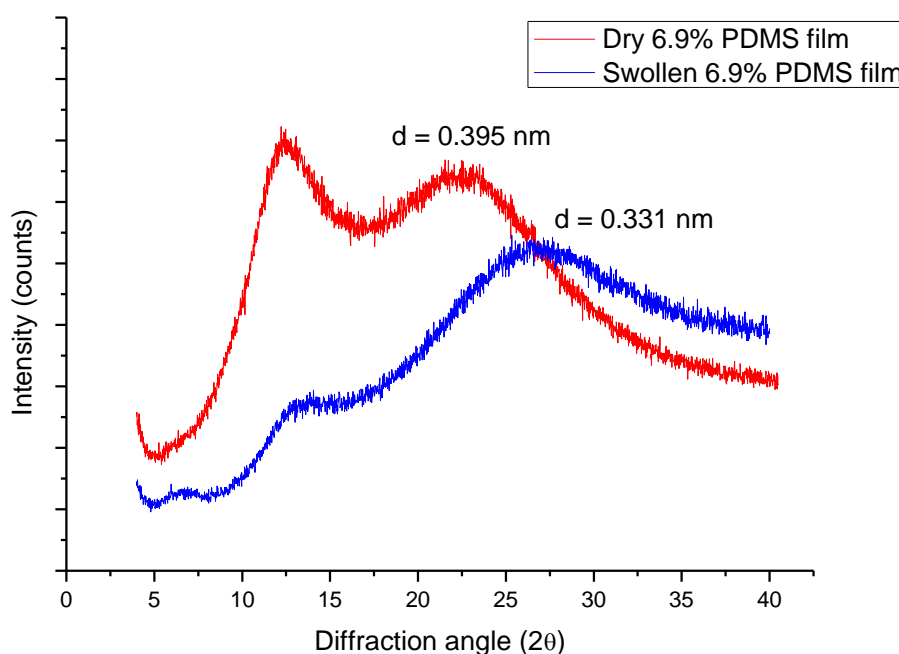


**Figure 4-32:** Effect of water on the XRD spectra of film samples of the 6.9 mol.% PDMS sample

_____
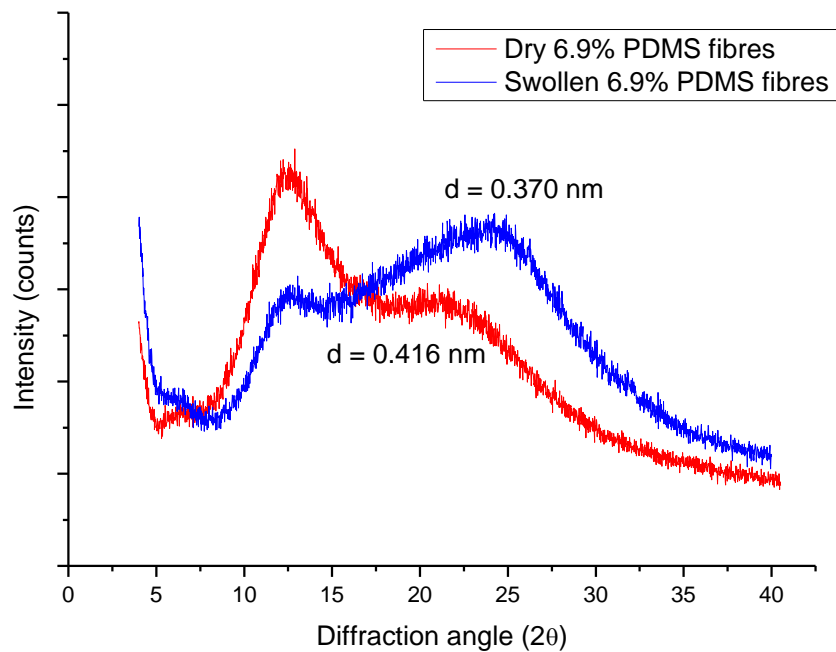


**Figure 4-33:** Effect of water on the XRD spectra of fibre samples of the 6.9 mol.% PDMS sample

Another indication of the difference in morphology between the films and nanofibres in the swollen state can be seen based off of the differing distances with regards to the intra chain correlations of the amide groups, which are longer in the fibre state than in the film state. The reason for this is unclear, however for now it is speculated that this could simply be a consequence of different chain conformations.

_____

## 4.6.5 Solid state NMR

Solid state NMR is a powerful technique in the study of material morphologies, due to its ability to probe interactions on the nanometer scale and identify different domains. In the liquid state, where molecules spin and tumble at intervals that are much faster than the time scale of the NMR experiment, narrow line widths are found as most directionally dependant interactions are cancelled out. In solid state NMR, where the molecules are locked in position, broadening of the peaks occurs as the directionally dependant interactions will affect the signal widths. Consequently, the highly rigid domains, such as crystalline areas, show relatively broad peaks in solid state NMR, while the more flexible and fast moving amorphous domains appear as narrower peaks.[25,27] Energy is transferred within and between these domains by spin diffusion, creating characteristic relaxation times. This can thus be used to detect phase segregated domains.[26] This technique is particularly useful when dealing with so called hard and soft domains, referring to domains below and above their $T_g$, respectively, where the technique can be used to determine the size of the microdomains.[27]

## 4.6.5.1 ^{13}C SP and CP experiments with MAS

Figure 4-34 shows the peak assignments in the solution state ^{13}C NMR spectrum (above) used as reference for the identification of the signals in the solid state ^{13}C SP-MAS NMR spectrum (below).
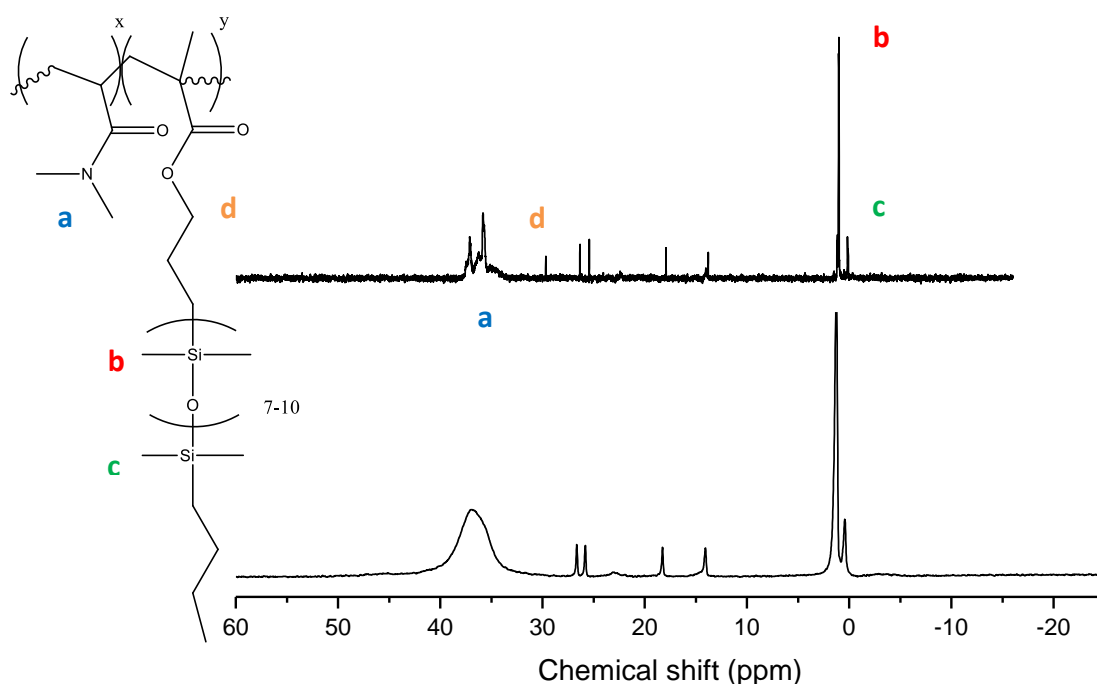


**Figure 4-34:** Liquid state ^{13}C NMR (above) and solid state ^{13}C SP-MAS (below) of the 4.9 mol.% PDMS sample with assignments

_____

The large peak centered around 37.5 ppm results from the methyl groups of the acrylamide, while the peak at 0 ppm originates from the methyl groups of the PDMS, with some fine splitting observed due to the terminal carbon atoms of the PDMS chain. The signals in the range of 30 – 10 ppm originate from the propyl group following the methacrylate in the PDMS macromonomer, as well as the butyl group on the graft chain end. The carbonyl groups appear as a single peak far upfield at 175 ppm (not shown here, see Figure 4-35 below). The narrow signal widths of all peaks associated with the macromonomer indicates that these areas have a high degree of mobility, in contrast to that of the acrylamide methyl groups which are relatively broad. This tentatively indicates the presence of a phase separated morphology in the film state.

Contrasting Figure 4-35 with Figure 4-36, it is seen that significant differences in relative signal intensity exist when the SP (single pulse) and CP (cross polarized) spectra are compared. In the CP experiment, the protons in the sample are irradiated so that their energy can be transferred to the $^{13}$C nuclei, resulting in an improved signal to noise ratio. This process appears to be less efficient in the PDMS phase, possibly due a greater degree of magnetic shielding. The PDMAA signals benefit disproportionately from the CP process, resulting in comparatively weak signals from the PDMS phase. In the SP experiment, the $^{13}$C nuclei are pulsed directly. For the purposes of this study, SP experiments provided clearer spectra, without significantly affecting the signal to noise ratio. However, for advanced experiments, such as the T1ρ relaxation measurements discussed in the next section, SP experiments are impractical due to the excessively long period of time that would be required to obtain results.
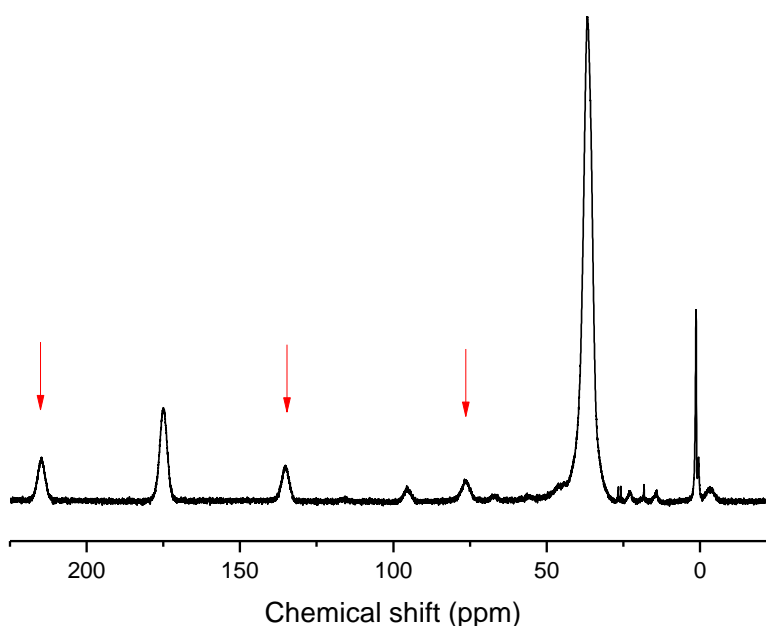


**Figure 4-35:** Solid state $^{13}$C CP-MAS NMR spectrum of the 4.9 mol.% PDMS sample. Spinning side bands are marked with arrows.

An overlay of the SP spectra of the 4.9 and 10.5 mol.% PDMS samples is shown in Figure 4-36. Two distinct differences can be observed. The first is the broadening of the peaks associated with the macromonomer aliphatic chain in the 10 – 30 ppm region, and the second is the splitting in the main PDMS signal which is reduced considerably in the high PDMS content copolymer. Both of these changes are indicative of a less phase separated system in which there is greater interaction between the domains.
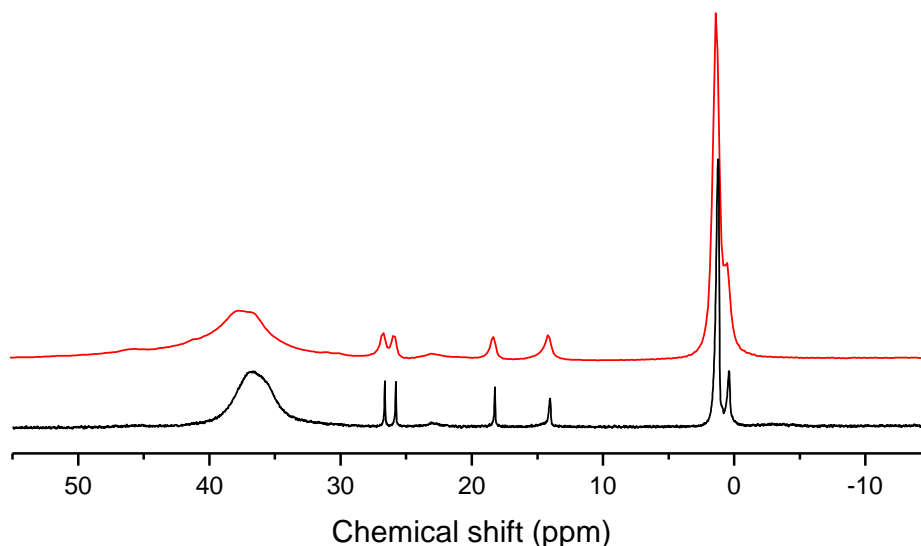


**Figure 4-36:** Comparison of $^{13}$C-SP-MAS spectra of the 4.9 mol.% PDMS (black, below) and the 10.5 mol.% PDMS (red, above) film samples

A comparison of $^1$H wideline spectra between the 4.9 and 10.5 mol.% PDMS film samples is shown in Figure 4-37. The PDMS peak appears narrower in the 10.5 mol.% sample, in comparison to the broader peak in the 4.9 mol.% PDMS sample. In static $^1$H wideline spectra, as in $^{13}$C-MAS spectra, broad peaks are indicative of rigid domains, while narrow peaks indicate soft or mobile domains.[28] Because of the limited spectral resolution in these experiments, the individual components can only be isolated through peak deconvolution. However, it can be seen that the 10.5 mol.% PDMS spectrum is more homogenous and Lorentzian in shape, suggesting more interaction between the domains in the higher PDMS content sample.
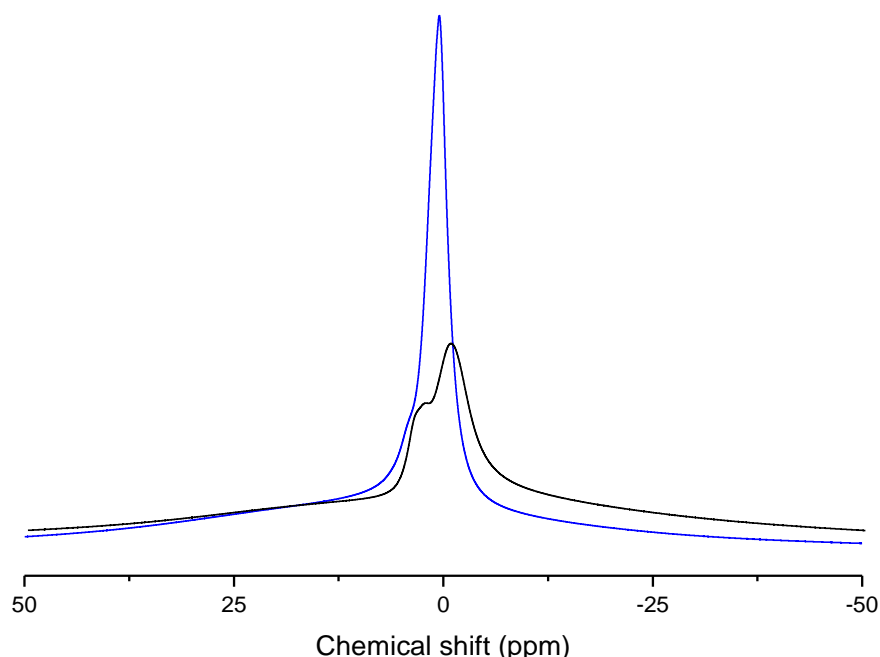
**Figure 4-37:** [1]H wideline spectrum of the 4.9 mol.% PDMS film (black, below) and 10.5 mol.% PDMS film (blue, above)

In the case of the electrospun fibres, the solution state morphology present prior to electrospinning can potentially be preserved due to the rapid evaporation of solvent from the fibres, effectively "freezing in" the morphology.[13] In Figure 4-38 the nanofibre and film state spectra of the 4.9 mol.% PDMS sample are compared. It is noted that the nanofibres show broader peaks associated with the PDMS domain, which is indicative of restricted motion in these domains.[25] Interestingly, an additional peak is observed at 29 ppm, just below the acrylamide moiety. This appears in both the 4.9 and 10.5 mol.% PDMS fibre spectra, but is absent in the film spectra. This was previously assigned to the carbon atom adjacent to the methacrylate group (Figure 4-34). Careful analysis of integrals indicates that this peak was previously concealed by the larger peak at 35 ppm; in the fibre state it becomes more shielded and consequently appears further downfield. It is tentatively proposed that the presence of this peak in the nanofibre state is therefore due to shielding by the electron clouds from the methyl groups on the amide. In the film state, these two groups are thus not in close enough contact for this phenomenon to occur. In terms of morphology, this implies that the polymer chains may be more coiled in the film state, as they attempt to maintain the most thermodynamically favourable conformation. In turn, this leads to more efficient crosslinking, since the PDMS grafts are able to bundle together and form larger clusters. Since ethanol is a non-solvent for the PDMS branches, the most likely solution conformation is micelle like structures. Upon removal of the solvent during electrospinning, these PDMS domains remain isolated inside the micelles and do not undergo much interaction with each other.

_____
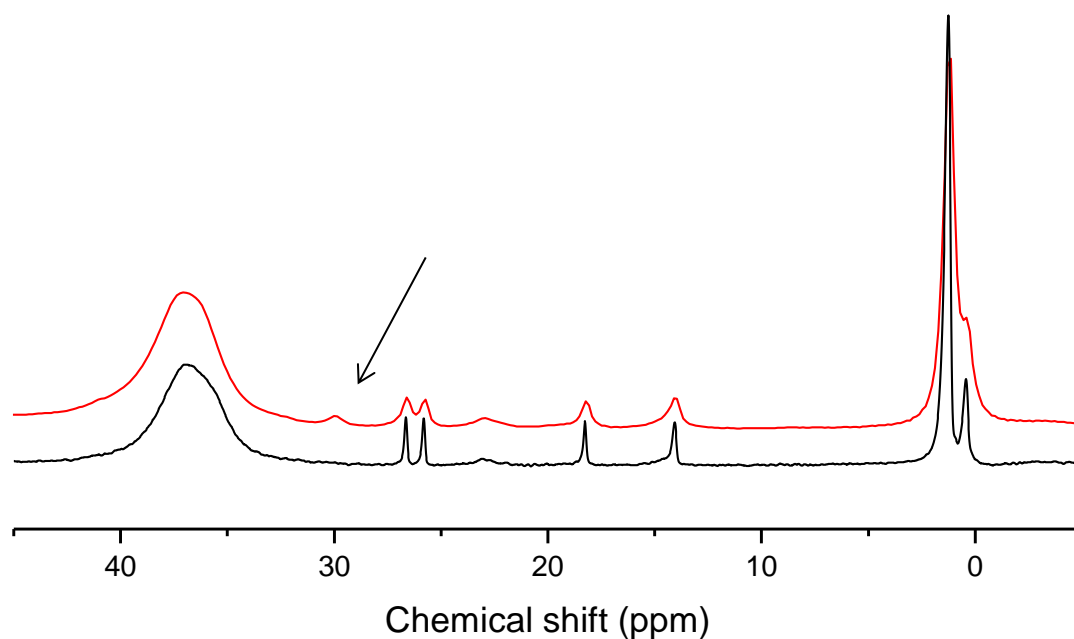


**Figure 4-38:** [13]C SP-MAS spectra of nanofibres (above) and film (below) of the 4.9 mol.% PDMS sample

In Figure 4-39 the ^{1}H wideline spectra of the nanofibre and film state are compared. As before, it is shown that the film state has a more phase separated morphology, with a sharp (mobile) peak and a broader (rigid) base peak, while the fibre state shows a more homogenous peak with less clearly defined components. Peak deconvolution (inset) indicates two main peaks present, originating from PDMS segment near 0 ppm, and the methyl groups of the acrylamide near 3 ppm.
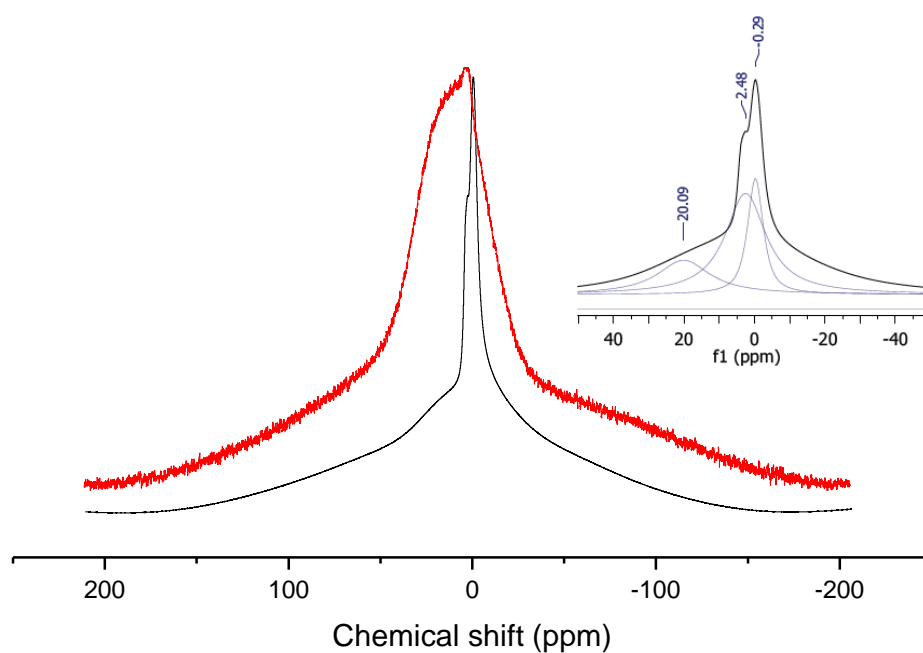


**Figure 4-39:** [1]H SP-MAS spectrum of 4.9 mol.% PDMS films (black) and nanofibres (red). The inset shows the deconvoluted peaks of the film spectrum.

_____

## 4.6.5.2 $^1$H T1ρ relaxation experiments

Peak intensities of the main acrylamide peak and the main PDMS peak were plotted as a function of relaxation time to produce T1ρ relaxation curves.  A three parameter exponential decay curve was then fitted to each data set, with the general formula

$$y = A + Be^{-\frac{t}{x}}$$
(4-8)

Where $x$ is the T1ρ relaxation time. The T1ρ relaxation curves for 4.9 mol.% PDMS film sample are shown in Figure 4-40. For the acrylamide moiety, the T1ρ relaxation time is substantially longer than that of the PDMS domain, which indicates phase separated domains within the film on the nanometer scale, under the assumption that the rate of spin diffusion is sufficient.[19] In other words, it is assumed that the different chemical components are able to interact with each other and exchange energy so as to lead to a common relaxation time. If this holds true, any significant difference in relaxation time must be due to physical segregation of the domains.[27]
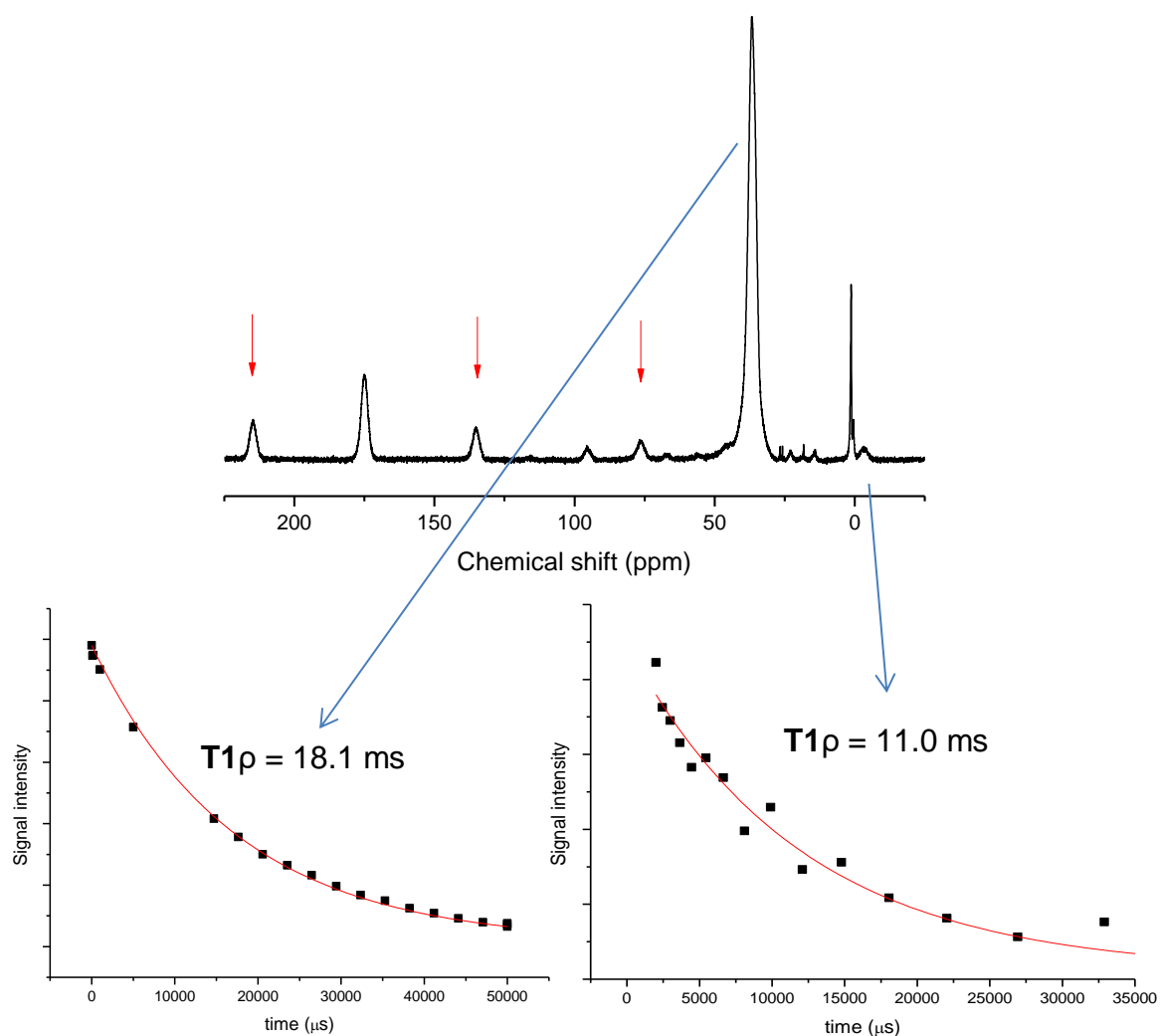


**Figure 4-40:** T1ρ relaxation curves of the acrylamide and PDMS peaks for the 4.9 mol.% PDMS film sample

_____

Because this data had to be obtained using CP rather than SP (which does not distort the signal intensity), the relative signal intensities for the PDMS domains are substantially lower and lead to some degree of uncertainty in the data. However, it is clear that the initial rate of decay is much higher in the PDMS domains. Additionally, multiple types of relaxation experiments were used to confirm these results, and in all cases the PDMS domains show relaxation times that are at least 40% shorter than that of acrylamide domains.

It is visually illustrated in Figure 4-41 that the relaxation time undergoes changes with increasing silicone content. The 10.5 mol.% PDMS sample shows a rapid decrease in the signal intensities of the acrylamide moiety. This data suggests that the PDMS in the 10.5 mol.% sample is in more intimate contact with the PDMAA domains, leading to rapid polarization transfer, and thus the difference between their respective T1ρ times is greatly reduced (see Table 4-10). This result is counter intuitive, as it indicates a reduced degree of phase separation for the 10.5 mol.% PDMS content sample, in contrast to what would normally be expected for a system comprised of immiscible polymers when the composition is altered to include a larger amount of the second monomer.
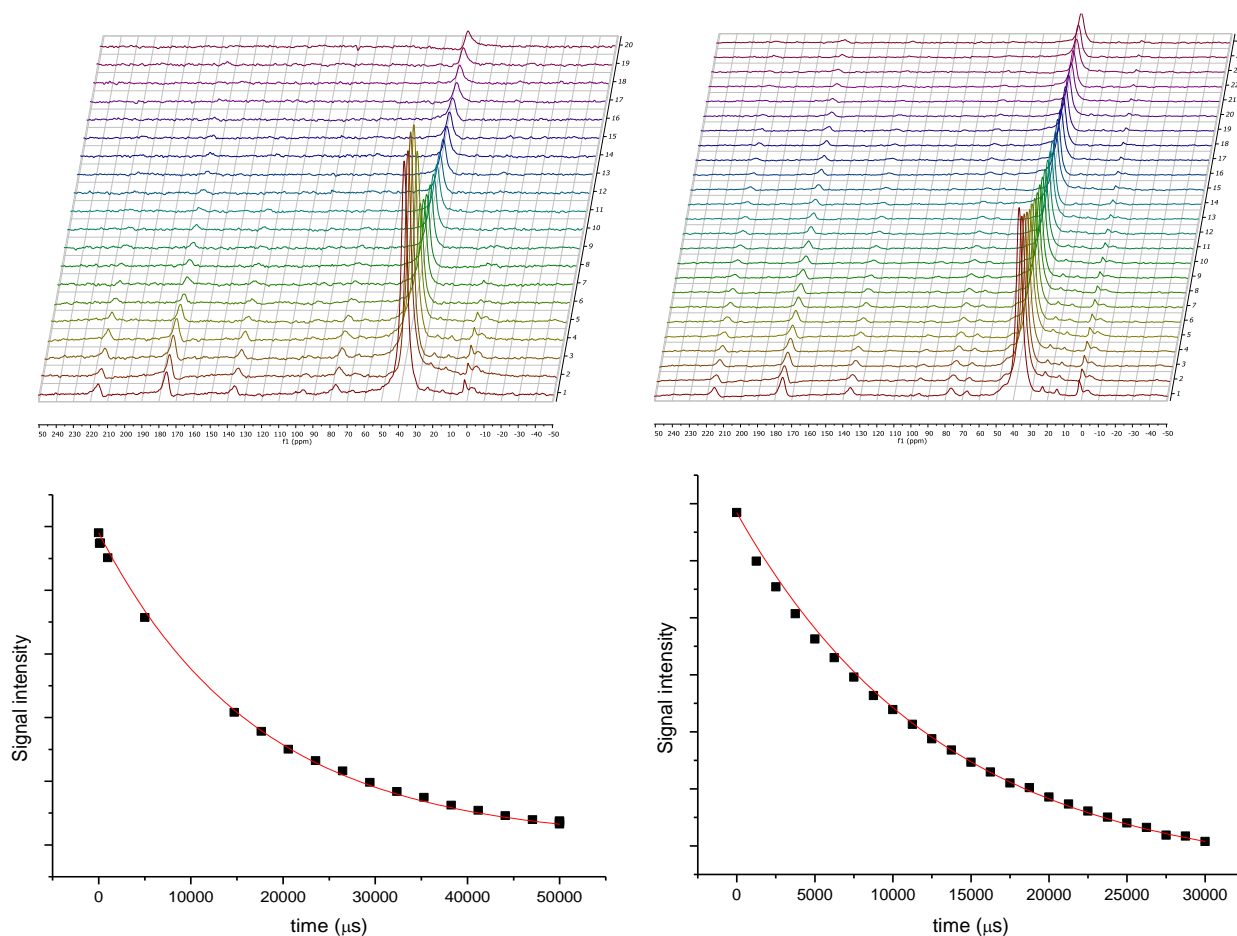


**Figure 4-41:** Effect of rising PDMS content on the T1ρ relaxation in the acrylamide region of the 4.9 mol.% PDMS sample (left) and the 10.5 mol.% PDMS sample (right)

_____

The next key point is to determine whether any difference can be observed for the nanofibres with regards to the relaxation data. It was theorized that the PDMS domains are more isolated in the nanofibre state, resulting in a visible broadening of the peaks associated with the macromonomer. Evidence for this change was present in the swelling studies, which showed a lower effective crosslink density and subsequently implied that the PDMS domains present are likely to be smaller and more isolated. This is rationalized by considering that there is insufficient time for the rearrangement of the PDMS domains in the nanofibre state, leading to isolated domains which are in more intimate contact with the surrounding acrylamide. In terms of relaxation time, some convergence between the two domains is thus likely to be observed.

The full set of calculated $T1\rho$ data is shown below in Table 4-11. Comparing the 4.9 mol.% PDMS film sample with the corresponding fibre sample shows significant shifts in the relaxation times of both the PDMS and methyl acrylamide peaks, with a 1.5 ms increase for the PDMS group and a 2.5 ms decrease in the acrylamide group, in agreement with both the swelling data and theoretical expectations. Given that the film state 10.5 mol.% PDMS sample already shows a significant degree of convergence in the relaxation times, it is unsurprising that the domains in the nanofibres of this sample have nearly identical relaxation times.

**Table 4-11:** $T1\rho$ values of functional groups per sample
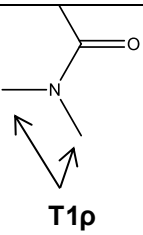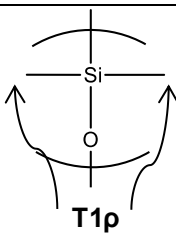
| Sample | $T1\rho$ | $R^2$ value of fit | $T1\rho$ | $R^2$ value of fit |
|---|---|---|---|---|
| 4.9 mol.% PDMS film | 18.1 ms | 0.99953 | 11.0 ms | 0.9291 |
| 4.9 mol.% PDMS nanofibre | 16.6 ms | 0.99939 | 11.7 ms | 0.9820 |
| 10.5 mol.% PDMS film | 13.0 ms | 0.99886 | 9.74 ms | 0.9876 |
| 10.5 mol.% PDMS nanofibre | 9.77 ms | 0.99694 | 9.29 ms | 0.9985 |

Solid state NMR data therefore provides conclusive evidence of large differences in the morphology of films containing different amounts of PDMS, and more importantly, key differences between films and nanofibres of the same sample.

## 4.6.6 Conclusions regarding morphology

It has been shown that the samples undergo a significant degree of phase segregation and that this leads to unexpected swelling behaviour. Before drawing conclusions about the behaviour of the copolymer system, it must be acknowledged what effect the presence or absence of water within the system can have on the observed morphology. The work by Niu *et al.*[22] illustrated from WAXD and SAXS spectra that physically crosslinked triblock copolymer systems underwent reversible changes from lamellar to hexagonal microstructure conformations, and similarly in this work it was shown that notable changes in peak intensity and some minor shifts occur in XRD experiments when swollen samples are used. However, in many experiments the use of fully swollen gels is simply not feasible. In solid state NMR, moisture within the samples leads to rapid loss of polarization and greatly distorts the obtained spectra because the imbibed water interacts almost exclusively with the hydrophilic moieties. In FE-SEM, the absolute vacuum required for imaging entirely precludes the use of even partially moist samples. This leads to an impasse, where it is difficult to fully characterize both states. However, it has been shown that the swelling studies and "dry" analytical techniques have generally been in strong agreement with one another. The difference between the wet and dry states, therefore, cannot be very significant since there are few inconsistencies in the overall data.

It was cited that a likely reason for the initial decrease in effective crosslinking density in the 4.2 – 6.7 mol.% PDMS samples may stem from localization of the PDMS rich polymer chains as observed under FE-SEM. However, this would only account for why the crosslink density does not increase further. In other words, it offers no real explanation for why a decrease is encountered. The best possible explanation comes from considering the effect of the grafts on the polymer chain conformations and the intermolecular distances. From the work of Ma *et al.*,[20] it was shown by means of Small Angle X-ray Scattering (SAXS) that the average inter domain distance between polymer chains increases with increasing graft density. Consequently, because the PDMS grafts in this system are relatively short and need to overlap with each other to act as crosslink points, an increase in these distances could hinder their ability to interact with each other, and therefore an overall decrease in crosslink density is observed. Given that the effective crosslink density nearly halves between the 4.2 and 6.7 mol.% PDMS samples, this serves to explain why the localized swelling in the PDMAA domains increases in spite of the increased amounts of hydrophobic monomers.

Above the 7.0 mol.% PDMS threshold, a morphological transition is seen to occur that leads to a decrease in swelling, and from solid state NMR data it was shown that the degree of phase separation appears to decrease greatly, with similar T1ρ relaxation times in both domains. This is indicative of a relatively homogenous system. FE-SEM images of the freeze fracture surface support this, showing fewer isolated PDMS rich domains present along fracture surfaces than in the lower PDMS content samples. This result is counter intuitive, and may merely be an artefact caused by the relatively large weight percentage of PDMS present in the samples. However, given the data at hand and a lack of evidence to provide a counter argument, for now it must be concluded that the 7.9 and 10.5 mol.% PDMS samples are less phase segregated than the lower PDMS content samples.

_____

In the fibre state, the micelle like structures that were present in solution before electrospinning are preserved, with the PDMS branches primarily facing toward the interior of the micelles. When the solvent is rapidly removed, these structures do not have time to reorganize, and consequently the PDMS branches remain isolated from each other, thus leading to a low effective crosslink density. This leads to the high degree of swelling observed in the fibre state, and the subsequent loss of structure when the fibres are immersed in water. Solid state NMR data confirms this in the case of the low PDMS content sample. However, the $T1\rho$ data shows that the PDMS and PDMAA domains converge for the 10.5 mol.% PDMS sample, indicating a continuous network. The difference in swelling between the films and fibres of 10.5 mol.% PDMS sample, in comparison to the 4.9 mol.% PDMS sample, corroborates this data. It is therefore apparent that the initial structures present in solution before electrospinning may differ for the two samples, and given the PDMS content, this is not at all surprising. A larger investigation into how the solvents used for electrospinning can be used to tailor the crosslink density is required, however this is beyond the scope of this work at present, and is discussed further under the future work section in Chapter 5.

_____

## 4.7 Physical properties

A common problem with physically crosslinked hydrogels is that they have poor mechanical properties. In the dry state, the hydrogel may be brittle, depending on its glass transition temperature. For the system at hand, the addition of PDMS provided a significant improvement in the physical properties of the material, due to silicone's elastic properties and extremely low glass transition temperature. Tensile testing was conducted on dry and moist gels to quantify the effect of these variables on the mechanical properties.

Tensile test results are shown in Figure 4-42. The addition of PDMS led to an improved yield strength and higher load at break in comparison to the homopolymer samples. The homopolymer samples also showed almost no recovery following elongation, whereas the PDMS containing samples contracted again after the load was removed. Comparisons between the copolymers containing varying amounts of silicones showed that the increase in silicone content did not necessarily result in a linear improvement of physical properties. Instead, it was found that the 6.7 mol.% PDMS sample exhibited a significantly higher load at break; the reason for this remains unclear.
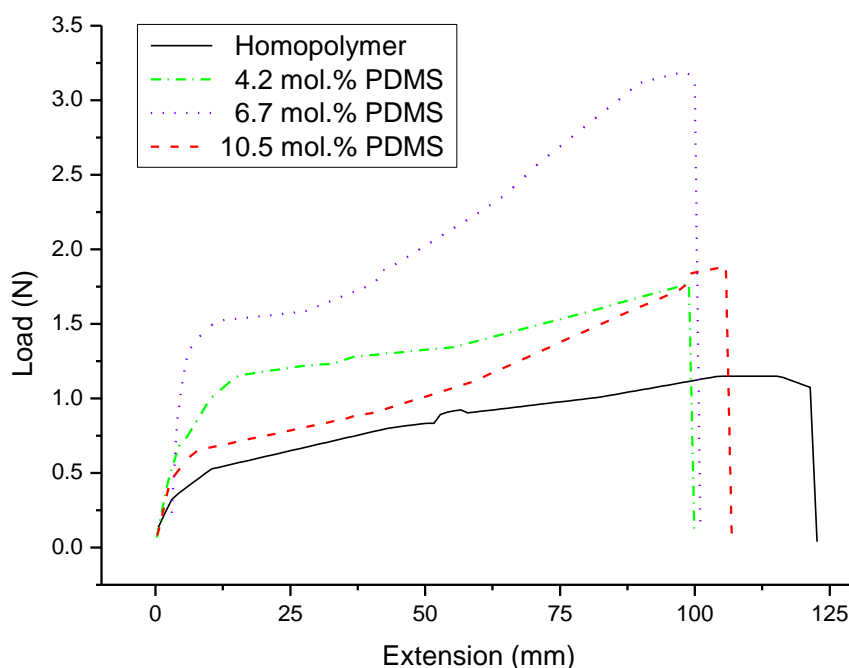


**Figure 4-42:** Comparison of tensile test results of samples equilibrated at 75% R.H.

The elastic behaviour is highly dependent on the ambient humidity, with the samples varying between rubbery and glass-like behaviour.  This phenomenon is due to a plasticizer-like effect brought about by the presence of water molecules between the chains, resulting in increased spacing between the molecules, and consequently more free movement. This result is presented graphically in Figure 4-43. Below 20% relative humidity, samples containing low amounts of PDMS undergo near instantaneous

_____

brittle failure, whereas at 75% relative humidity they undergo significant elongation. This effect is less pronounced for the high PDMS content samples, where the large amounts of PDMS significantly improve the dry physical properties of the material.
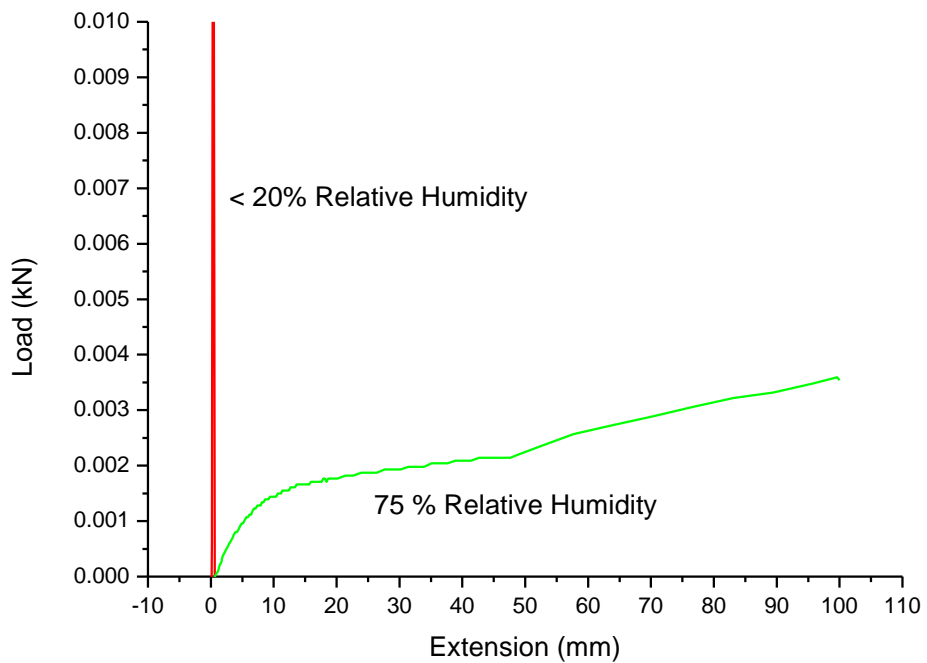


**Figure 4-43:** Comparison of 20% and 75% relative humidity equilibrated 6.9 mol.% PDMS samples

_____

## 4.8 References

**1**   Meltz, F. Master's Thesis, University of Stellenbosch, **2014.**

**2**   Erdodi, G.; Kennedy, J. P. *J. Polym. Sci. Part A Polym. Chem.* **2007**, *45*, 295–307.

**3**   Saha, S.; Sarkar, P.; Sarkar, M.; Giri, B. *Rsc Adv.* **2015**, *5*, 27665–27673.

**4**   Xia, Z.; Patchan, M.; Maranchi, J.; Elisseeff, J.; Trexler, M. *J. Appl. Polym. Sci.* **2013**, *127*, 4537–4541.

**5**   Gundogan, N.; Okay, O.; Oppermann, W. *Macromol. Chem. Phys.* **2004**, *205,* 814–823.

**6**   He, C.; Erdodi, G.; Kennedy, J. P. *J. Polym. Sci. Part B Polym. Phys.* **2006**, *44*, 1474–1481.

**7**   Okuzaki, H.; Kobayashi, K.; Yan, H. *Macromolecules* **2009**, *42*, 5916–5918.

**8**   Sundar, S. S.; Sangeetha, D. *J. Mater. Sci. Mater. Med.* **2012**, *23*, 1421–1430.

**9**   Kim, Y.-J.; Ebara, M.; Aoyagi, T. *Sci. Technol. Adv. Mater.* **2012**, *13*, 064203.

**10**   Chuang, W.-J.; Chiu, W.-Y. *Polymer* **2012**, *53*, 2829–2838.

**11**   Lu, P.; Hsieh, Y. Lo. *Polymer* **2009**, *50*, 3670–3679.

**12**   Kim, S. H.; Kim, S. H.; Nair, S.; Moore, E. *Macromolecules* **2005**, *38*, 3719–3723.

**13**   Bayley, G. M.; Mallon, P. E. *Polymer* **2012**, *53*, 5523–5539.

**14**   Fragiadakis, D.; Pissis, P. *J. Non. Cryst. Solids* **2007**, *353*, 4344–4352.

**15**   Bennour, S.; Louzri, F. *Adv. In Chem.* **2014**, *2014, 1-10.*

**16**   Ikeda-Fukazawa, T.; Ikeda, N.; Tabata, M.; Hattori, M.; Aizawa, M.; Yunoki, S.; Sekine, Y. *J. Polym. Sci. Part B Polym. Phys.* **2013**, *51*, 1017–1027.

**17**   Li, W.; Xue, F.; Cheng, R. *Polymer* **2005**, *46*, 12026–12031.

**18**   Bigg, E. K. *Proc. Phys. Soc. Sect. B* **2002**, *66*, 688–694.

**19**   Wagler, T.; Rinaldi, P. L.; Han, C. D.; Chun, H. *Macromolecules* **2000**, *33*, 1778–1789.

**20**   Ma, Y.; Cao, T.; Webber, S. E. *Macromolecules* **1998**, *9297*, 1773–1778.

**21**   Guan, Y.; Ding, X.; Zhang, W.; Wan, G.; Peng, Y. *Macromol. Chem. Phys.* **2002**, *5*, 900–908.

**22**   Niu, H.; Wang, F.; Weiss, R. A. *Macromolecules* **2015**, *48*, 645–654.

**23**   Xu, J.; Qiu, M.; Ma, B.; He, C. *ACS Appl. Mater. Interfaces* **2014**, *6*, 15283–15290.

**24**   Bragg, W.L.; Bragg, W.H. *Proceedings of the Roy. Soc. of London: Series A.* **1913**, 428 – 438.

**25**   Geppi, M.; Veraeini, C. A.; Forte, C.; Cecchin, G.; Ferrari, P. *Polymer* **1997**, *38*, 5713–5723.

**26**   Elhrari, W.; Assumption, H.; Mallon, P. E. *Polymer* **2015**, *77*, 95–101.

**27**   Mokeev, M. V; Zuev, V. V. *Eur. Polym. J.* **2015**, *71*, 372–379.

**28**   Solid State NMR Application Notes, *University of Durham Solid State NMR Service,* **2002.**

**29**   Fineman, M.; Ross, S. D. *J. Polymer Sci.* **1950**, *5*, 259.

**30**   Painter, P.C; Coleman, M.M. *Essentials of Polymer Science and Engineering,* DEStech Publications Inc, **2008**.

**31**   Mochizuki, A.; Namiki, T.; Nishimori, Y. *J. Biomater. Sci. Polym. Ed.* **2015**, *26*, 750–765.

_____

# Chapter 5: Conclusions and Recommendations

## 5.1 Conclusions

A selection of hydrogel monomers, namely 2-hydroxy ethyl methacrylate, acrylic acid, and N,N'-dimethyl acrylamide were tested as potential candidates in the synthesis of novel physically crosslinked amphiphilic hydrogels by copolymerizing them with poly(dimethyl siloxane) macromonomers. Of the graft copolymers synthesized, only DMAA with the 1 000 g/mol PDMS macromonomer resulted in the formation of hydrogels which swelled to a significant degree and which had useful physical properties. Therefore, these monomers were chosen as a focus of this study and a series of copolymers with varying PDMS contents were prepared by a simple free radical polymerization process. The sample compositions and formation of the copolymer was confirmed by means of FTIR, $^1$H NMR and SEC. The molecular weights varied from 46 000 - 84 000 g/mol, with dispersity values ranging between 2.3 and 2.9.

Kinetics studies from in-situ $^1$H NMR, and analysis of composition vs. feed ratios via the Fineman-Ross equation was used to determine the general reaction kinetics and reactivity ratios of the system. It was found that random copolymers with a significant degree of compositional drift were formed for the range of feed ratios used in this study. The reactivity ratios for DMAA and the PDMS macromonomer in toluene were found to be 0.926 and 4.31, respectively. Fractionation of the samples by HPLC revealed that a homopolymer and copolymer fraction was present, with the homopolymer fraction diminishing significantly as the PDMS in the feed ratio was increased, while the retention time of the copolymer fraction increased linearly across the series.

The addition of PDMS was shown to be an effective means of inducing reversible physical crosslinking. The material was readily soluble in a number of common organic solvents such as THF, acetone, ethanol and chloroform, but remained insoluble in water and hexane. The degree of swelling of the material in water is dependent on both the amount of added PDMS and the morphology induced by the method of preparation. The material was optically transparent and had rubber-like properties as long as it was contained in a humid environment. Swelling occurred rapidly, reaching 90% of the equilibrium maximum in less than 5 minutes.

DSC analysis showed a weak glass transition temperature around 98°C, within the expected range for PDMAA. An unknown secondary event was also detected, tentatively ascribed to the presence of either moisture or possibly a secondary transition due to interactions between the amide side groups.

DSC analysis was also used to track the fractions of freezing and non-freezing water within swollen samples. The fraction of non-freezing water initially increased as the PDMS content was increased, until the occurrence of a morphological transition at PDMS contents greater than 6.7 mol.%. Relative crosslink densities were also calculated for the system and it was found that between 4.2 – 6.7 mol.% PDMS, increases in the PDMS content led to diminishing returns in the effective crosslink density of the PDMAA domains. It was noted that the 4.2 and 7.9 mol.% PDMS samples have similar degrees of

swelling and similar crosslink densities in the PDMAA domains, even though the latter sample has almost twice as much PDMS.

Nanofibres of the material were prepared for the first time by means of electrospinning, and were found to have an average diameter of around 700 nm. The fibre diameters decreased slightly with increasing PDMS content. When exposed to water, the nanofibres were found to be unstable and underwent amalgamation, consequently losing most of their fibrous structure. The stability improved with increasing PDMS content. Swelling in the fibre state was much higher than in the film state, and it was shown by way of DSC that the amount of non-freezing water present in the fibres was larger than that of the films, thereby proving that the nanofibres do not only absorb more water due to the presence of interstitial spaces, but rather due to a change in internal morphology.

A combined approach, using data from the swelling studies, DSC, FE-SEM, WAXD and solid state NMR was used to elucidate the morphology of the system. It was shown that the PDMS domains in the lower PDMS content samples are mostly found in isolated clusters, as evidenced by the swelling of the material in hexane, FE-SEM images and the T1ρ relaxation data. As the PDMS content was initially increased, the degree of swelling in water did not decrease substantially, and it was therefore concluded that most of the PDMS must remain isolated inside of these clusters. However, once a threshold PDMS content is exceeded, the material undergoes a morphological transition and less phase segregation appears to occur. This leads to similar T1ρ relaxation times in both the PDMAA and PDMS domains, a decrease in water swelling and an increase in swelling in hexane. The morphology observed from FE-SEM images of freeze fracture surfaces is also found to differ from the lower PDMS content samples. This result is unusual, given that we generally expect to see an increased degree of phase segregation as the composition changes to include more of the immiscible comonomer. This raises some questions as to whether some secondary effects, such as the large weight percentage of PDMS, may lead to some distortions in the data. However, it was concluded that since no contrary results were obtained by any of the analytical techniques employed, this result has to be accepted as valid for the time being.

Before comparing the nanofibre state with the film state, the effect of the solvent used for the preparation of each type of material was addressed and it was concluded that the induced morphology was as a result of the rate of drying, rather than the type of solvent itself. It was also shown that a superswollen morphology could be induced by use of the appropriate procedure. Comparisons between the nanofibres and the film state using solid state NMR indicated that the degree of phase separation in the fibre state was less extreme than in the film state. It is stated that this is because there is insufficient time for rearrangement of the polymer chains during the electrospinning process, and consequently the PDMS domains are not able to cluster together sufficiently to produce a well crosslinked material. The appearance of a previously unseen peak in the nanofibres' solid state NMR spectra served as further proof of the altered morphology, and suggested that some changes in rotation and in conformation around the polymer backbone had occurred as a result of the electrospinning process. Differences in the intra chain amide correlation distances were also noted from WAXD data.

_____

Finally, at the outset it was stated that developing a "smart" material was one of the objectives. No such properties were observed during the course of this study, but some potential was noted in the nanofibre state with regards to solvent responsive shape memory. However, we believe the ability of this material to readily dissolve in a number of solvents, while maintaining its ability to behave as a crosslinked network in water and non-polar solvents, alongside its anticipated biocompatability and its rapid swelling behaviour, will likely make it useful for a variety of practical applications in the near future.

_____

## 5.2 Recommendations

With a basic understanding of the material properties and morphology in place, the next step will be to determine how the use of different solvents in electrospinning can alter the effective crosslink density of the resulting material. This may make it possible to produce highly crosslinked nanofibers using relatively small amounts of PDMS, or conversely, produce high swelling nanofibres from the high PDMS content material. There is also the possibility of manipulating the PDMS chain lengths to find an optimal value.

Controlled polymerization by means of RAFT (Radical Addition Fragmentation Transfer) or anionic polymerization could potentially produce a more structurally regular material with improved physical properties, as well as allowing for better control over the crosslink density.

The biocompatibility of PDMAA-g-PDMS should be assessed for its potential use as a means of controlled drug release. Due to the material's amphiphilic nature, it may be useful in the delivery of both hydrophilic and hydrophobic drug compounds. Its high solubility in ethanol, which is relatively non-toxic and could be diluted with water to further lower the toxicity, also makes it a potential candidate as an injectable hydrogel system. The use of a modified PDMS macromonomer that can undergo *in-vitro* hydrolysis should also be explored, as this could allow the material to slowly dissolve inside of body tissue and be excreted once its drug reservoirs are depleted.

In this study, only two samples could be examined with solid state NMR, and it is therefore recommended that the full series should be analysed to better understand the changes in morphology as the PDMS content is increased throughout the series.

Dynamic Mechanical Analysis (DMA) over a series of temperatures and different degrees of swelling will likely provide a clearer understanding of the thermal events detected by DSC, since the material exhibited a weak glass transition, and the nature of some of the other detected thermal events remained unclear. The exact "transition point" between rubber-like and glassy behaviour as the ambient humidity is altered could potentially also be detected more clearly using this analytical technique.

Finally, application testing should be conducted for drug release. Due to its amphiphilic nature, it is likely that this system will have the ability to store and release both hydrophilic and hydrophobic drug compounds. The ability to easily tweak its hydrophilicity by the incorporation of varying amounts of PDMS will also allow it to be tailored more easily to create specific drug release rate profiles.

_____

# Appendix A: Calculations

**1.      Determination of sample PDMS content from NMR data:**

| Sample | Acrylamide peak integral[a] | Number of associated protons | PDMS peak integral[b] | Number of associated protons[c] |
|---|---|---|---|---|
| S1 | | | 0.44 | |
| S2 | | | 0.51 | |
| S3 | 1 | 6 | 0.72 | 60 |
| S4 | | | 0.86 | |
| S5 | | | 1.17 | |

Formula: $Mol\ fraction\ PDMS = \dfrac{\frac{PDMS\ peak\ integral}{\#\ Protons}}{\frac{PDMS\ peak\ integral}{\#\ Protons} + \frac{Acrylamide\ peak\ integral}{\#\ Protons}}$

*a: "Acrylamide peak integral" is defined as the range from 3.23 to 2.74 ppm*

*b: "PDMS peak integral" is defined as 0.18 to -0.05 ppm.*

*c: Number of protons determined by using 900 g/mol the average molecular weight of the PDMS macromonomer (product is specified as 800 – 1 000 g/mol); protons on the carbon directly after the PDMS chain are also accounted for.*

**2.      Reactivity ratio calculation via Fineman-Ross method:**

$G = \dfrac{f_1(2F_1-1)}{(1-f_1)F_1}$  and      $H = \left[\dfrac{f_1^2(1-F_1)}{(1-f_1)^2 F_1}\right]$

With H plotted against G, the slope is equal to $r_1$ and the intercept $-r_2$ with a linear fit.

The PDMS content of each sample (at 10% conversion) was calculated by adding the difference between the fraction of residual PDMS monomers (determined from the CH3 peak at 4.0 ppm and the vinyl peak at 5.5ppm) and the PDMS feed ratio, thus yielding the fraction of PDMS actually incorporated in the sample. This methodology was necessary to avoid altering the monomer ratios, since the macromonomer is non-volatile, while DMAA evaporates readily.

Appendix A

_____

**Table A:** PDMS fractions in copolymer at 10% conversion

| Sample | PDMS fraction in polymer @ 10% conversion |
|--------|--------------------------------------------|
| S1 | 0.039 |
| S2 | 0.062 |
| S3 | 0.086 |
| S4 | 0.130 |
| S5 | 0.163 |

**3.      $Q_S$ and $Z_S$ value determination of swollen gels:**

$$Q_S = \left( \frac{Q - 1}{(1 - Weight\ fraction\ PDMS)} \right) + 1$$

and

$$Z_S = \left( \frac{Z - 1}{Weight\ fraction\ PDMS} \right) + 1$$

Explanation: Suppose sample X weighs 1 g and contains 1 ml water. Therefore, Q = 2. But the sample is 25 wt.% PDMS, therefore 0.75 g of the sample holds the 1 g water, meaning that the effective  swelling is 1 g water / 0.75 g = 1.333. But, since Q is the wet sample divided by the dry sample, the sample weight needs to be added to the nominator, and the equation becomes (1 g water + 0.75 g sample / 0.75 g dry sample) =  $Q_S$ = 2.33.